Western Research
INSTITUTE

Asphalt Research Consortium

Quarterly Technical Progress Report
October 1 - December 31, 2007

January 2008

Prepared for
Federal Highway Administration
Contract No. DTFH61-07-H-00009

By
Western Research Institute
Texas A&M University
University of Wisconsin-Madison
University of Nevada-Reno
Advanced Asphalt Technologies

www.westernresearch.org
www.ARC.unr.edu

TABLE OF CONTENTS

INTRODUCTION

This document is the Quarterly Report for the period of October 1 to December 31, 2007 for the Federal Highway Administration (FHWA) Contract DTFH61-07-H-00009, the Asphalt Research Consortium. The Consortium is coordinated by Western Research Institute with partners Texas A&M University, the University of Wisconsin-Madison, the University of Nevada Reno, and Advanced Asphalt Technologies.

The Quarterly Report is grouped into seven areas, Moisture Damage, Fatigue, Engineered Paving Materials, Vehicle-Pavement Interaction, Validation, Technology Development, and Technology Transfer. The format of the report is based upon the Research Work Plan and is grouped by Work Element and Subtask. The Moisture Damage and Fatigue areas report on Work Elements and Subtasks that are interrelated and thus work together to advance the knowledge of mechanisms and models in these areas.

The research areas of Engineered Paving Materials, Vehicle-Pavement Interaction, and Validation generally report work elements that are more "stand-alone" in nature but this doesn't mean that these work elements operate independently because in most cases, at least two Consortium partners are teaming to conduct the work. These work elements also provide useful information to the other research activities in the Consortium.

Finally, the areas of Technology Development and Technology Transfer report where the research deliverables have been transmitted to the user community. The Technology Development area reports the progress to take promising research developments and refine them into useful tools for engineers and technologists involved in the design, construction, and maintenance of flexible pavement systems. The Technology Transfer area reports on the transfer of Consortium research findings to the asphalt community using the Consortium website, presentations, publications, and workshops.

In December 2007, the Consortium members met to discuss the details of preparing the Annual Work Plans for Year 2 and other Consortium matters.

SUPPORT OF FHWA AND DOT STRATEGIC GOALS

The Asphalt Research Consortium research is responsive to the needs of asphalt engineers and technologists, state DOT's, and supports the FHWA Strategic Goals and the Asphalt Pavement Road Map. More specifically, the research reported here supports the Strategic Goals of safety, mobility, and environmental stewardship. By addressing the causes of pavement failure and thus determining methods to improve asphalt pavement durability and longevity, this research will provide the motoring public with increased safety and mobility. The research directed at improved use of recycled asphalt pavement (RAP), warm mix asphalt, and cold mix asphalt supports the Strategic Goal of environmental stewardship.

GENERAL CONSORTIUM ACTIVITIES

PROGRESS THIS QUARTER

Several Consortium members traveled to McLean, Virginia to meet with FHWA personnel regarding the Materials Selection plan. The Materials Selection Plan was prepared as part of the Annual Work Plans for Year 2.

Consortium members Dr. Dallas Little, Dr. Amit Bhasin, Dr. Hussain Bahia, Dr. Peter Sebaaly, Dr. Ramon Bonaquist, Dr. Raymond Robertson, Mr. Fred Turner, and Mr. Michael Harnsberger met in Denver to discuss the preparation of the Annual Work Plans for Year 2 and other Consortium matters. Consortium members and staff began preparation of the Year 2 work plans that included addressing the reviewer comments on the Year 1 work plan. The reviewer comments and the responses from the Consortium are included as part of the Annual Work Plans for Year 2 and addressed in the Work Plan where necessary.

WORK PLANNED FOR NEXT QUARTER

Many Consortium members planned to attend the 87th Annual Meeting of TRB where several members have presentations. Consortium members are also planning on attending the project review that is organized by Western Research Institute on the Friday after TRB concludes. Attendance at the WRI project review was requested by FHWA.

All Consortium members and staff will complete the preparation of the Annual Work Plan for Year 2 and deliver the plan to FHWA in January 2008. In addition, a Quarterly Report on the Consortium activities for the period October 1, 2007 to December 31, 2007 will be prepared and delivered.

Consortium members are also expecting that attendance at the February 2008 ETG meetings in Tampa, Florida will be required although there has been no specific request as of January 31, 2008.

PROGRAM AREA: MOISTURE DAMAGE

CATEGORY M1: ADHESION

Work Element M1a: Affinity of Asphalt to Aggregate

Subtask M1a-1: Select Representative Asphalt Binders and Mastics, and Aggregate Materials (All Year 1 start)

Progress This Quarter

A Materials Selection Plan was prepared as part of the Year 2 Work Plan.

Work Planned Next Quarter

Receive comments on the Materials Selection Plan from FHWA and discuss any needed changes.

Subtask M1a-2: Use the Modified DSR Tests to Evaluate Various Moisture Testing Conditions Including Control of Rate and Temperature and to Measure Affinity of Asphalts to Aggregates and also Cohesion of Binders (UWM Year 1 start)

Subtask M1a-3: Evaluate the Moisture Damage of Asphalt Mixtures with Selected Material Combinations by the TSR Test or an Alternative Test System (UWM)

(Note: These two subtasks will be reported together.)

Task Lead: Dante Fratta

In order to evaluate the susceptibility of moisture damage within asphalt pavements, the chemical and/or physical affinity is commonly measured with loose asphalt mixtures or compacted asphalt mixtures in a field-simulated environment. Although some of these tests show results comparable with real field data, the actual mechanism of moisture damage and the role of components in the failure response cannot be sorted from these tests due to the complexity of the interacting mechanisms (Kanitpong 2005). Therefore, there is significant room for improvement, mainly because of the structural complexity of asphalt mixtures, the interaction with different mineral surfaces, and the confounding effects that result from it.

The difficulty of accurately measuring the role of the various variables (e.g., binder cohesion, adhesive bond, air voids, aggregate surface characteristics and shape, etc.) makes an analytical approach for selecting materials that will resist moisture damage very complex. The use of simplified testing systems that can separate the contribution of different components under the effect of water could provide a more effective method for moisture damage analysis, prediction of damage risk, and the evaluation of mixture components that can reduce and/or control

moisture damage. Among the many ideas proposed in the last 10 years, two systems show the greatest potential for satisfying the simple analytical approach criteria. One is the Pneumatic Adhesion Tensile Testing Instrument (PATTI) and the other is the testing procedure developed using a Dynamic Shear Rheometer (DSR) to measure cohesive strength (Cho and Bahia 2007).

The PATTI device was initially developed by the National Institute of Standards and Technology (NIST) and was utilized by Youtcheff and Aurilio (1997) at FHWA to evaluate the adhesive loss of asphalt-aggregate systems exposed to water. The PATTI device is advantageous for several reasons: it allows the use of different aggregate surface, the aggregate specimen can be conditioned in water after applying the binder, and it allows one to observe the failure surface to define adhesive versus cohesive failure. In addition, the device is low-cost, simple, and well described by an ASTM standard (ASTM 2002). The PATTI device and methodology are therefore considered as a good testing procedure for measuring moisture damage properties of binders.

The DSR thin film cohesion test methodology was recently developed, and its main advantage is the very precise control of temperature, film thickness, and rate of loading. The DSR test allows precise measurements of time-based responses such as load and deflection. These parameters are then used to evaluate the rheological properties of binder-aggregate surface systems. The DSR and PATTI tests also permit the application of different loading paths (e.g., shearing or uniaxial loading in the DSR methodology and uniaxial in the PATTI testing methodology). Testing data have shown the potential of the methodology for measuring factors affecting moisture damage for a wide variety of testing conditions. For example, by combining different aggregate-made discs and varying the binder film thickness, we will be able to gain more insight on the binder's cohesive properties and aggregate-binder adhesive responses.

This work element includes objectives focused on the PATTI and DSR thin film rheology tests. It is expected that both of these systems will be evaluated to define factors that have significant effect on binder-aggregate responses: Modification of the pull-off test to allow measuring load and deflection and control film thickness. The cost and practicality of the modification as well as the precision and bias will be evaluated.

Further development of the DSR thin film test is done by evaluating the following factors:

- The effect of different pulling rates on the PATTI and DSR responses.
- The testing temperature plays an important role in adhesion and cohesion. The testing temperature effect on the adhesion and cohesion results will be quantified and used to define role of climate on moisture damage. The testing temperature will also help in establishing relationships between different mixture testing temperatures.
- Changing loading frequencies in the shear mode will have an important effect on the cohesion and adhesion test results and it will better simulate different traffic speeds.
- The temperature during the water conditioning plays an important role in the effect of water on cohesion and adhesion of binders or mastics.

Progress This Quarter

Since the start of Year 1 work plan, the team has extensively evaluated the modification of the traditional pullout test methodology and the proposed modification on the measured parameters. Major tasks include:

(a) Design and build the testing component

The different components of the modified PATTI test methodology were selected and put together. These components include an 8-channel data acquisition card, pressure transducer, displacement transducer and support for the pullout stub, and displacement transducer frame. The system was put together and testing and evaluation began.

(b) Design of the test methodology

The proposed testing methodology was developed considering all testing parameters and condition. The step-by-step methodology includes

Binder preparation. Put the binder in the oven at 135°C until it becomes fluid. Stir the hot binder in one direction to homogenize the temperature in the binder. Pour the molten binder in a clean silicone mold. Dress the binder as shown in figure M1a.1 and let the binder cool down to room temperature.

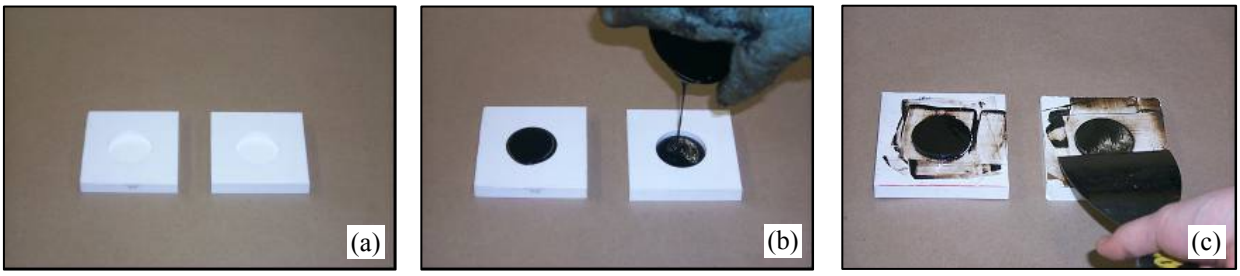

Figure M1a.1. Photos. (a) Prepare clean silicone molds. (b) Pour the molten binder. Let the binder to cool down to room temperature (approx. one hour). (c) Dress the binder with a heated putty knife (Pictures by Kitae 2005).

Aggregate surface preparation. Place the flat surface of the aggregate to be tested on a hot plate or oven set at the required preparation temperature (typically 135 °C). Leave the aggregate surface on the plate until the surface temperature of the aggregate equilibrates with the temperature of the hot plate. The aggregate surface temperature is measured with an infrared thermometer. At the same time, place the bottom of the pullout stub on the surface of the hot plate or in an oven set at 135 °C. The stub needs to be heated to allow binding to the asphalt binder.

Place the binder onto the heated aggregate surface. Remove the aggregate from the hot plate or oven (however keep the pullout stub on the hot plate). Measure the aggregate surface

temperature with the infrared thermometer (this is the preparation temperature). Place the silicone mold face down on the heated aggregate surface so that the binder makes contact with the heated aggregate.

Remove the silicone mold. Let the binder-mineral system cool to room temperature and carefully remove the silicone mold (to facilitate the binder demolding, place the silicone mold and binder in a refrigerator for about 5 minutes). The silicone mold should be easily removed and the binder must remain on the aggregate surface. If the binder peels off from the aggregate, repeat procedure from the first step using a fresh mineral surface.

Attach the pullout stub to the binder. Place the split pull-off stab support around the binder. Remove the pullout stab from the hot plate and rapidly place it on the center of the pullout stab support (see figure M1a.2 – use gloves when handling the pullout stub as it will be hot). This support leaves a binder thickness equal to 0.5 mm. Let the system pullout stub cool down until it reaches the ambient temperature.

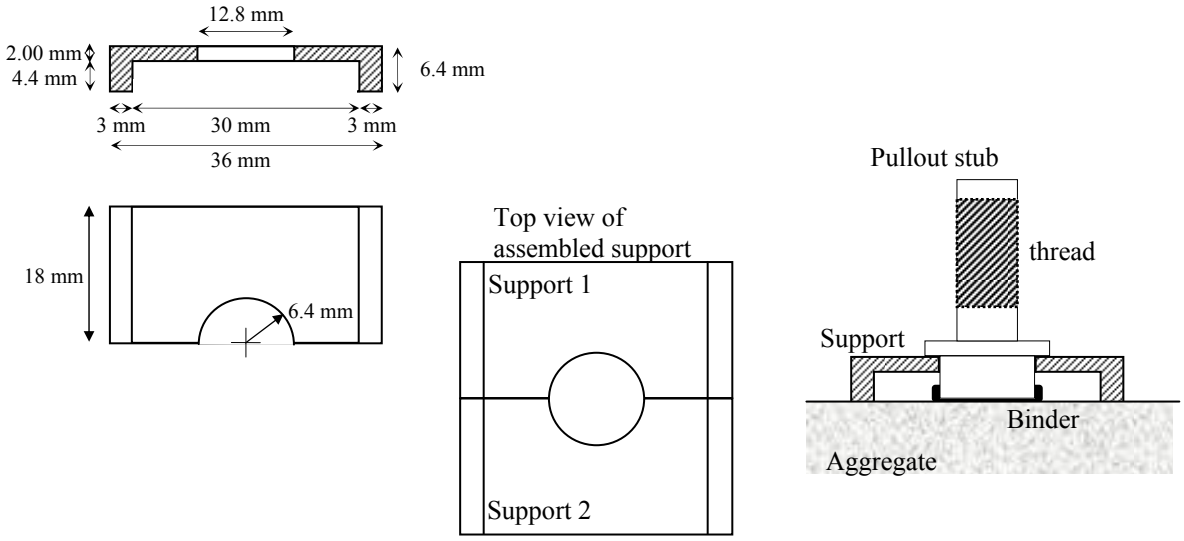

Figure M1a.2. Illustration. Details of the split pullout stub support and assembled aggregate, binder, support and pullout stub.

Binder mineral conditioning. Submerge the assembled aggregate-binder-pullout stub system in a temperature-controlled water or salt aqueous-solution bath for a predetermined period of time. Once this process is complete, the aggregate-binder system is ready for the pullout testing. If the system will be tested without conditioning, let the system equilibrate with the testing temperature (for example, room temperature or 10 °C) for at least one hour.

Setting the pullout test. Place the aggregate, binder and pullout system on a bench top for ambient temperature testing or in an environmental chamber for temperature control testing. Separate the split support and use them as spacer (figures M1a.3 andM1a. 4). Assemble the PATTI test pressure ring (on top of the spacers), silicone gasket, and the pressure line to the

PATTI pressure controller. The added spacers allow a pullout deformation of about 6 mm (at total strain of 1200%).

Screw the self-aligning bearing plate following the procedure described in ASTM standard D4541. Set the three-leg LDVT frame on top of the mineral rock and align the high resolution LVDT on the top of the pullout stab. The modified PATTI test also includes a pressure transducer to monitor the pressure history during the test (see figures M1a.4 and M1a.5). Connect the pressure transducer and LVDT to the data acquisition card. The recorded data allow for the reconstruction of the deformation-force history and the evaluation of the energy dissipated during the pullout test. Set the pullout rate in the PATTI pressure controller and the test is ready to begin.

Run the pullout test. Set the pressure rate in the PATTI pressure control panel. Run the test by applying pressure to the line. The data acquisition system will collect the data post failure. Once the test is completed, remove the pullout stab and take a picture of the failure surface to document if the failure was cohesive or adhesive. Use the deformation-load history data to evaluate the energy dissipated during testing and the type of failure (ductile or brittle).

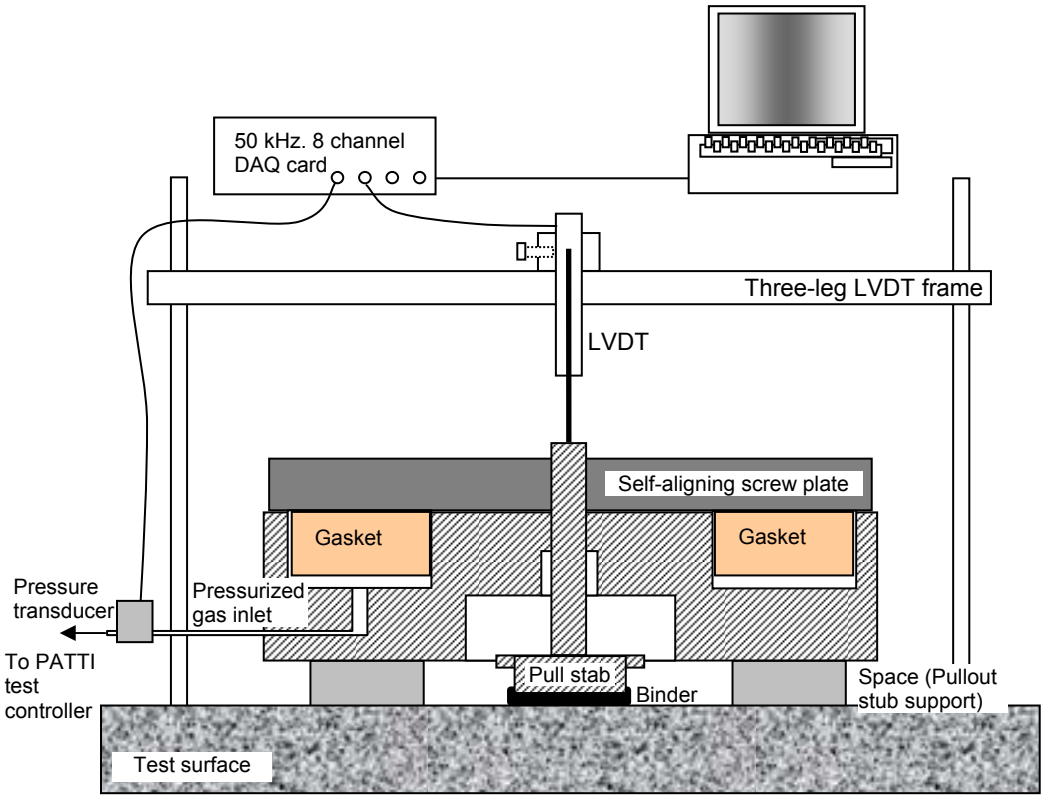

Figure M1a.3. Illustration. Schematic of the complete ensemble modified PATTI test.

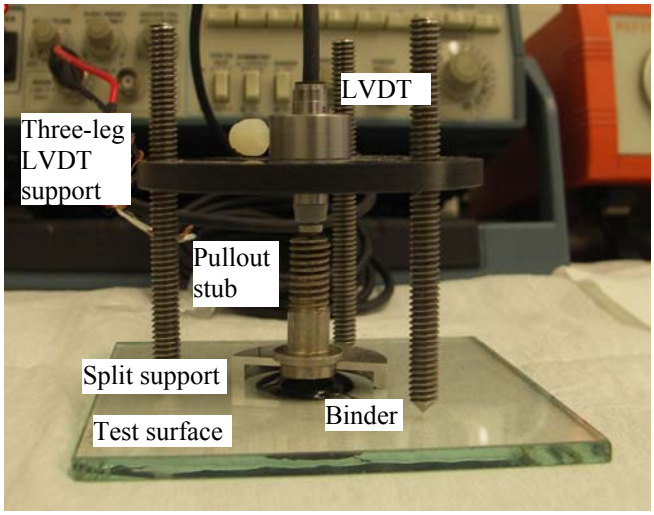

Figure M1a.4. Photo. Picture of the ensemble modified PATTI test setup (the PATTI pressure ring is not shown).

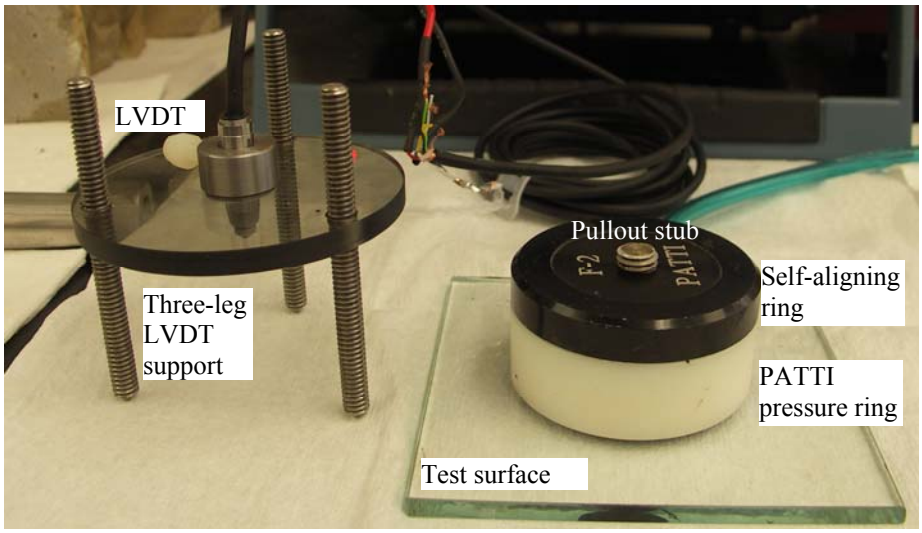

Figure M1a.5. Photo. Picture of the ensemble modified PATTI test setup (the PATTI pressure ring is not shown).

(c) Evaluation of the modified testing methodology

Several controlled tests were run to calibrate and validate the proposed methodology. These tests include:

- The calibration of the pressure transducer and linear variable displacement transducer and linear potentiometer
- The calibration of the pressure rate applied by the PATTI pressure panel

- The evaluation of the relative location of the pressure transducer to reduce the air pressure losses
- The initial evaluation of the binder-aggregate response

Initial set of results are presented in figures M1a.6 and M1a.7.

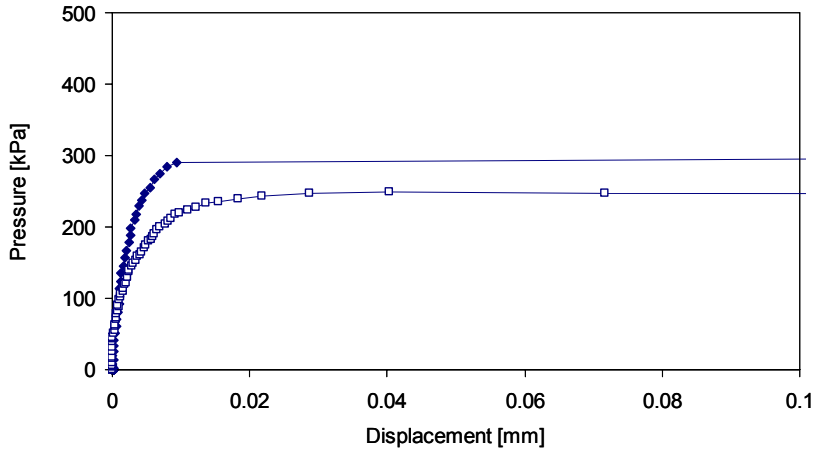

Figure M1a.6. Chart. Typical modified PATTI test results: PG 58-22 neat binder, glass plate test surface and slow and fast pressure rates.

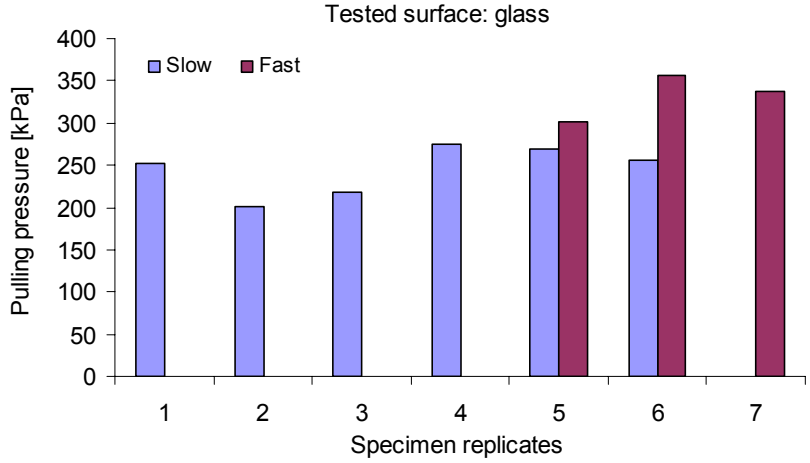

Figure M1a.7. Chart. Summary modified PATTI pulling pressure test results: PG 58-22 neat binder, glass plate test surface and slow and fast pressure rates.

Problems Encountered and Solutions

None

Work Planned Next Quarter

During the first quarter of 2008, the research team will continue with the validation of the modified PATTI test methodology and will further evaluate the results by comparing binder-aggregate system behavior with results using the DSR testing methodology. Additional test will be performed using different mastics.

The testing program was proposed and testing began to further to validate the modified PATTI test methodology and evaluate both binder-aggregate system behavior under moisture damage. The following parameters will be tested:

- Mineral surfaces (3): granite, limestone, glass plates
- Binders (3): neat PG58-22 binder, PG64-22 SBS-modified binder, and PG64-22 Elvaloy-modified binder
- Binding temperatures: 65 and 135 °C
- Conditioning temperatures (1): 60 °C
- Conditioning times (1): 24 hours.
- Conditioning environment (4): unconditioned, de-ionized water, 0.5 M NaCl solution and 0.5 M $CaCl_2$ solution
- Testing temperatures (2): 10°C and 25°C (room temperature)
- Pullout rates (2): one slow and one fast (as determined from a parametric pullout rate study)

Total number of tests: 96 tests (+ duplicates). The summary of materials and tests are presented in the following tables. Test will be performed using the modified PATTI tests and the results will be validated with DSR testing.

Table M1a.2. Proposed testing materials

Mineral surfaces	Granite	Conditioning environment	Air
	Limestone		0.5 M NaCl (aq)
	Glass Plate		0.5 M $CaCl_2$ (aq)
Binders	neat PG58-22 binder		
	PG64-22 SBS-modified binder		
	PG64-22 Elvaloy-modified binder		

Table M1a.3. Proposed testing parameters

Testing technique	Modified PATTI	Binding temperatures	Two (65 and 135 °C)
	DSR	Condit. temperature	One (65 °C)
Mineral surfaces	Three	Testing temperatures	Two (10 and 25 °C)
Binders	Three	Pullout rates	Two (slow and fast)
Conditioning environments	Three		

Two types of data interpretation analysis are proposed. The first analysis methodology proposed is a statistical evaluation of the tested parameters. PATTI tests have problems with repeatability and the evaluation of the maximum pullout pressure, the energy dissipated, and failure type (adhesion vs. cohesion) variability during testing will allow identifying spurious events and will affect the quality of the data. Once the validity of the testing results is confirmed, material behavior will be evaluated. Moisture damage studies will be performed to evaluate material behavior with the proposed new methodology. Emphasis will be placed on the evaluation of the conditioning environment and surface mineralogy on the strength and failure mechanism of the aggregate-binder system.

References

ASTM, 2002, D 4541 – 02 Standard Test Method for Pull-Off Strength of Coatings Using Portable Adhesion Testers. *American Society of Testing and Materials*. 100 Barr Harbor Drive, P.O. Box C700, West Conshohocken, PA 19428-2959, United States.

Bahia, H., and K. Kanitpong, 2003, Role of Adhesion and Thin Film Tackiness of Asphalt Binders in Moisture Damage of HMA. *Journal of the Association of Asphalt Paving Technologists*, 72: 502-528.

Cho, D.-W., and H. Bahia, 2007, Effects of Aggregates' Surface and Water on Rheology of Asphalt Film, Accepted to the *Transportation Research Record*, 2007.

Kanitpong, K., 2005, *Evaluation of the Roles of Adhesion and Cohesion Properties of Asphalt Binders in Moisture Damage of HMA*. Ph.D. Thesis. University of Wisconsin-Madison.

Youtcheff, J. and V. Aurilio, 1997, Moisture Sensitivity of asphalt Binders: Evaluation and Modeling of the Pneumatic Adhesion test Results. *Canadian Technical Asphalt Association proceedings*.

Subtask M1a-4: Correlate Moisture Damage as Measured by the Modified DSR Test with the Mixture Test Results - Analyze Results on Each Combination and Material (UWM)

Progress This Quarter

No activity this quarter.

Work Planned Next Quarter

No work planned next quarter.

Subtask M1a-5: Propose a Novel Testing Protocol (UWM)

Progress This Quarter

No activity this quarter.

Work Planned Next Quarter

No work planned next quarter.

Work Element M1b: Work of Adhesion Based on Surface Energy

Subtask M1b-1: Surface Free Energy and Micro-Calorimeter Based Measurements for Work of Adhesion (TAMU Year 1 start)

Progress This Quarter

In the previous quarter, a protocol to determine the enthalpy of adhesion or heat of immersion between the aggregate and asphalt binder at room temperatures using a micro calorimeter was developed. At room temperatures, liquid asphalt binder was used in the form of a solution with toluene as a solvent. During this quarter, the sensitivity of this test method was evaluated using other solvents. The following is a short summary of the conclusions based on trial tests conducted using solvents other than toluene:

i) Cyclohexane: The coefficient of variation was typically higher and certain types of asphalt binders such as ABD did not dissolve completely.
ii) Dichloromethane: This solvent was found to be extremely volatile which made it extremely difficult for the micro calorimeter to attain thermal equilibrium prior to mixing.
iii) n Propyl Bromide: Results were similar to those obtained using toluene in terms of sensitivity and precision.

Tests to evaluate the sensitivity of this methodology to different types of asphalt binders are in progress.

Work Planned Next Quarter

The planned activity for the next quarter is to use the micro-calorimeter to evaluate: i) the effect of treatment of asphalt binder with active fillers and liquid anti strip agents on the total energy of adhesion, ii) the sensitivity of this methodology to differentiate reactivity of different asphalt binders to hydrated lime, and iii) the possible use of this technique to detect presence of clay

contamination that may be present in the filler material used in the production of asphalt mixtures.

Subtask M1b-2: Work of Adhesion at Nano-Scale using AFM (WRI Year 2 start)

Progress This Quarter

No activity this quarter.

Work Planned Next Quarter

No work planned next quarter.

Subtask M1b-3: Identify Mechanisms of Competition Between Water and Organic Molecules for Aggregate Surface (TAMU Year 1 start)

Progress This Quarter

Trial tests with pure minerals and model organic compounds using a flow calorimeter are in progress. We expect to have some results before the end of next quarter.

Work Planned Next Quarter

The planned activity for the next quarter is to develop a synthesis of mechanisms of interaction between organic functional groups and mineral surfaces. In addition this synthesis will also identify: i) minerals that can be used to represent aggregate surfaces, ii) model organic compounds that can be used to represent the most common functional groups in asphalt binders, and iii) a list of candidate test methods that can be used to investigate the interfacial interactions

Work Element M1c: Quantifying Moisture Damage Using DMA (TAMU)

Progress This Quarter

The experimental and analytical procedure to evaluate the performance of moisture conditioned FAM specimens is very similar to the procedure used for unconditioned or dry specimens. Therefore, the work being developed and reported in Task F2b also applies to this work element.

Work Planned Next Quarter

As compared to the procedures developed in Task F2b, two additional components that are required to quantify moisture damage in FAM specimens are: i) a methodology or protocol to moisture condition FAM specimens, and ii) an analytical method to combine results from tests on dry and moisture conditioned specimens. A probabilistic method was developed to address the latter during the previous quarter. The work planned for the next quarter is to focus on the review and finalization of a protocol to moisture condition the FAM specimens.

CATEGORY M2: COHESION

Work Element M2a: Work of Cohesion Based on Surface Energy

Subtask M2a-1: Methods to Determine Surface Free Energy of Saturated Asphalt Binders (TAMU Year 1 start)

Progress This Quarter

No activity this quarter.

Work Planned Next Quarter

No work planned next quarter.

Subtask M2a-2: Work of Cohesion Measured at Nano-Scale using AFM (WRI Year 2 start)

Progress This Quarter

No activity this quarter.

Work Planned Next Quarter

No work planned next quarter.

Work Element M2b: Impact of Moisture Diffusion in Asphalt Mixtures

Subtask M2b-1: Measurements of Diffusion in Asphalt Mixtures (TAMU Year 1 start)

Progress This Quarter

A method to measure diffusivity of water through films of asphalt binder was developed in the previous quarter. This methodology was further refined and developed as follows during this quarter:

i. An improved methodology to prepare thin films on the ATR-IR window using a spin coater was developed after several trials by varying the concentration of the asphalt binder, rotational speed of the spin coater, and volume of material added. Spin coating for 15 seconds at 1000 rpm produced 0.3±0.03 micron thick films. The objective of this exercise was to create thin films with uniform thickness on the entire ATR window. A uniform geometry is essential in order to obtain accurate estimates for the diffusivity of water. The spin coated film of asphalt binder is purged under dry nitrogen gas to eliminate any residual solvent and annealed to eliminate any alterations caused due to vaporization of the solvent.

ii. The film thickness and optical properties (refractive index) of the binder are important inputs in order to determine the concentration of water across the thickness of the thin

film of asphalt binder. These properties were determined for a few selected asphalt binder using ellipsometry. A refractive index value of about 1.62 was obtained for the selected asphalt binders. The refractive index was verified to be constant for different film thickness of the asphalt binder.

Research is underway to determine the long term diffusivity of water through films of asphalt binder.

Work Planned Next Quarter

The planned activity for the next quarter is to continue the experiments described above, using different asphalt binders. For the FTIR, a second setup is being prepared to have humid air flow through the chamber (controlled relative humidity) in order to evaluate the hysteretic effect of a humid-dry cycle on the moisture diffusivity of asphalt binders.

Subtask M2b-2: Kinetics of Debonding at the Binder-Aggregate Interface (TAMU)

Progress This Quarter

The rate of debonding due to moisture at the binder-aggregate or filler interface is one of the factors that controls the overall rate of moisture damage within the asphalt mixture. The objective of this task was to use a similar set up as M2b-1, such as an FTIR, to determine the rate or kinetics of debonding at a binder-solid interface. Another objective of this subtask is to validate the hypothesis that the rate or kinetics of debonding at the binder-aggregate interface is largely dictated by the work of adhesion between these two materials (in addition to extrinsic properties such as temperature, geometry etc). A literature review to investigate available methods to determine the rate of moisture transport at the interface (or the rate of debonding) was conducted. Findings from the literature indicate that it is possible to evaluate the rate of moisture transport at the polymer film-solid interface using spectroscopic techniqes. For example, Linossier et al. (1999) used a double sided ATR cell to track rate of movement of water at the polymer film-solid interface as well as the diffusion of water through the polymer film. Figure M2b-2.1 illustrates the schematic of the process used by these authors and others to determine rate of moisture transport through interfaces.

Work Planned Next Quarter

Pilot tests will be conducted based on the principles identified from the literature review and summarized above.

Reference

Linossier, I., F. Gaillard, M. Romand, and T. Nguyen, 1999, A Spectroscopic Technique for Studies of Water Transport Along the Interface and Hydrolytic Stability of Polymer/Substrate Systems. *Journal of Adhesion*, 70: 221-239.

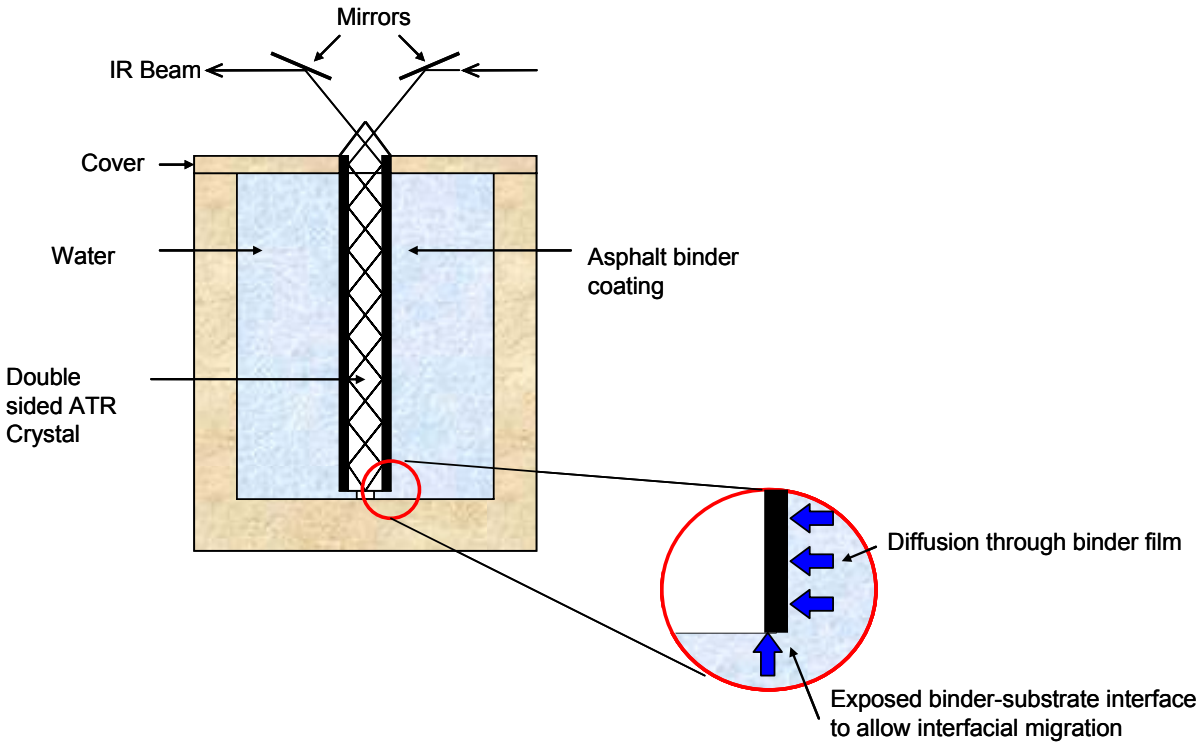

Figure M2b-2.1: FTIR set up to determine diffusion and interfacial coupled moisture transport.

Work Element M2c: Measuring Thin Film Cohesion and Adhesion Using the PATTI Test and the DSR (UWM)

Subtask M2c-1: Evaluate Load and Deflection Measurements using the Modified PATTI Test (UWM Year 1 start)
Subtask M2c-2: Evaluate Effectiveness of the Modified PATTI Test for Detecting Modification Effects (Year 1 start)
Subtask M2c-3: Validation of the Modified PATTI Test using Results from DSR Testing
Subtask M2c-4: Testing of Mastics Using Modified PATTI and DSR Tests
Subtask M2c-5: Commercialization and Practicality Evaluation of the Modified PATTI Test
Subtask M2c-6: Analysis and Recommendations for the Modified PATTI Test
Note: The above subtasks will be reported together.

Work Element Lead: Codrin Daranga

Progress This Quarter

A comprehensive materials library has been put together. Materials prepared under ARC task F2a are included in this study. This will help investigate the influence of different modifiers over the moisture damage properties of binders. On the aggregate side of the materials list, three types of filler (acidic, basic, and neutral) have been identified and acquired (sandstone, limestone, and Ottawa sand, respectively). Testing procedure has been developed for this project

based on the stress sweep test and tack test developed at UW-Madison. Representative data for the modified DSR test with wet and dry testing is shown in figure M2c.1. The preliminary conclusions of for the testing performed this up to this quarter can be summarized as follows:

- The developed modified DSR moisture damage test can evaluate moisture effects of asphalt-aggregate interaction and can differentiate between different materials. The key benefit of this test is that it allows isolation of the physical and chemical effects of the interactions from mixture variables, which commonly confound the evaluation of moisture damage.
- The parameter, defined as W/D YSS (wet-conditioned yield shear strength / dry-conditioned yield shear strength) Ratio, is sensitive enough to evaluate moisture effects of asphalt-aggregate combinations.
- The use of linear visco-elastic (LVE) G* as a performance-related parameter is shown to be insensitive to effects of moisture effects. This raises some concerns regarding the practice of using LVE rheology to evaluate moisture effects.

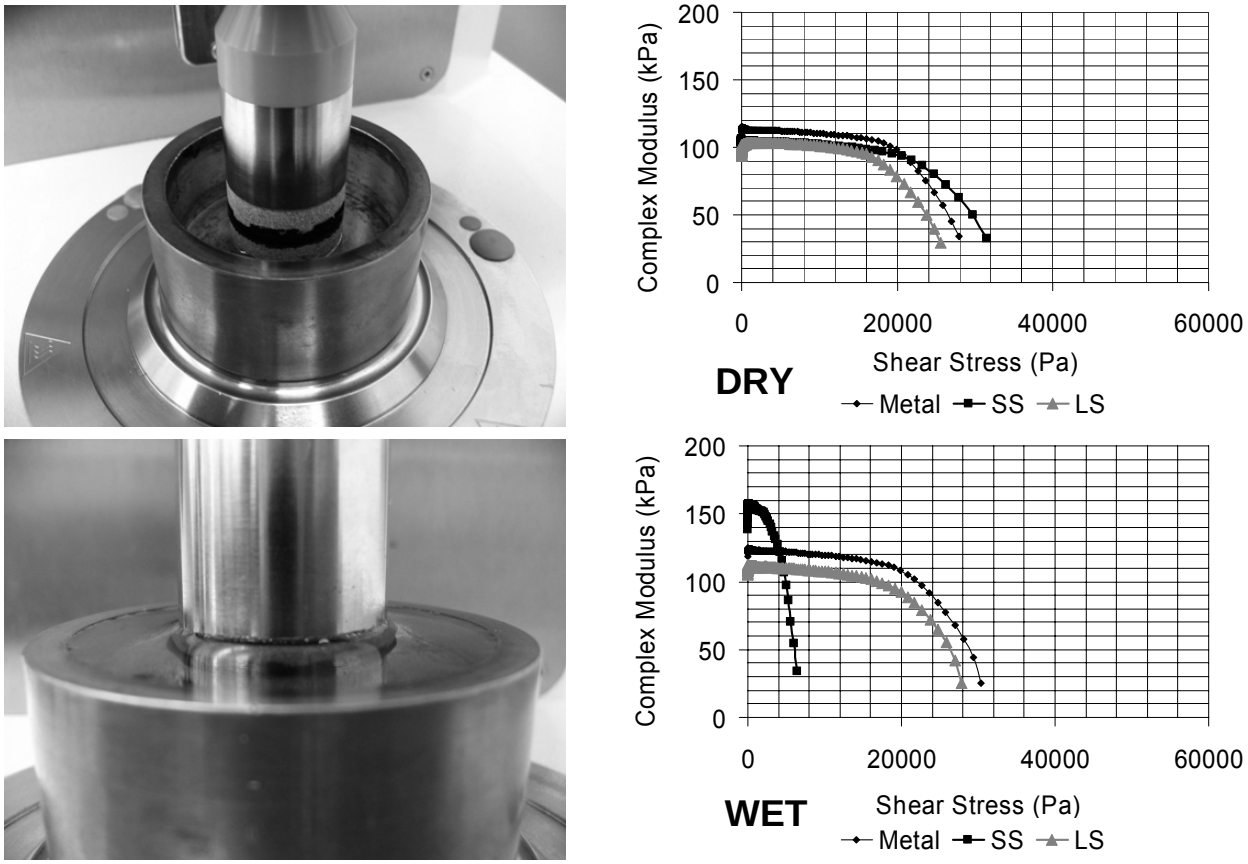

Figure M2c.1. Photos and charts. Representative data for the modified DSR test with wet and dry testing (SS = sandstone, LS = limestone).

Problems Encountered and Solutions

No notable problems were encountered this quarter.

Work Planned Next Quarter

Testing for the next quarter will include stress sweep tests and tack tests to be performed on the previously prepared materials, as detailed in table M2c.1.

Table M2c.1. Stress sweep & tack test experimental matrix.

Neat Binders	PG 58-28	Mineral Fillers	Limestone
	PG 64-22		Sandstone
Modifiers	D1101 Kraton SBS		Ottawa Sand
	D1184 Kraton SBS	Conditioning Media	Distilled water
	Elvaloy AM		NaCl (aq)
	Elvaloy 4170		$CaCl_2$ (aq)
	PPA 115 (or 105)	Conditioning Time	24 hours
Testing Temperature	19° C		No Time
	25° C	Conditioning Temperature	60° C
Aggregate Disks	Limestone	Granite	Sandstone

This test setup will be used to collect data for shear stress sweep at different conditioning conditions, temperatures, and rates of loading. A wide range of combinations of materials (see table M2c.1) will be included. The results will be analyzed in coordination with Texas A&M University research activities to verify that what is being measured is, in fact, explainable by fundamental surface energy measurements, and that the conditions selected for measurements are effective in determining adhesive bond strength as well as cohesive strength.

References

Al-Omari, A., and E. Masad, 2004, Three Dimensional Simulation of Fluid Flow in X-ray CT Images of Porous Media. *International Journal for Numerical and Analytical Methods in Geomechanics*, 28: 1327-1360.

Bhasin, A., and D. N. Little, 2006, Application of Micro-Calorimeter to Characterize Adhesion Between Asphalt Binders and Aggregates. *Journal of Materials in Civil Engineering*, In Review.

Hueckel, T., 2002, Reactive Plasticity for Clays during Dehydration and Rehydration. Part I: Concepts and Options. *International Journal of Plasticity*, 18(3): 281-312.

Kringos, N., and N. Scarpas, 2005a, Raveling of Asphaltic Mixes Due to Water Damage: Computational Identification of Controlling Parameters. *Transportation Research Record,* 1929, 79-87.

Kringos, N., and A. Scarpas, 2006, Numerical Simulation of the Physical Processes Inducing Moisture Damage in Asphaltic Mixtures. *Proc.,* 10th International Conference on Asphalt Pavements (ICAP), Quebec, Canada, 732-741.

Kutay, E. M., M. Aydilek, E. Masad, and T. Harman, 2007, Evaluation of Hydraulic Conductivity Anisotropy in Asphalt Specimens. *International Journal of Pavement Engineering*, 8(1): 29-43.

CATEGORY M3: AGGREGATE SURFACE

Work Element M3a: Aggregate Surface Characterization (TAMU Year 1 start)

Progress This Quarter

This activity was pending the final selection of core aggregates that will be used by all consortium partners. We have generated a tentative list of these core aggregates and we are in the process of obtaining representative samples from their respective quarries.

Work Planned Next Quarter

A list of aggregate surface properties, such as mineral composition and specific surface area and corresponding test methods by which to measure these properties will be compiled. Measurement of selected properties will commence immediately upon the receipt of representative samples of aggregates selected for this project.

CATEGORY M4: MODELING

Work Element M4a: Micromechanics Model (TAMU)

Progress This Quarter

A detailed literature review was conducted and summarized in the previous quarterly report. This review was used as a basis for the development of a finite element model to simulate the loss of adhesive bonds in the presence of moisture at aggregate – binder interface with idealized geometry. The model is being developed in the commercial finite element package ABAQUS®. The finite element model relies on coupling moisture diffusion and fracture at adhesive interfaces to account for two deterioration processes: 1) degradation of the mastic properties due to the presence of moisture, and 2) deterioration of the aggregate-mastic interface as a function of moisture content (figure M4a.1). Other processes, such as fracture in the mastic and deterioration by mechanical loads, will be incorporated in the model in the future.

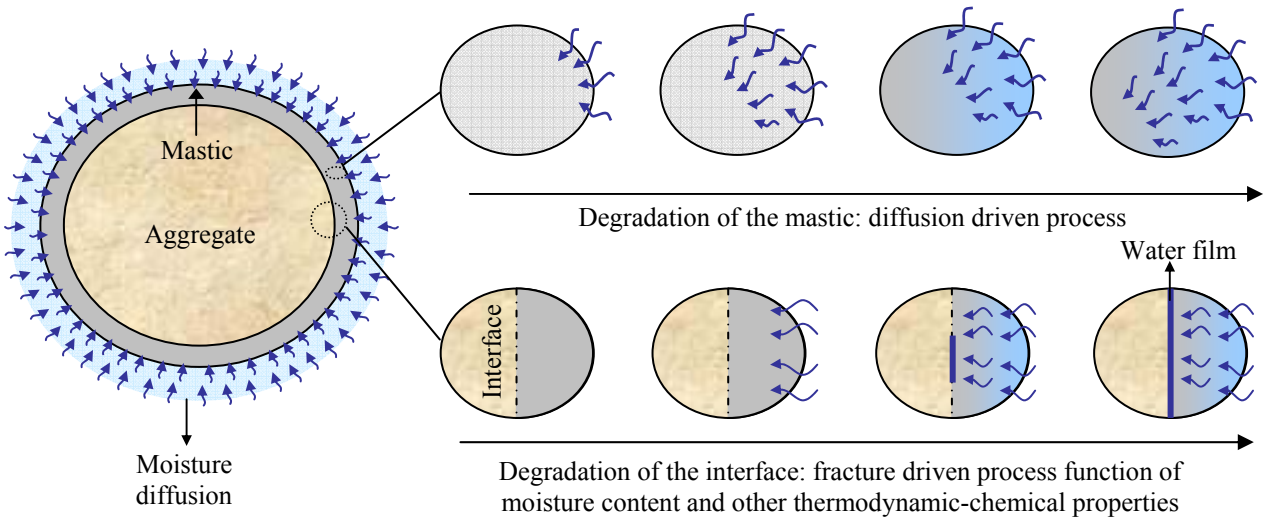

Figure M4a.1. Schematic of the moisture degradation processes considered in the model.

The aggregate-mastic interface is modeled using the cohesive zone elements of zero nominal thickness available in the ABAQUS® software. The constitutive behavior of these cohesive (or adhesive) elements is dictated by a traction-separation law, i.e. fracture nucleation at the interface occurs when the maximum traction capability of an element is overcome. The maximum traction capability is a function of the interface strength, which is in turn a function of moisture content. In addition, the fracture model accounts for the thermodynamic potential and is controlled by the absolute rate of hydrolysis reaction (displacement of interfacial bonds by the presence of water molecules) at the interface.

Work Planned Next Quarter

The plan for next quarter is to use the finite element model to conduct a parametric analysis on the influence of moisture diffusion, thermodynamic potential, and absolute rate of reaction on the rate of moisture damage at the asphalt-aggregate interface. We will also develop an experimental setup to measure the constitutive and fracture parameters of the asphalt-aggregate interface at different moisture contents. The experiments will rely on the pull-off test and peeling test. The two researchers working on this task will spend about one month (May 15 to June 15) at the University of Nottingham and adhesive group in Imperial College working on the development of the experimental setup.

Work Element M4b: Analytical Fatigue Model for Mixture Design (TAMU)

Progress This Quarter

No activity this quarter.

Work Planned Next Quarter

No work planned.

Work Element M4c: Unified Continuum Model (TAMU)

Progress This Quarter

No activity this quarter.

Work Planned Next Quarter

No work planned.

CATEGORY M5: MOISTURE DAMAGE PREDICTION SYSTEM (Later start TAMU, UWM, UNR, WRI, AAT)

Progress This Quarter

No activity this quarter.

Work Planned Next Quarter

No work planned.

PROGRAM AREA: FATIGUE

CATEGORY F1: MATERIAL AND MIXTURE PROPERTIES

Work Element F1a: Cohesive and Adhesive Properties

Subtask F1a-1: Critical Review of Measurement and Application of Cohesive and Adhesive Bond Strengths (TAMU Year 1 start)

Progress This Quarter

A detailed literature review was conducted with emphasis on the test and analytical methods to determine the practical work of cohesion for different binders and the work of adhesion between binders and standard surfaces. In this context, researchers from the Texas A&M University visited University of Nottingham and Imperial College in the United Kingdom as a part of the "Collaborating for Success through People" program sponsored by the United Kingdom. Researchers from the Imperial College, London, led by Dr. Kinloch, have pioneered the development of several industry standards that are used to determine the practical work of adhesion and cohesion for different polymeric adhesives. Drs. Little and Masad from Texas A&M University had a detailed discussion on the recently developed methodologies and experience related to the use of test methods to determine the practical work of adhesion and cohesion with Dr. Kinloch and his team.

Work Planned Next Quarter

The detailed literature review will be continued to address following areas relevant to the cohesive and adhesive bond strengths of materials:

i. Need for revision and/or improvement of existing methods to determine work of adhesion and cohesion for modified asphalt binders and recommendations for changes or improvements that may be required.
ii. Experimental and analytical methods to determine the work of cohesion or adhesion using mechanical tests, including approaches based on contact mechanics.
iii. Sources of differences between thermodynamic work of adhesion or cohesion and mechanical work of adhesion or cohesion, and methods to account for these differences.
iv. Acid-base scale to determine the surface free energy components of asphalt binders and aggregates and use of an alternate scale that may improve the sensitivity of the measured surface energy components and is consistent with the use of dissipated energy partitions applied to fracture mechanics and viscoplasticity.
v. Effect of oxidative aging on the surface free energy components of the asphalt binder.

Subtask F1a-2: Develop Experiment Design (TAMU Year 1 start)

Progress This Quarter

No activity this quarter.

Work Planned Next Quarter

A detailed experiment design to determine the practical work of adhesion and cohesion for different materials will be developed. The experiment design will be based on tests identified from the literature review in Task F1a-1 as well as the tests recommended by the research experts in this area from the Imperial College. In the first stage of the experiments limited materials will be used to determine the practical work of cohesion for different asphalt binders. After evaluating the test results, only one or two test methods will be screened and used to test a larger suite of materials.

Subtask F1a-3: Thermodynamic Work of Cohesion and Adhesion (TAMU Year 1 start)

Progress This Quarter

The objective of this subtask is to determine the surface energy properties of binders modified using active fillers, polymers, and other chemical additives. A protocol to prepare smooth surfaces of polymer modified binders for testing with the Wilhelmy plate device was developed. Essentially, the polymer is filtered out of the modified binder at high temperatures to enable specimen preparation. The basis for this specimen preparation methodology is that the physical chemistry of the binder will remain unaltered after the polymer has been blended in the binder. However, after this change has occurred the surface free energy of the binder phase can be determined independently without the physical presence of the polymer in the specimen. Note, that the objective of this exercise is to determine the effect of polymer addition to the intrinsic performance related thermodynamic properties of the binders. The researchers are cognizant of the fact that on a larger length scale the presence of polymers and the mechanical interaction between the two phases will also significantly effect the performance of the binder and mixture.

Work Planned Next Quarter

The plan for the next quarter is to continue the testing of select binders that were modified using polymers as well as active fillers.

Subtask F1a-4: Mechanical Work of Adhesion and Cohesion (TAMU)

Progress This Quarter

The test equipment required to conduct mechanical tests to determine the practical work of adhesion and cohesion was mobilized. Fixtures that allow testing of thin films of asphalt binder in tension using various configurations were obtained (eg. T-peel, Mandarin T-peel).

Work Planned Next Quarter

Following the experiment design developed in Subtask F1a-2, select asphalt binders will be tested to determine the practical work of cohesion for different film thickness.

Subtask F1a-5: Evaluate Acid-Base Scale for Surface Energy Calculations (TAMU)

Progress This Quarter

No activity this quarter.

Work Planned Next Quarter

No work planned.

Work Element F1b: Viscoelastic Properties (Year 1 start)

Subtask F1b-1: Separation of Nonlinear Viscoelastic Deformation from Fracture Energy under Cyclic Loading (TAMU)

Progress This Quarter

The objective of this subtask is to characterize fatigue damage in fine aggregate matrix specimens of asphalt by incorporating the nonlinear viscoelastic response of the material (table F1b-1.1).

Table F1b-1.1. Methodology to characterize fatigue damage by incorporating the non linear viscoelastic response of the material.

	Procedure	Purpose
Step 1	Identify the limiting stress or strain amplitude that generates nonlinear viscoelastic response without causing damage	This information will also be used to select a suitable magnitude of stress or strain amplitude for the specific material to ensure that incremental crack growth occurs with each consecutive cycle
Step 2	Model and monitor **the change in** the nonlinear viscoelastic **parameters with increasing number of load cycles** during the fatigue test	A change in the nonlinear viscoelastic parameters with increasing number of load cycles indicates accumulation of damage. Therefore, this change can be used to quantify the accumulated fatigue damage in the test specimen
Step 3	Model and monitor **the change in** the nonlinear viscoelastic **parameters within each cycle** during the fatigue test	A change in the nonlinear parameters within each cycle can be modeled and monitored to determine the type of damage that is being accumulated during the fatigue load test and also to accurately partition the dissipated energy due to damage versus nonlinear viscoelastic dissipated energy

In the previous quarter we reported progress on step 1 and 2 of this subtask. During this quarter we developed the model for step 3. As described in table F1b-1.1, a change in the viscoelastic response such as phase angle and damage within each cycle can be monitored using this approach. This model was derived by assigning a functional form to the non linear parameter g_2 in the following non linear model originally proposed by Schapery.

$$\varepsilon = g_0 D_0 \sigma + g_1 \int_0^t \hat{D}(t-\tau) \frac{\partial g_2 \sigma}{\partial t} d\tau \qquad \text{(F1b-1.1)}$$

where,g_0, g_1, and g_2 are non linear parameters, σ is the stress, ε is the strain, D represents the creep compliance parameters. The functional form for g_2 is dependent on two additional material properties α and β, as well as the magnitude of stress at any given time. Using this approach, it is possible to compute the change of the phase angle within each cycle due to the non linear behavior of the material as follows:

$$\frac{\varepsilon_0}{\sigma_0} \cos\delta_t = D_0 + \Delta g_1 \left\{ \hat{D}^*_\omega \cos\hat{\delta}_w + \alpha \sigma_0^\beta \hat{D}^*_{(1+\beta)\omega} \cos\left(\hat{\delta}_{(1+\beta)\omega} + \omega\beta t\right) \right\} \qquad \text{(F1b-1.2)}$$

$$\frac{\varepsilon_0}{\sigma_0} \sin\delta_t = \Delta g_1 \left\{ \hat{D}^*_\omega \sin\hat{\delta}_w + \alpha \sigma_0^\beta \hat{D}^*_{(1+\beta)\omega} \sin\left(\hat{\delta}_{(1+\beta)\omega} + \omega\beta t\right) \right\} \qquad \text{(F1b-1.3)}$$

where, δ_t is the phase angle at any time *t*, ε_0 is the strain amplitude, σ_0 is the stress amplitude, $\hat{D}^*_x$ is the linear dynamic compliance at frequency *x*, and $\hat{\delta}_x$ is the linear phase angle at frequency *x*, and ω is the frequency at which the material is being tested.

Work Planned Next Quarter

We are continuing to conduct tests on select materials to obtain data relevant to the analysis indicated in steps 1 through 3. The work planned for next quarter is to use the test data and verify and refine the model described above.

Subtask F1b-2: Separation of Nonlinear Viscoelastic Deformation from Fracture Energy under Repeated and Monotonic Loading (TAMU)

Progress This Quarter

No activity this quarter.

Work Planned Next Quarter

Same work planned as subtask F1b-1.

Work Element F1c: Aging

Subtask F1c-1: Critical Review of Binder Oxidative Aging and Its Impact on Mixtures (TAMU Year 1 start)

Progress This Quarter

Recent research has expanded knowledge of binder oxdiation kinetics and the impact of oxidation on binder physical properties, especially during the slower constant-rate oxidation period that follows the fast, but declining rate initial reaction period. Review of prior work conducted this quarter has been directed at comparing some of the early work on binder oxidation with the more recent work, for the purpose of understanding better the two reaction periods as a whole. Both reaction periods contribute to binder hardening but which is more significant over the long term depends on climate and oxygen availability to the binder (air voids), in addition to the reaction characteristics of the the specific binder, i.e., to the amount of oxidation that occurs during the fast rate period for a given asphalt (termed the initial jump in oxidation and hardening).

Also in this quarter, literature from previous TxDOT Projects 0-4468, "Evaluate the Fatigue Resistance of Rut Resistant Mixes" and 0-4688, "Development of a Long Term Durability Specification for Modified Asphalt" was gathered for review in terms of the different responses of different mixtures to aging measured in terms of fatigue life predicted by the calibrated mechanistic with surface energy (CMSE) approach.

Work Planned Next Quarter

The review of prior work is ongoing and will be used to determine appropriate experimental procedures, conditions, and materials as well as to provide background for the development of a transport model (Subtask F1c-3).

Subtask F1c-2: Develop Experimental Design (TAMU Year 1 start)

Progress This Quarter

In this quarter, experimental design commenced with consideration of the mixture parameters that may affect mixture response to binder oxidation and subsequent performance. These parameters include binder content, aggregate gradation, presence of additives such as lime, and the resulting air void distribution and binder film thickness. In addition, literature from previous TxDOT Projects 0-4468, "Evaluate the Fatigue Resistance of Rut Resistant Mixes" and 0-4688, "Development of a Long Term Durability Specification for Modified Asphalt" was gathered for review in terms of the mixtures tested in direct tension and evaluated in terms of fatigue life predicted by the calibrated mechanistic with surface energy (CMSE) approach. The initial discussion of the experiment design was coordinated with TxDOT Project 0-6009 "Evaluation of Binder Aging and its Influence in Aging of Hot Mix Asphalt Concrete" that starts in the next quarter.

Work Planned Next Quarter

The planned activity for the next quarter is to continue the experimental design, estimate quantities of component materials required, and begin material procurement. Interconnected air voids or those with access to oxygen and binder film thickness will be explored further as candidates for a key mixture parameter controlling mixture response to binder oxidation and subsequent performance.

Subtask F1c-3: Develop a Transport Model of Binder Oxidation in Pavements (TAMU Year 1 start)

Progress This Quarter

Work has proceeded towards developing a combined heat and mass diffusion transport model for reaction of binders in compacted mixtures and pavements. Issues are the relative importance of diffusion and reaction rates in the binder as well as the accessibility of oxygen to the binder from the porous structures of the mixtures. The model that is being developed is conceived to provide oxygen to the binder radially from pores that pass through the mixture. Complicating the model is the presence of aggregate that forces a tortuous path for the oxygen, thereby producing a reduced effective diffusivity. The extent to which diffusion resistance slows the oxidation process relates directly to the oxidation rate relative to the diffusion rate. The model is essential to guide the efficient and effective use of both laboratory and field mixture aging data for assessing the rate of binder hardening in pavements and its impact on pavement durability. The model is also relevant to Category F3, Modeling. The schematic for the binder oxidation transport model is shown in figure F1c.1.

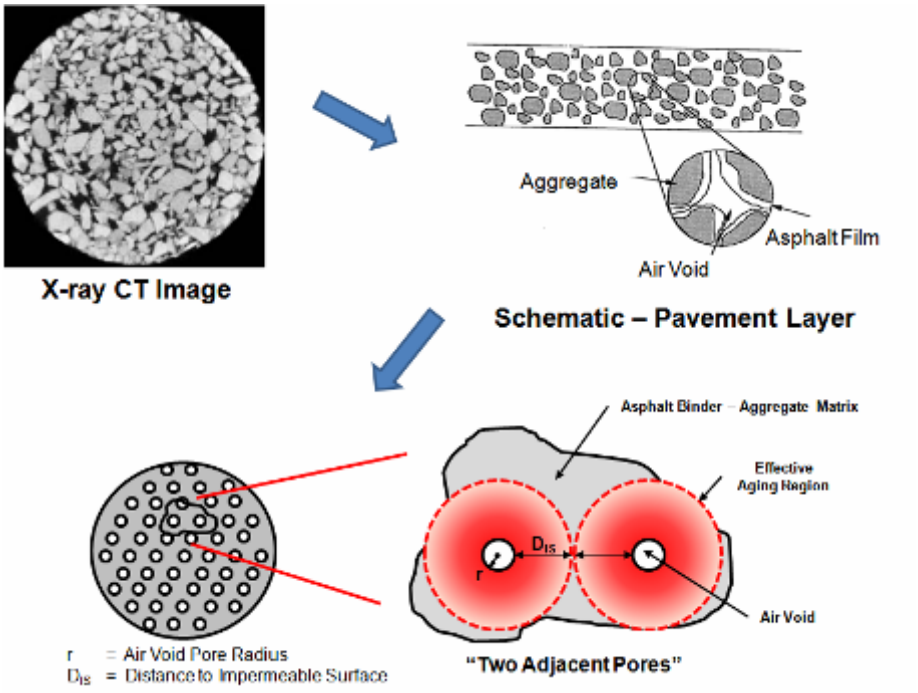

Figure F1c-3.1. Modeling concept for oxygen transport.

The pavement oxidation transport model is based on three interlinked processes: (1) diffusion of oxygen into the asphalt binder mastic in the pavement, (2) heat transfer into the pavement that results in temperature variations with depth and time, and (3) asphalt binder oxidation, which is a function of oxygen concentration and temperature in the binder. A fourth issue that affects the oxygen transport and concentration is the air voids distribution in the mixture because it affects the availability of oxygen to the binder. The diffusion process is coupled to both temperature and oxidation because both of these factors affect oxygen diffusivity. A quantitative model is further developed below.

A reaction and diffusion model accounting for O_2 in a differential volume is represented in equation F1c.1 in which the accumulation rate of oxygen at a point in the binder occurs because of oxygen diffusion to and from that point coupled with oxygen depletion because of the oxidation reaction.

$$\left(\frac{\partial C_{O_2}}{\partial t}\right) = -\nabla \cdot N_{O_2} - r_{O_2} \tag{F1c-3.1}$$

As can be expressed by Fick's first law of diffusion, the molar flux of oxygen, N_{O_2}, is given in equation F1c.2.

$$N_{O_2} = -\mathcal{D}_{O_2} \nabla C_{O_2} \tag{F1c-3.2}$$

Substituting into equation F1c.1 and allowing for $\mathcal{D}_{O_2}$ variations with temperature and oxidation over position gives Equation F1c.3.

$$\left(\frac{\partial C_{O_2}}{\partial t}\right) = \nabla \mathcal{D}_{O_2} \cdot \nabla C_{O_2} + \mathcal{D}_{O_2} \nabla^2 C_{O_2} - r_{O_2} \tag{F1c-3.3}$$

Assuming a Henry's law absorption of oxygen by the binder at low oxygen pressure, together with an ideal gas law conversion of pressure to concentration gives the oxygen concentration in the asphalt in terms of the oxygen pressure in the air

$$C_{O_2} = h\left(\frac{P_{O_2}}{RT}\right) \tag{F1c-3.4}$$

From a previous study by Lau et al. (1992) and Martin et al. (1990), it was discovered that the rate of oxygen depletion r_{O_2} is proportional to the rate of formation of carbonyl content, r_{CA} in the binder.

$$r_{O_2} = c\, r_{CA} \tag{F1c-3.5}$$

In a cylindrical coordinate system, Equation F1c.3 combined with Equations F1c.4 and F1c.5 leads to Equation F1c.6.

$$\frac{\partial P_{O_2}}{\partial t} = \frac{1}{r}\frac{\partial}{\partial r}\left(r\mathcal{D}_{O_2} \frac{\partial P_{O_2}}{\partial r} \right) - \left(\frac{cRT}{h} \right) r_{CA} \tag{F1c-3.6}$$

where r is the radial distance from air void-binder interface.

According to Reid et al. (1983), under isothermal conditions, the diffusivity of oxygen in liquids is dependent on the viscosity of the liquid according to Equation F1c.7.

$$\mathcal{D}_{O_2} = \mathcal{D}_0 \left(\eta_0^* \right)^B \tag{F1c-3.7}$$

For any specific asphalt, $\mathcal{D}_0$ and B are estimated constant parameters.

η_0^* is related to CA by hardening susceptibility (HS) and log-viscosity intercept (m).

$$\eta_0^* = \exp\{HS \cdot CA + m\} \tag{F1c-3.8}$$

HS and m are functions of temperature. CA represents the level of oxidation of the binder and increases at rate r_{CA} so that the amount of oxidation can be represented by

$$CA(t) = \int_0^t r_{CA} d\theta + CA_0 \tag{F1c-3.9}$$

The rate of carbonyl formation, r_{CA}, and thus of log viscosity, is a function of temperature (Lau et al. 1992) according to an Arrhenius relationship (Froment and Bischoff 1979).

$$r_{CA} = A \exp\left(\frac{-E_a}{RT} \right) \tag{F1c-3.10}$$

To obtain oxygen partial pressure profiles in the pavement model, the PDE system (equation F1c.6 together with boundary and initial conditions) is solved for the oxygen partial pressure as a function of time and distance away from air void-binder interface. In principle the oxygen partial pressure profile can be used to calculate CA and viscosity profiles and histories in the pavement, which then can be combined with an appropriate performance model to estimate pavement durability and performance, taking into account binder oxidative hardening.

Some initial calculations are shown in figure F1c-3.2. The binder used for these calculations is an Ampet AC-20 with the shell thickness of 1 mm, from radius of 0.5 – 1.5 mm, and was simulated to age at 333.3 K for 90 days. The inner surface (IS) refers to the air void-binder interface, whereas, the outer surface (OS) refers to the surface of the radius at the half distance between two adjacent air voids.

Also from the figure, carbonyl area and viscosity were predicted to increase with aging time while diffusivity decreased with aging time, which means the efficiency of oxygen diffusion is decreased over time.

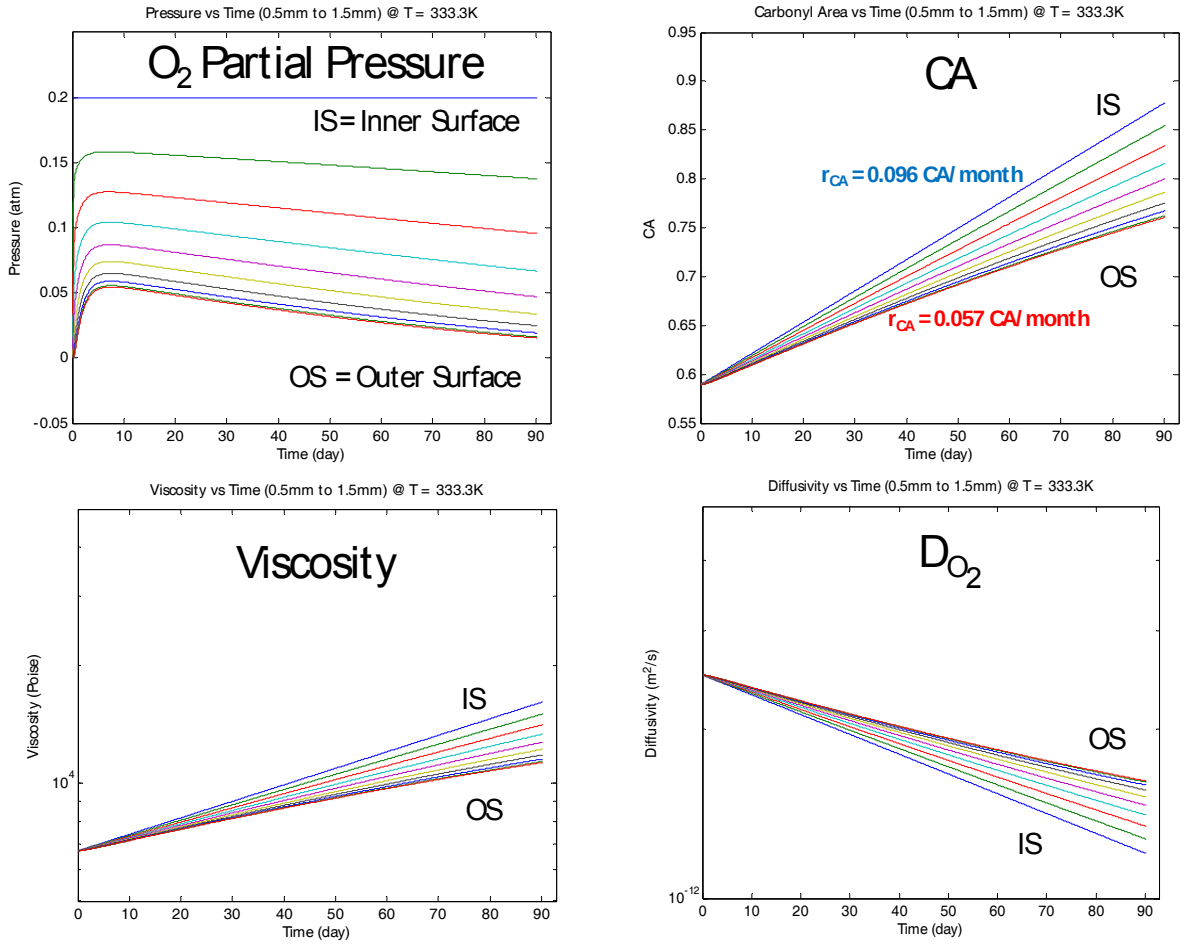

Figure F1c-3.2. Initial results from transport model of binder oxidation in pavements.

Work Planned Next Quarter

Work in the next quarter is expected to finish formulation of the basic transport model and then to use the model as a guide to designing field and laboratory experiments for the purpose of evaluating the impact of diffusion resistance on the oxidation rate of binders in pavements as a function of air voids, binder content, and other parameters.

A review of research work on the prediction of pavement temperature profiles will be conducted, and the presented methods and models will be studied and compared. Then an improved model will be developed to estimate the pavement temperature as a function of depth and time for the determination of binder oxidation rates in pavements, and for different pavement locations.

The methods and models to be reviewed fall into three types. The first type uses a heat transfer model, and it's based on a simplification that daily and annual pavement temperatures are sinusoidal functions of time with a surface periodic temperature boundary condition (Won Jun

2006). The resulting model yields an analytical solution of pavement temperature versus depth over time. The second approach also uses a heat transfer model, but assumes a surface flux boundary conditions and employs a finite different approximation to obtain a discrete solution; hourly temperature data are obtained (Ake Hermansson 2001; Ake Hermansson 2004; Manuel J. C. Minhoto et al. 2005; Jooseng Gavin Gui et al. 2007). The third type is a statistical model, the parameters of which are obtained using regression methods (Brian K. Diefenderfer et al. 2006; Peter J. Bosscher et al. 1998) to establish pavement maximum and minimum temperatures as a function of depth. Complete temperature profiles, however, are not obtained.

Based on comparison of these three types of models and their outputs with measured field data, we will develop an improved model designed expressly to provide temperature profiles suitable for calculating binder oxidative hardening as a function of time and depth in the pavement. The primary source of raw temperature data is the Long Term Pavement Performance (LTPP) database, which contains the temperature data of pavement in depth.

Subtask F1c-4: The Effects of Binder Aging on Mixture Viscoelastic, Fracture, and Permanent Deformation Properties (TAMU)

Progress This Quarter

No activity this quarter.

Work Planned Next Quarter

No work planned.

Subtask F1c-5: Polymer Modified Asphalt Materials

Progress This Quarter

No activity this quarter.

Work Planned Next Quarter

No work planned.

References for F1c

Ake Hermansson, 2001, Mathematical Model for Calculation of Pavement Temperatures Comparison of Calculated and Measured Temperatures. Transportation Research Record 1764, Paper No. 01-3543.

Ake Hermansson, 2004, Mathematical model for paved surface summer and winter temperature: comparison of calculated and measured temperatures. *Cold Regions Science and Technology*, 40.

Brian K. Diefenderfer, et al., February 2006, Model to Predict Pavement Temperature Profile: Development and Validation. *Journal of Transportation Engineering*, 162-167.

Fromont, G.F., and K.B. Bischoff, 1979, *Chemical Reactor Analysis and Design*, John Wiley and sons, New York, NY.

Jooseng Gavin Gui, et al., August 2007, Impact of Pavement Thermophysical Properties on Surface Temperatures. *Journal of Materials in Civil Engineering*, 683-690.

Lau, C. K., K. M. Lunsford, C. J. Glover, R. R. Davison, and J. A. Bullin, 1992, Reaction Rates and Hardening Susceptibilities as Determined from POV Aging of Asphalt. *Trans. Res. Rec*., 1342, 50.

Manuel J. C. Minhoto, et al., 2005, Predicting Asphalt Pavement Temperature with a Three-Dimensional Finite Element Method. Transportation Research Record: *Journal of the Transportation Research Board, No. 1919*, Transportation Research Board of the National Academies, Washington, D.C., 96–110.

Martin, K. L., C. J. Glover, R. R. Davison, and J. A. Bullin, 1990, Asphalt Aging in Texas Roads and Test Sections. *Trans. Res. Rec*., 1269, 9.

Peter J. Bosscher, et al., 1998, Relationship between Pavement Temperature and Weather Data: Wisconsin Field Study to Verify Superpave Algorithm, Transportation Research Record 1609, Paper No. 98-0944.

Reid, R. C., J. M. Prausnitz, and T. K. Sherwood, 1983, *The Properties of Gases and Liquids*, McGraw-Hill, 4th, ed., New York, NY.

Won Jun Woo, et al., November 2006, Polymer Modified Asphalt Durability in Pavements, Chapter 5, Report No. FHWA/TX-07/0-4688-1.

Work Element F1d: Healing

Subtask F1d-1: Critically Review Previous Work on Healing under FHWA Contracts DTFH61-C-92-00170 and DTFH61-C-99-00022 (TAMU Year 1 start)

Progress This Quarter

During the last quarter a detailed literature review was conducted to synthesize the state of the art in understanding and characterization of the healing mechanism in asphalt materials. A summary of this review was also presented in the last quarterly report. The review was continued in this quarter with emphasis on areas other than bituminous materials. An important finding from this review was the use of a DSR type test method to determine the interfacial diffusion properties of polymer like materials. This is further discussed in Subtask F1d-4.

Work Planned Next Quarter

Researchers will continue the literature review in the area of healing with emphasis on areas other than bituminous materials.

Subtask F1d-2: Select Materials with Targeted Properties (TAMU Year 1 start)

Progress This Quarter

The use of molecular modeling techniques was investigated to identify key material properties that govern the healing process in asphalt binders. Molecular modeling has two benefits; i) it allows the researchers to determine intrinsic material properties that significantly affect the healing process thus enabling a more targeted selection of materials for further tests and experiments, and ii) it allows the verification of the hypothesis for healing mechanism which is the basis of analytical modeling. A brief summary of the progress from this modeling effort is presented here.

The molecular modeling was conducted using a software developed by Accelrys. The general procedure for molecular modeling is as follows. An amorphous cell is constructed using constituent molecules to achieve a target density. The molecules within the cell have an amorphous form and the cell itself can be considered as a representative volume element (RVE) that repeats itself in three dimensions. Each atom in the amorphous cell is assigned a force field that is unique to the atom and depends on the element, location of the atom within the molecule, neighboring atoms, and neighboring bonds. The total energy of the amorphous cell is minimized using molecular dynamics. An artificial surface or thin film of the material is created by padding the amorphous cell with a layer of vacuum, followed by energy minimization processes as before. The surface energy of the material can then be estimated as follows (Prathab et al. 2007):

$$\gamma = \frac{E_{thin\ film} - E_{amorphous\ cell}}{2A} \qquad \text{(F1d-2.1)}$$

where, A is the surface area of the cell.

During the initial stages of this study, two approaches were adopted to determine the surface and self diffusion properties of different asphalt binders. In the first approach, the average molecular structure for two asphalt binders AAM and AAD was used to create the amorphous cell. The average molecular structure was obtained from pervious NMR studies on these materials (Jennings et al. 1999). Figure F1d-2.1 illustrates the average molecular structure for AAM and AAD used for this analysis.

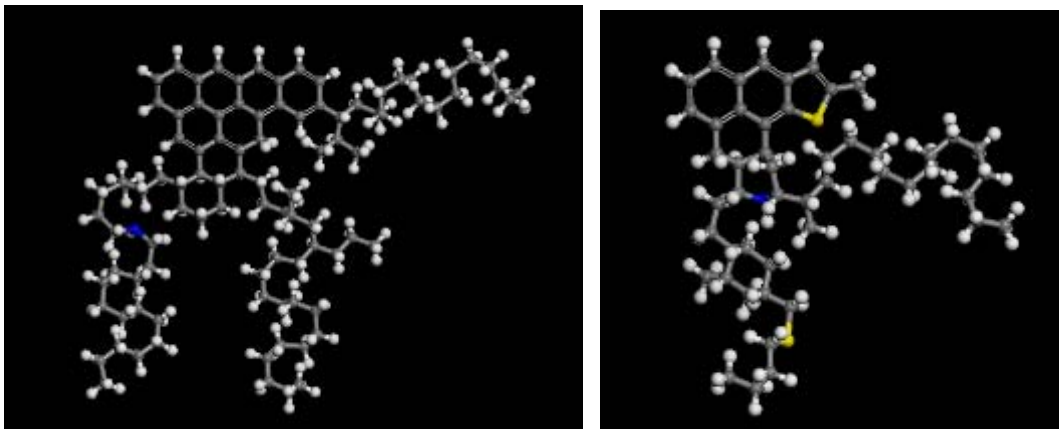

Figure F1d-2.1. Average molecular structure for AAM (left) and AAD (right).

Using the approach described above, the surface energy for AAM and AAD was computed to be 91 ergs/cm^2 and 61 ergs/cm^2, respectively. The measured surface energy values for these two materials using the Wilhelmy plate test method is 50 ergs/cm^2 and 38 ergs/cm^2, respectively. The order of magnitude and relative values for these two materials obtained using molecular modeling as compared to the measured values are encouraging. Since average molecules do not accurately reflect certain properties of interest, an alternative second approach was used. In this approach, an ensemble of representative molecules of asphaltene, napthenes, and saturates were used in a proportion representative of a typical asphalt binder. Figure F1d-2.2 illustrates the the representative structures of the napthene, saturate, and asphaltene (Greenfield 2006), and figure F1d-2.3 illustrates an amorphous cell constructed using these three molecules. The surface energy of this hypothetical asphalt binder was computed to be 81 ergs/cm^2. We are currently refining the protocols used with molecular modeling to obtain better estimate of these properties. Furthermore, we are using a similar approach to determine the rate of healing between thin films of these cells.

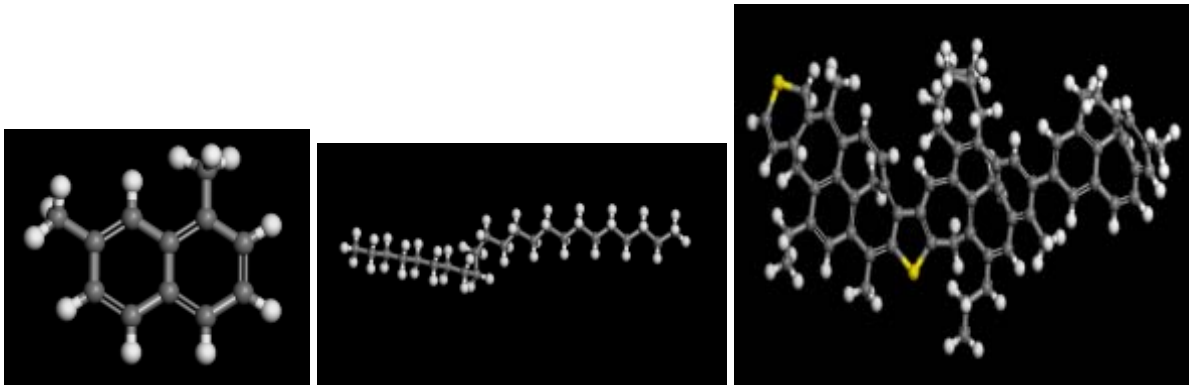

Figure F1d-2.2. Strcutures for the representative molecules of napthene, saturate, and asphaltene components (left to right).

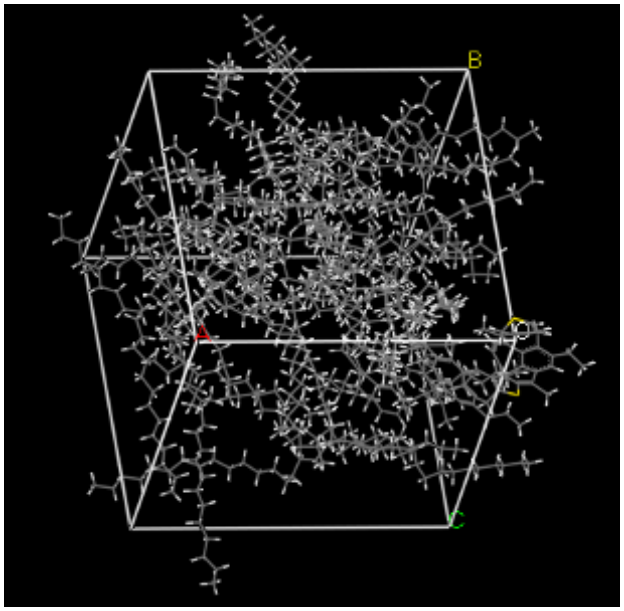

Figure F1d-2.3. Amorphous cell using the three consituent molecules.

Work Planned Next Quarter

We will conduct a parametric analysis using the hypothetical asphalt binder to determine the constituent properties that have the most significant impact on the healing rate. For example, Kim et al. (1990) used a combination of mechanical tests and spectroscopic techniques to demonstrate that asphalt binders with longer chain lengths and less branching will have faster healing rates. This hypothesis can easily be validated or refined by conducting a parametric analysis using molecular modeling techniques. In addition, materials selected for other areas of work will be tested for their healing related properties such as surface free energy and intrinsic healing function using the newly developed DSR test method (reported in Subtask F1d-4 of previous quarter).

Subtask F1d-3: Develop Experiment Design (TAMU Year 1 start)

Progress This Quarter

No activity this quarter.

Work Planned Next Quarter

The literature review conducted in subtask F1d-1 and the material properties measured in subtask F1d-3 will be used to develop a detailed experiment design for this work element.

Subtask F1d-4: Investigate Test Methods to Determine Material Properties Relevant to Asphalt Binder Healing

Progress This Quarter

In the previous quarter a simple test method based on the use of a DSR was developed to determine the intrinsic healing function of the asphalt binder. Continued literature review in this area revealed that a similar test method can be used with a different analytical approach to determine the self diffusion properties of the asphalt binder, which are also related to healing. For example, Qiu and Bousmina (1999) used a similar technique with a diffusion model to determine the diffusion at the interface of different polymers. More recently, Karlsson (2007) used a similar approach to characterize the diffusion between different types of asphalt binders with reference to the use of recycled aggregates that have a residual binder coating.

Work Planned Next Quarter

We will apply the test data from the DSR based test method with the analytical approach described above to determine self diffusion properties for different asphalt binders.

Subtask F1d-5: Testing of Materials (TAMU)

Progress This Quarter

Testing of different asphalt binders using the DSR was continued in this quarter.

Work Planned Next Quarter

We plan to continue testing of different asphalt binders using the DSR to obtain the intrinsic healing function as well as measurement of surface energy for the selected materials.

Subtask F1d-6: Evaluate Relationship Between Healing and Endurance Limit of Asphalt Binders (UWM Year 1 start)

Task Lead: Carl M. Johnson

Progress This Quarter

During this quarter, the research was focused on two main tasks: critical literature review of test methods to quantify healing, and evaluation of the applicability of the test methods uncovered during the literature review to binder healing characterization.

Literature Review

The ultimate fatigue performance of a pavement relies on many factors, but the two that this study will focus on is the ability of asphalt binder to both resist damage from occurring, and also heal the damage that has already occurred. Fatigue performance of asphalt mixtures has been

widely tested in the lab, but binder fatigue characterization is still in progress. This section will discuss two concepts that have been applied to mixtures, and how they can be applied to binder testing.

1. Sinusoidal Cyclic Loading with the Inclusion of Rest Periods (RP's)

Typical fatigue testing, also known as time sweep testing, is performed by applying sinusoidal cyclic loading at a given frequency and controlled level for either a specified amount of time or specified level of achieved damage (e.g. 50% loss of G*, max phase angle). The healing qualities of the material are typically measured by comparing the differences of the measured material properties between standard time sweep tests and those that have had rest periods introduced into them. It has been clearly shown that RP's increase the number of cycles that a sample can withstand before reaching its predetermined failure criterion. Below are two examples of this method:

a) TTI's Method (Kim et al. 2003)

A standard strain-controlled time sweep is applied to the material until failure, in this case δ_{max}. Another time sweep test is then run with the addition of multiple RP's of predetermined duration spaced at equal intervals. The length of the interval depends on the ability of the material to withstand damage; weaker materials will be assigned shorter intervals in order to recover some of the accumulated damage. An example of these tests is shown in figure F1d-6.1.

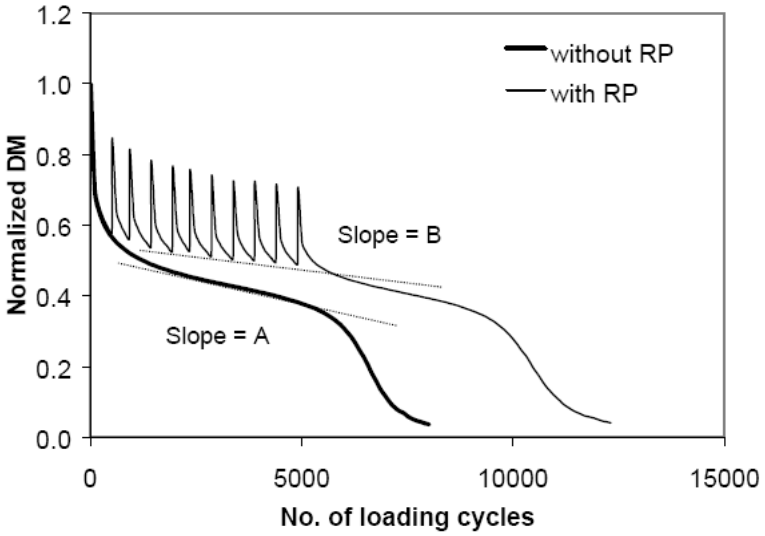

Figure F1d-6.1. Chart. Effect of microdamage healing due to rest periods (from Kim et al. 2003).

The quantification of the material's healing index is then calculated using a parameter known as the Healing Potential Index (*HPI*):

$$HPI = \frac{A - B}{A} \quad (1)$$

Where *A* and *B* equal the absolute value of the slope representing microcracking speed (shown in figure F1d-6.1) with and without rest periods, respectively.

Performing this analysis method requires time sweep testing with and without rest periods. It also requires a predetermined failure criterion and a systematic way of determining rest period interval spacing.

b) Baglieri's Method (Baglieri 2007)

Similar to the previous method, Baglieri's method involves measuring the comparison between time sweep tests with and without rest periods. However, the basis for comparison lies within measuring the Dissipated Energy Ratio (*DER*) over the course of the time sweep test. A standard stress-controlled time sweep is run in this case, and the *DER* is plotted for the duration of the test. Then, depending on the amount of damage in the specimen that the healing properties of the material are to be evaluated for, one RP is inserted into the time sweep at the desired level of damage (e.g., DER_{max}, 75% DER_{max}, 50% DER_{max}). The duration of this RP is equal to three times the duration of the time sweep test up until introduced RP, measured from the precious time sweep with no RP's. The test then resumes until the predetermined failure criterion is reached.

The Healing Index (*HI*) is calculated as follows:

$$HI = \left| \frac{W_{\mathrm{Re}load} - W_{Load}}{W_{Load}} \right| \quad (2)$$

Where W_{Load} is the dissipated energy per cycle at the end of the loading phase and W_{Reload} is the dissipated energy per cycle at the first cycle of the reloading phase.

Performing this analysis method requires time sweep testing with and without rest periods. It also requires a predetermined failure criterion, but the duration of the RP is determined as described above. The point at which the RP is introduced must be predetermined.

2. Repeated Haversine Loading

This method of fatigue and healing testing is derived from the method of determining resilient modulus of asphalt mixtures using the Superpave Indirect Tension test (IDT). Typically, a 0.1 second loading pulse is applied to the material, followed by a rest period of 0.9 seconds in order to simulate the action of traffic on a pavement. As the number of loading pulses increases, the internal structure of the material begins to accumulate damage and the specimen becomes unable to withstand additional loading. The testing can either be run to a specified number of cycles, or until a failure criterion is reached (e.g. 50% loss in dynamic modulus). The RP's are introduced

either directly after the loading pulses by controlling the length of the repeated RP's, or after a certain number of loading cycles with standardized RP's during each cycle. An example of each is shown below:

a) Carpenter's Method (Carpenter and Shen 2006)

Rest periods using this method are controlled by adjusting the length of the RP directly after the pulse. Typically, a 0.9 sec rest period is applied after each 0.1 sec loading pulse; by changing the length of the RP, the material has more opportunity to heal accumulated damage.

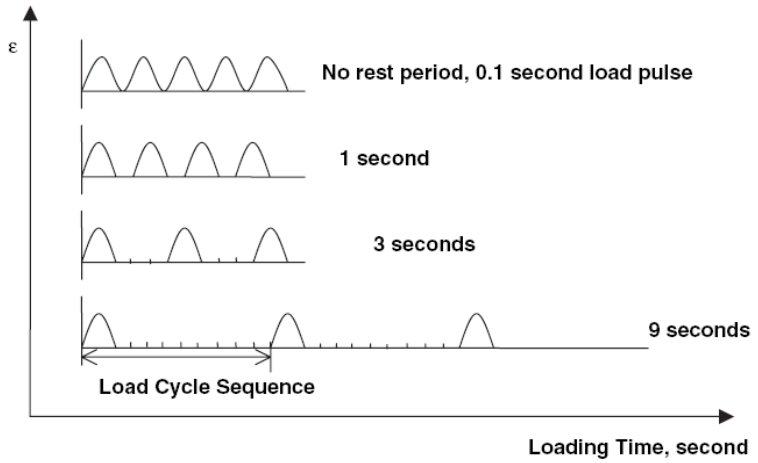

Figure F1d-6.2. Chart. Haversine load pulse sequence of fatigue-healing test (from Carpenter and Shen 2006).

By measuring number of cycles until failure (typically defined as 50% loss in stiffness) for each RP duration, a characteristic curve can be developed. This curve can be used to predict the duration of the RP needed to reach a predetermined number of cycles to failure; this idea can be extrapolated to the idea of a pavement's fatigue endurance limit. By lowering the strain level of the loading pulse, the duration of the RP needed to achieve the predetermined number of cycles to failure shortens. Once this duration reaches a level that is applicable to a desired traffic loading, the material can be engineered to perform within the expected loading levels, i.e., pavement layer thicknesses can be calculated such that the asphalt concrete experiences strain levels at or below the material's fatigue endurance limit.

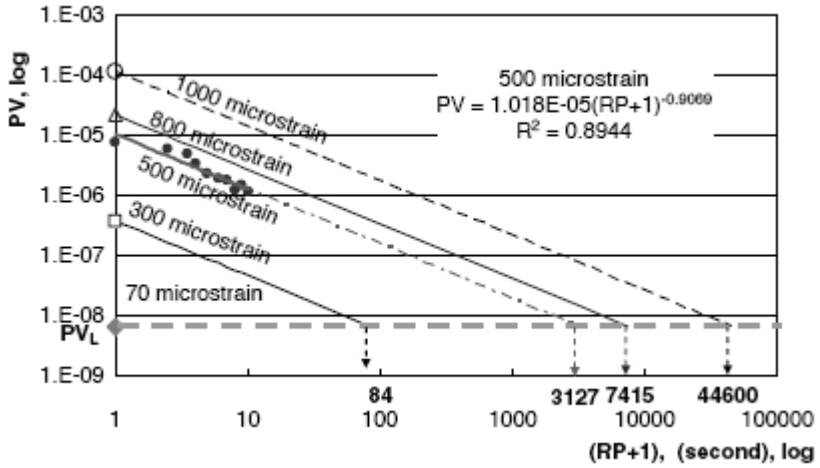

Figure F1d-6.3. Chart. Plot of PV versus Rest Period Duration + 1 (PV is a parameter derived from the inverse of N_f); (From Carpenter and Shen 2006).

This method requires the ability to test using haversine loading with the ability to adjust the duration between load pulses. The number of cycles to failure can be plotted against the duration of the RP's in order to evaluate the material's healing potential.

b) Roque's Method (Roque 2006)

This method uses the procedure set forth in AASHTO TP 31-94 to determine resilient modulus as its basis. In other words, the repeated haversine loading is standardized at 0.1 sec of loading with 0.9 sec of rest. Healing is evaluated by interrupting the loading cycles to include RP's of varying durations, then comparing the level of damage in the material before and after RP's. Damage is accounted for by measuring the deformation in the specimen against the number of loading cycles.

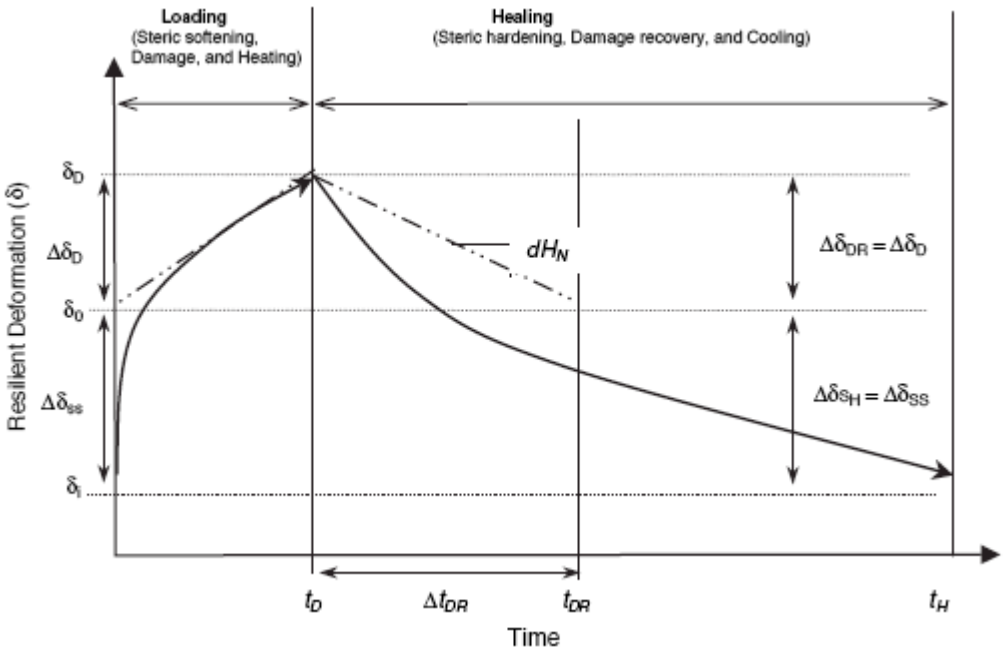

Figure F1d-6.4. Chart. Resilient deformations during loading and healing (From Roque 2006).

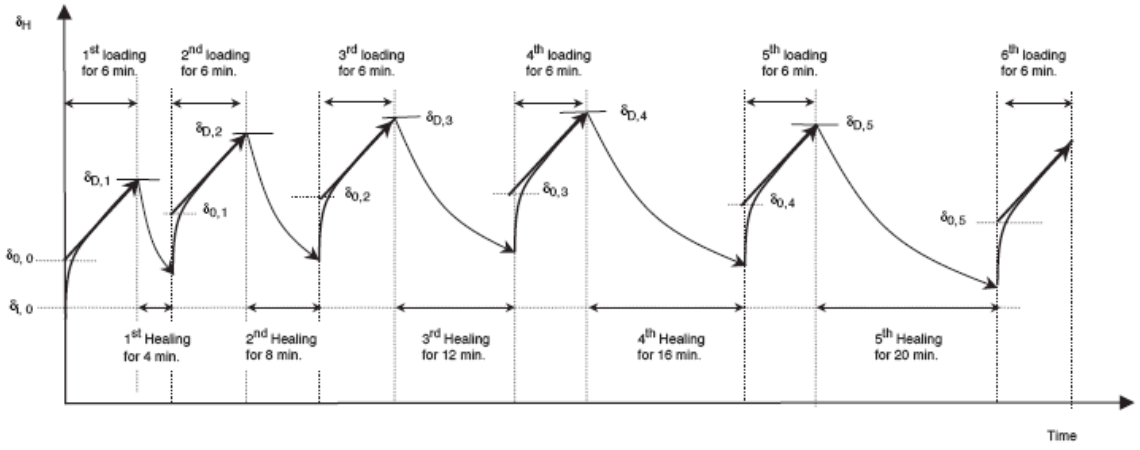

Figure F1d-6.5. Chart. Concept of repeated loads for determining damage recovery rate (from Roque 2006).

From Roque (2006), the healing characteristics are calculated as follows using the parameters shown in figures F1d-6.4 and F1d-6.5:

Net normalized damage:

$$(D_{NN,i}) = (\delta_{D,i} - \delta_{0,i-1})/\delta_{0,i-1} \qquad i = 1 \sim 5$$

Normalized damage:

$$(D_{N,i}) = D_{NN,i} + D_{NR,i-1} \qquad i = 1 \sim 5, D_{NR,0} = 0$$

Remaining normalized damage:

$$(D_{NR,i}) = D_{N,i} - H_{N,i} \qquad i = 1 \sim 5$$

Normalized damage recovery:

$$(H_{N,i}) = (\delta_{D,i} - \delta_{0,i})/\delta_{0,i-1} \qquad i = 1 \sim 5$$

Relative damage recovery:

$$H_{N,i}/D_{N,i} \qquad i = 1 \sim 5$$

With the relative damage recovery plotted with rest periods, the rate of normalized damage recovery (dH_N) was determined as the slope of a linear regression curve. Time to the full recovery of damage (Δt_{DR}) was then calculated by extrapolation of the regression curve (figure F1d-6.4).

To complete this analysis, haversine loading needs to be applied to the specimen at the standard 0.1 sec loading with 0.9 sec of rest per loading cycles. Testing can then be suspended at predetermined intervals in order to allow the specimen to heal, at which point the material's healing characteristics can be evaluated.

Laboratory Testing Evaluation

Interrupted cyclic fatigue testing was started during this quarter, as it is easy to implement with existing DSR controller software. A standard time sweep protocol was modified to include rest periods at controlled intervals. For the preliminary research, a neat PG 64-22 PAV-aged binder was used to evaluate the testing protocol. The 8-mm parallel plate geometry was used, and the sample was subjected to strain-controlled loading (3% peak strain for the example shown below) at 10 Hz and 25 °C. The temperature was chosen as a compromise to represent the higher limit of the intermediate temperatures typically associated with fatigue, with higher temperatures typically being perceived as more conducive to healing behavior. Three different types of tests were performed: a "control" time sweep test consisting of repeated cyclic loading without any rest periods (RP's); a time sweep test with ten equally-spaced five-minute RP's beginning at the number of cycles corresponding to a 10% reduction in complex shear modulus from the control

test, with subsequent RP's occurring at each point corresponding to a 5% reduction in shear modulus from the control test; and a time sweep test with one 50-minute rest period corresponding to the number of cycles at which the 10th RP occurred during the previous 10-RP test procedure. This procedure was selected to both evaluate the effect of rest periods on the stiffness reduction over the course of time sweep testing, as well as the effect of specimen damage level on the material's healing potential. The results from the test are shown in figure F1d-6.6.

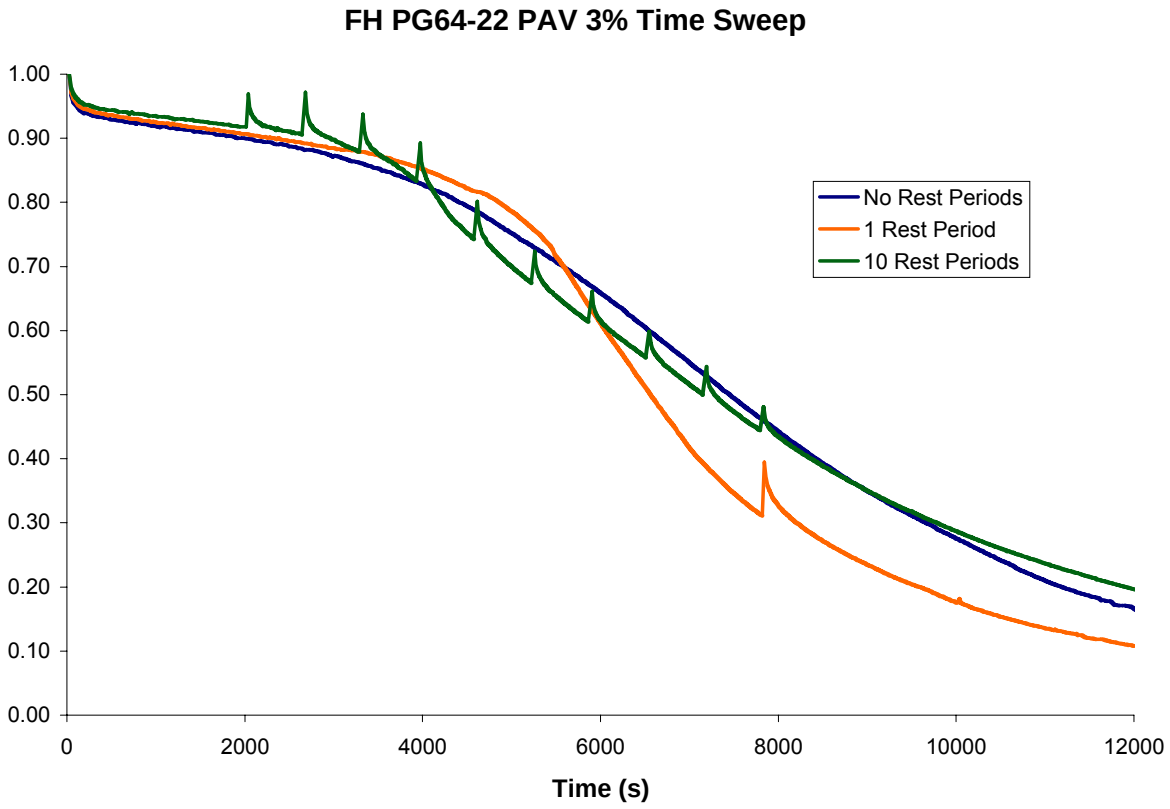

Figure F1d-6.6. Chart. Results from time sweep testing with and without RP's.

As has been shown in other studies on asphalt healing, the curves appear to follow an asymptotic behavior regardless of the number of rest periods (or lack thereof). The first 20,000 cycles show a consistent modulus loss behavior for each test, but specimen variability appears to take control of the test past that point. However, this is only one binder sample, and the effect of polymer modification has yet to be established.

Regardless of the shape of the curves shown in the above plot, the healing potential does present itself by viewing the hysteresis loops produced from cyclic loading. Both the angle of the major axis of the loops as well the area contained within them are significant indicators to energy dissipation characteristics of the material. Figures F1d-6.7 and F1d-6.8 show the hysteresis behavior for the time sweep tests with 1 RP and 10 RP's, respectively.

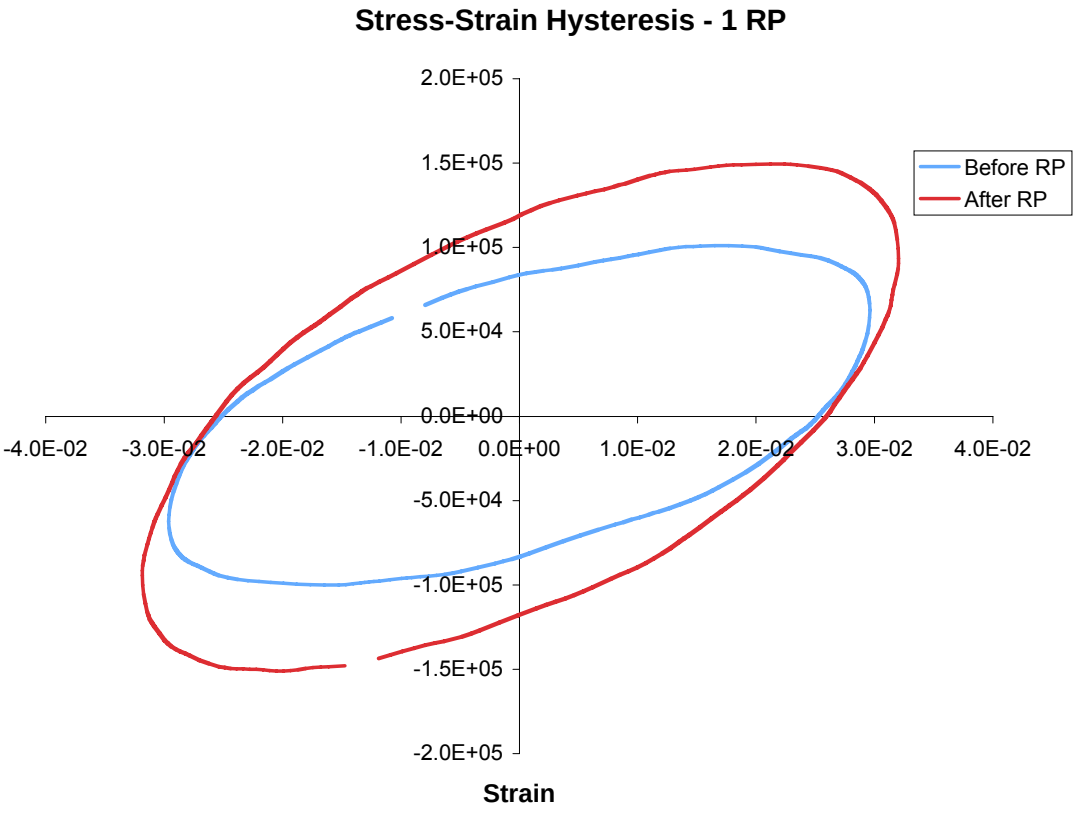

Figure F1d-6.7. Chart. Stress-strain hysteresis of the time sweep test with 1 RP.

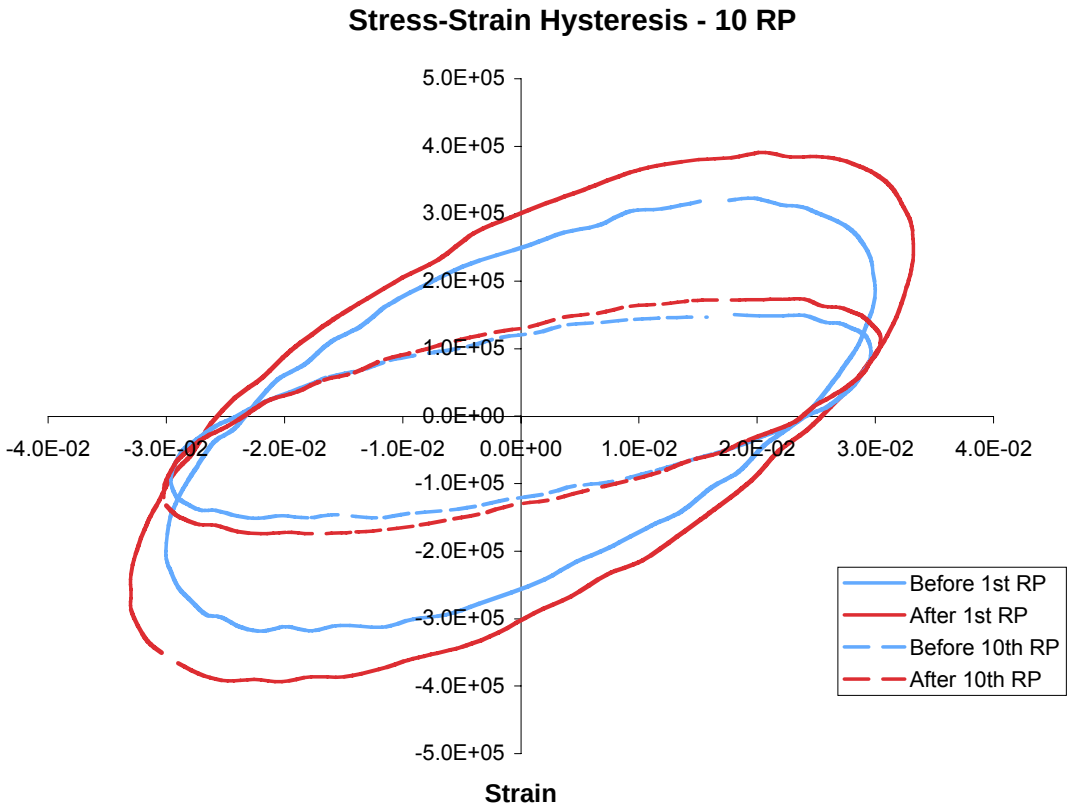

Figure F1d-6.8. Chart. Stress-strain hysteresis of the time sweep test with 10 RP's.

Table F1d-6.1. Dissipated energy at selected cycles.

Test Conditions		W_i [Pa]	% Increase
10 RP's	Before 1st RP	23,093	
	After 1st RP	31,209	35.14%
	Before 10th RP	11,084	
	After 10th RP	12,553	13.25%
1 RP	Before RP	7,645	
	After RP	11,868	55.24%

Both the plots and table show from preliminary results that the healing potential of asphalt binders is indeed dependent upon both the level of damage in the specimen as well as the duration of the testing time. This appear to be intuitive, but it stresses the fact that traffic level (corresponding to rest period duration), pavement structure (corresponding to level of damage), and binder fatigue performance could all play an important role in the determination of endurance limits for asphalt pavements.

Work Planned Next Quarter

Further evaluation of different binders will continue for the test procedure shown above. Once the trends and characteristics of interrupted cyclic become apparent, the other healing test protocols outlined in the literature review will be evaluated for their applicability to binder testing. This may involve modification of existing test protocols in the DSR, but the translation of mixture testing protocols to binder testing may require new protocols to be developed. For example, haversine loading is not typically included in most DSR controller software. A surrogate method may need to be developed to create a corollary to haversine mixture loading.

References

Baglieri, O., 2007, Preliminary investigation on healing of bituminous binders, *Internal Report*, *UW-Madison*.

Carpenter, S. H., and S. Shen, 2006, A Dissipated Energy Approach to Study HMA Healing in Fatigue. 85th Annual Meeting of the Transportation Research Board, Washington D.C.

Kim, Y. R., D. N. Little, and R. L. Lytton, 2003, Fatigue and Healing Characterization of Asphalt Mixes. *Journal of Materials in Civil Engineering (ASCE)*, 15: 75-83.

Kim, B., and R. Roque, Evaluation of Healing Property of Asphalt Mixture. 85th Annual Meeting of the Transportation Research Board, Washington, D.C.

Subtask F1d-7: Coordinate with Atomic Force Microscopic (AFM) Analysis. (WRI Year 2 start)

Progress This Quarter

No activity this quarter.

Work Planned Next Quarter

No work planned next quarter.

Subtask F1d-8: Coordinate Form of Healing Parameter with Micromechanics and Continuum Damage Models. (TAMU)

Progress This Quarter

No activity this quarter.

Work Planned Next Quarter

In the previous quarter we developed a framework to model the healing phenomenon with explicit relationships for the wetting and intrinsic healing function and a test method to

determine parameters for the latter. In the next quarter we will focus on development of test and/or analytical methods to determine the two remaining unknowns for this model, the wetting length and bond stresses.

References for F1d

Jennings, P. W., J. A. Pribanic, M. A. Desando, and M. F. Raub, 1993, *Binder Characterization and Evaluation by Nuclear Magnetic Resonance Spectroscopy*. *SHRP-A-355*, Strategic Highway Research Program, National Research Council, Washington, DC.

Little, D. N., and A. Bhasin, 2006, Using Surface Energy Measurements to Select Materials for Asphalt Pavement. *Final Report for Project 9-37*, Texas Transportation Institute, Texas.

Greenfield, M. L., 2006, Modeling for Nanoengineering: Molecular Simulation of Asphalt-like Materials. Presented at NSF Workshop on Nanomodification of Cementitious Materials.

Prathab, B., V. Subramanian, and T. M. Aminabhavi, 2007, Computation of surface energy and surface segregation phenomena of perfluorinated copolymers and blends - A molecular modeling approach. *Polymer*, 48(1): 417-424.

Kim, Y. R., D. N. Little, and F. C. Benson, 1990, Chemical and Mechanical Evaluation on Healing Mechanism of Asphalt Concrete. *Proc.*, Association of Asphalt Paving Technologists, 59, 240275.

Qiu, H., and M. Bousmina, 1999, New technique allowing the quantification of diffusion at polymer/polymer interfaces using rheological analysis: Theoretical and experimental results. *Journal of Rheology*, 43(3): 551-568.

Karlsson, R., U. Isacsson, and J. Ekblad, 2007, Rheological Characterisation of Bitumen Diffusion. *Journal of Materials Science*, 42: 101-108.

Subtask F1d-9: Design Experiment on Selected Binders with Synchrotron (TAMU)

Progress This Quarter

No activity this quarter.

Work Planned Next Quarter

No work planned.

CATEGORY F2: TEST METHOD DEVELOPMENT

Work Element F2a: Binder Tests and Effect of Composition

Subtask F2a-1: Analyze Existing Fatigue Data on Polymer Modified Asphalts (UWM Year 1 start)
Subtask F2a-2: Select Virgin Binders and Modifiers and Prepare Modified Binder (UWM Year 1 start)
Subtask F2a-3: Subject Samples of Virgin and Modified Binder to Several Laboratory Aging Procedures. (UWM)
Subtask F2a-4: Collect Fatigue Test Data for All Samples (UWM)
Subtask F2a-5: Analyze Data and Propose Mechanisms by which Aging and Modification Influence Fatigue of Binders (UWM)

Note: These subtasks will be reported together.

Task Lead: Codrin Daranga

Progress This Quarter

Three binders (one neat, one SBS modified and one Elvaloy® modified) were treated with polyphosphoric acid (PPA). The effect of PPA modification was then studied on storage time and presence of mineral filler. Notable results are as follows:

The starting materials are shown below:

- A1 PG 70-22 SBS Modified;
- A5 PG 58-22 Neat;
- B9 PG 64-28 Elvaloy Modified;
- X 115 PPA (polyphosphoric acid);
- Y 105 PPA;
- Z 85 OPA (ortho-phosphoric acid).

Table F2a.1 summarizes the PG properties for the starting asphalt binders included in this study. Note that the polymer modified binders were acquired already modified with unknown concentrations of the respective polymer modifiers.

Table F2a.1: PG grading of starting materials.

	A1 SBS PG 70-22		c.v.%	A5 Neat PG 58-22		c.v.%	B9 Elvaloy PG64-28		c.v.%
Original									
G*/sinδ (kPa)	@70°C	1.26	1.61	@58°C	1.12	1.66	@64°C	1.22	1.23
True Grade (°C)	**@1.00 kPa**	**72.5**		**@1.00 kPa**	**59.5**		**@1.00 kPa**	**66.3**	
RTFO									
G*/sinδ (kPa)	@70°C	2.43	0.20	@58°C	2.44	0.24	@64°C	2.76	0.77
True Grade	**@2.20 kPa**	**71.2**		**@2.20 kPa**	**58.9**		**@2.20 kPa**	**66.6**	
PAV									
G*·sinδ (kPa)	@13°C	4939	6.64	@16°C	3831	3.70	@07°C	4161	7.03
True Grade	**@5000 kPa**	**12.4**		**@5000 kPa**	**13.6**		**@5000 kPa**	**5.4**	
Stiffness (MPa)	@-18°C	267.0	2.12	@-18°C	273.3	10.76	@-24°C	258.3	6.45
True Grade	**@300MPa**	**-29.9**		**@300MPa**	**-29.4**		**@300MPa**	**-29.6**	
m-value	@-12°C	0.358	0.40	@-12°C	0.369	7.26	@-24°C	0.310	0.46
True Grade	**@0.300**	**-26.8**		**@0.300**	**-27.8**		**@0.300**	**-28.0**	
TEMP RANGE	**98.0**			**86.7**			**94.3**		

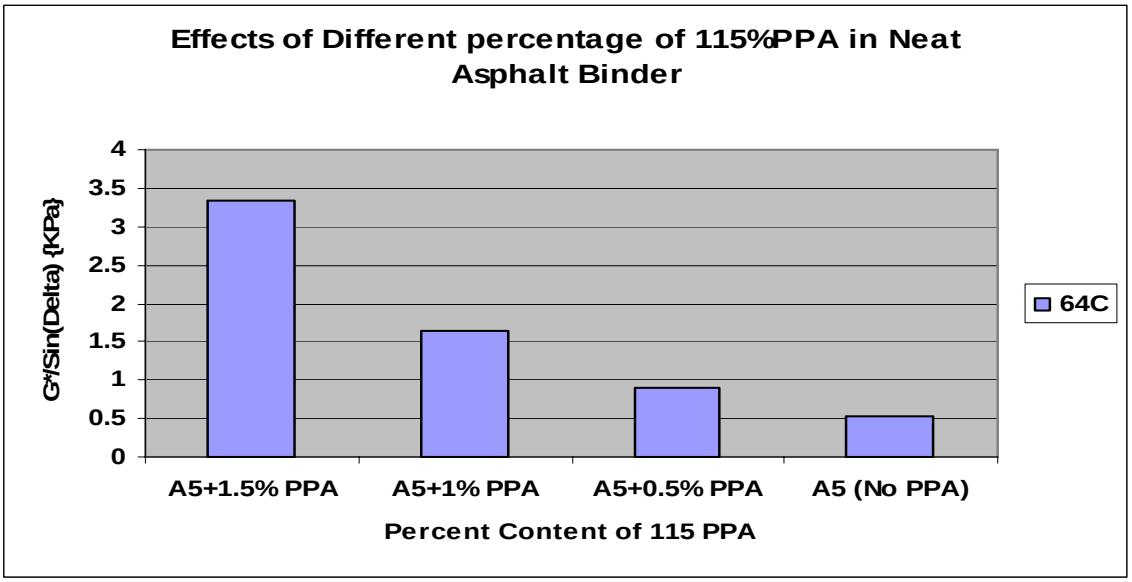

Figure F2a.1. Chart. Effect of PPA concentration on neat asphalt binder.

A small percentage of PPA (between 0.5 and 1%wt) raises the high PG grade of the binder by six degrees (one PG grade); 1.5 to 2% wt PPA will bring an additional PG grade raise. The effect of increasing the high end of the PG grade is more pronounced on the polymer modified materials than on the neat binder. There is also a surprising improvement on the low temperature grade of the binders.

The storage experiment was performed at 135 °C in closed containers for 24 and 72 hours. For all binders there is a definite trend of increased stiffness with increased storage time.

Table F2a.2. PG grading of binders after modification with 1% 105 PPA.

	A1 SBS PG 70-22		c.v.%	A5 Neat PG 58-22		c.v.%	B9 Elvaloy PG64-28		c.v.%
Original									
G*/sinδ (kPa)	@82°C	1.24	2.87	@64°C	1.25	0.79	@82°C	1.12	5.07
True Grade (°C)	**@1.00 kPa**	**84.7**		**@1.00 kPa**	**66.0**		**@1.00 kPa**	**83.3**	
RTFO									
G*/sinδ (kPa)	@88°C	2.86	3.73	@64°C	2.76	0.18	@88°C	2.68	8.31
True Grade	**@2.20 kPa**	**91.5**		**@2.20 kPa**	**66.0**		**@2.20 kPa**	**91.0**	
PAV									
G*·sinδ (kPa)	@13°C	4046	6.71	@13°C	4472	4.02	@07°C	4775	--
True Grade	**@5000 kPa**	**10.8**		**@5000 kPa**	**11.9**		**@5000 kPa**	**6.5**	
Stiffness (MPa)	@-18°C	200.7	1.39	@-18°C	222.0	3.82	@-24°C	231.0	6.45
True Grade	**@300MPa**	**-31.5**		**@300MPa**	**-30.4**		**@300MPa**	**-36.5**	
m-value	@-18°C	0.307	0.23	@-18°C	0.311	4.55	@-24°C	0.304	0.46
True Grade	**@0.300**	**-28.6**		**@0.300**	**-29.1**		**@0.300**	**-34.7**	
GRADE	**PG 82-28**			**PG 64-28**			**PG 82-34**		
TEMP. RANGE	**113.3°C**			**95.1°C**			**118.0°C**		

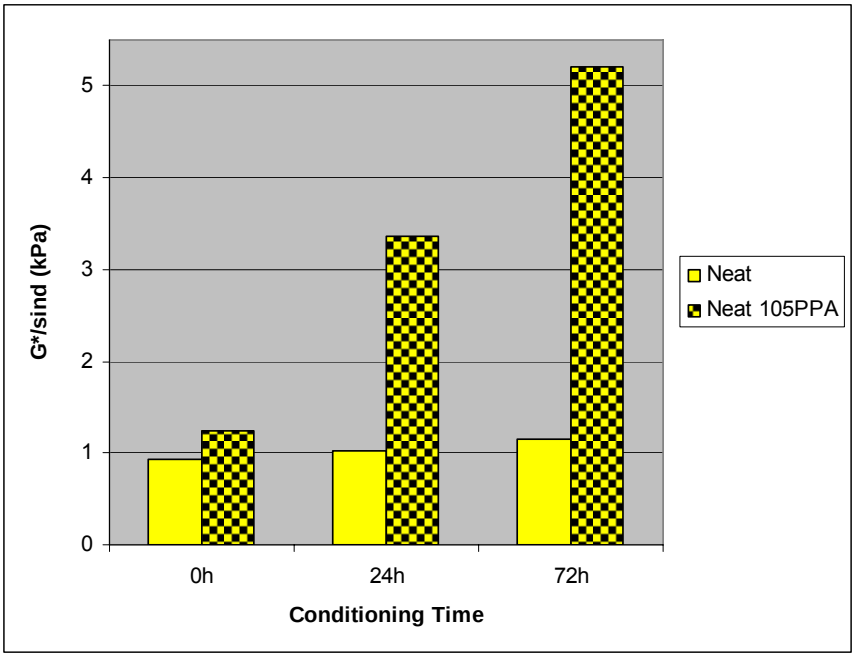

Figure F2a.2. Chart. Effect of conditioning on neat binder @ 135 ºC.

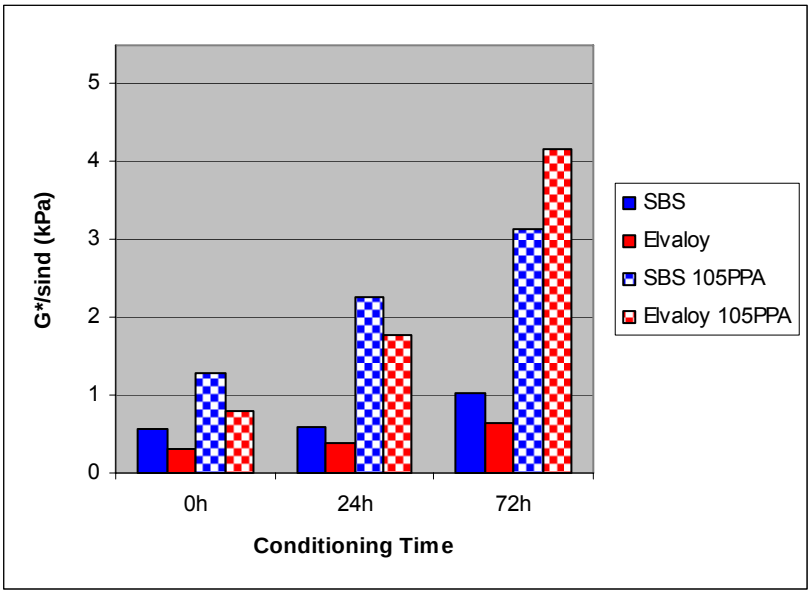

Figure F2a.3. Chart. Effect of conditioning on polymer modified binder @ 135ºC

This trend is valid for both binders and mastics. As in the case of the high PG grade, this trend is more pronounced for the polymer modified binders than for the neat binder.

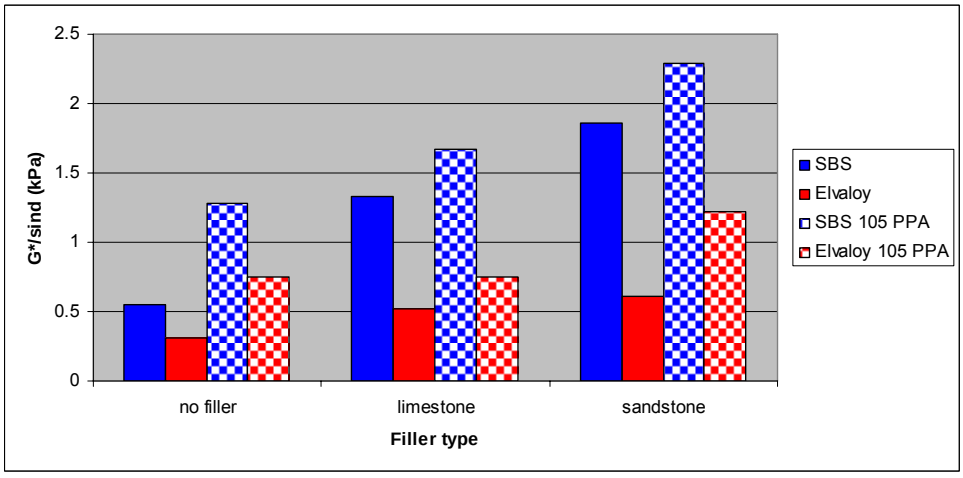

Figure F2a.4. Chart. Effect of filler on polymer modified binders.

In the case of the mastics, the presence of PPA doesn't seem to have as much of an effect as in the case of binders. However, the trend showing an increase in stiffness when PPA is added is still present.

The increase in stiffness observed in the presence of the PPA is greater than expected. One explanation could be the formation of a gel like structure in the presence of an acid like PPA. In order to investigate this hypothesis we subjected four samples of binders (two PPA modified and two without PPA) to stress sweep testing. If a gel like structure is contributing to the increase in stiffness, then that structure would be expected to collapse under increasing shear stress.

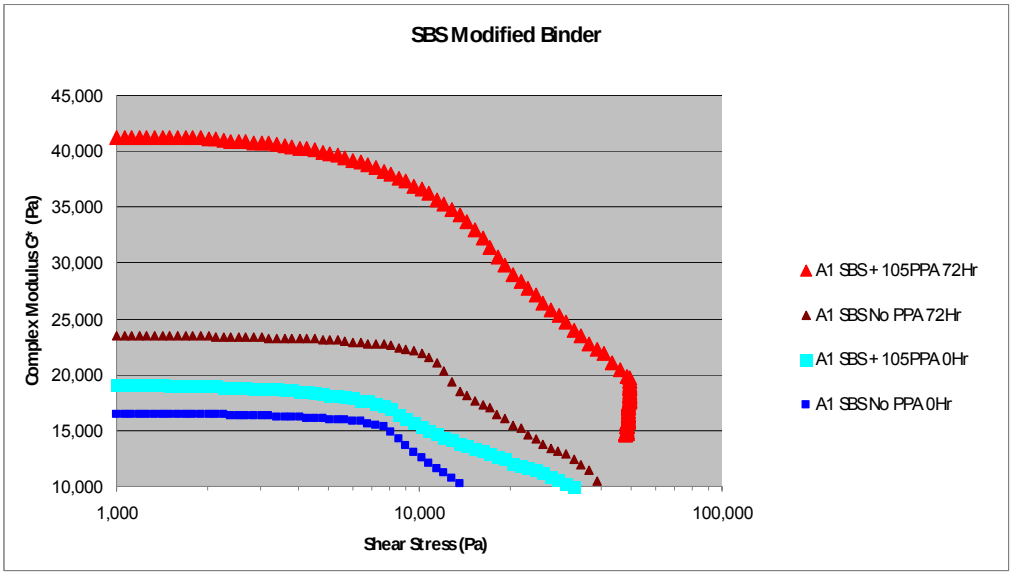

Figure F2a.5. Chart. Stress sweep test results on SBS modified binder with and without PPA, before and after 72 hours of conditioning @135 ºC.

As shown in figure F2a.5, we see no evidence of a gel like structure collapsing, which would indicate the absence of such a structure. However these are just preliminary results and we are continuing to investigate this matter.

Problems Encountered and Solutions

No significant problems were encountered.

Work Planned Next Quarter

The experimental test matrix is described in table F2a.3.

Table F2a.3. Stress sweep and monotonic test experimental matrix.

Binders	Flint Hills PG 58-28	Mineral Fillers	Limestone
	Flint Hills PG 64-22		Sandstone
	Marathon PG 58-28	Modifiers	PG xx-34
	Marathon PG 64-22		D1101 Kraton SBS
Testing Temp	19 °C		D1184 Kraton SBS
	25 °C		Elvaloy AM
Storage time	0h		Elvaloy 4170
	24h		PPA 115
	72h		PPA105
Storage Temperature	135 °C		OPA 85

Stress sweep tests will be performed on these materials in order to asses their fatigue properties. Also the new monotonic test developed at University of Wisconsin-Madison will be performed. This will give us a better picture of the influence of different modifiers on fatigue properties of binders, but also will help further validate the monotonic test.

Analysis

The data analysis on this project will be focused on two main areas: rheological properties and damage resistance characterization.

The rheological properties investigation serves as a tool to classify and rank starting materials, as well as a monitoring tool during the modification and conditioning process. This is accomplished by measuring parameters like $G^*/\sin\delta$, an indication of the rutting resistance of binders, as well as performing Multiple Stress Creep Recovery tests on the binders. This will provide us with important information on how the modification of binders affects not only fatigue but also rutting performance of binders.

The damage resistance characterization part of the investigation will focus on classifying and ranking different modifiers and/or modification techniques based on their impact over the binder's ability to resist damage. This is mainly focused on fatigue damage, but it uses rutting damage control tests to maintain perspective on improving the overall binder properties.

References

Bhasin, A., and D. N. Little, 2006, Characterization of aggregate surface energy using the universal sorption device. *Journal of Materials in Civil Engineering (ASCE)*, Accepted for publication.

Della Volpe, C., and S. Siboni, 2000, Acid base surface free energies of solids and the definition of scales in the Good van Oss Chaudhury theory. *Journal of Adhesion Science and Technology*, 14(2): 235-272.

Hefer, A. W., A. Bhasin, and D. N. Little, 2006, Bitumen surface energy characterization using a contact angle approach. *Journal of Materials in Civil Engineering (ASCE)*, 18(6): 759-767.

Huang, C. W., E. Masad, A. Muliana, and H. Bahia, 2007, Development and Numerical Implementation of a Nonlinear Viscoelastic Model for Hot Mix Asphalt. *Mechanics of Time Dependent Materials* (In Review).

Little, D. N., and A. Bhasin, 2006, Using Surface Energy Measurements to Select Materials for Asphalt Pavement. *Final Report for Project 9-37*, Texas Transportation Institute.

Masad, E., 2004, X-ray Computed Tomography of Aggregates and Asphalt Mixes. *Materials Evaluation Journal, American Society for Nondestructive Testing*, 62(7): 775-783.

Masad, E., V. Castelo Branco, D. Little, and R. Lytton, 2007, A Unified Method for the Analysis of Controlled-Strain and Controlled-Stress Fatigue Testing. *International Journal of Pavement Engineering* (Accepted for Publication).

Sharon, E., S. P. Gross, and J. Fineberg, 1996, Energy Dissipation in Dynamic Fracture. *Physical Review Letters*, 76(12): 2117-2120.

Work Element F2b: Mastic Testing Protocol

Subtask F2b-1: Develop Specimen Preparation Procedures (Year 1 start) (TAMU)

Progress This Quarter

During the last quarter a refined procedure for design and preparation of FAM test specimens for use with DMA was presented. The new design procedure allows the use of a FAM that is an exact representation of the asphalt mixture without the coarse aggregates. In this quarter several FAM specimens were prepared using different material combinations based on the new design and fabrication procedure. For the material combinations and designs used thus far, no problems in fabrication of the test specimens were found.

We commenced testing of the specimens using the DMA in order to obtain data that is required to model the fatigue response of FAM specimens according to the approach presented in Work Element F1b.

Work Planned Next Quarter

We will continue testing of the FAM specimens for select material combinations.

Subtask F2b-2: Document Test and Analysis Procedures in AASHTO Format

Progress This Quarter

No activity this quarter.

Work Planned Next Quarter

No work planned.

Work Element F2c: Mixture Testing Protocol (TAMU)

Progress This Quarter

Trial tests were conducted in direct tension mode to determine the fatigue cracking characteristics of asphalt mixtures. A test protocol was developed such that analytical tools developed for FAM specimens in task F1b can also be applied to characterize the non linear and fatigue damage properties for full asphalt mixtures.

Work Planned Next Quarter

The planned activity for next quarter is to continue testing of select asphalt mixtures as described above.

Work Element F2d: Tomography and Microstructural Characterization

Progress This Quarter

In the previous quarter we proposed the design of a micro scale loading frame. The loading frame will facilitate better understanding of the physio-chemical and morphological changes associated with the following four processes with the aid of an FTIR microscope and AFM:

i. relaxation,
ii. plastic deformation and fatigue crack initiation,
iii. fatigue crack propagation, and
iv. healing

In this quarter fabrication of the loading frame was completed. A function generator and a signal amplifier are used with the loading frame to apply various loading configuration related to the four mechanisms described above (figure F2d-1.1)

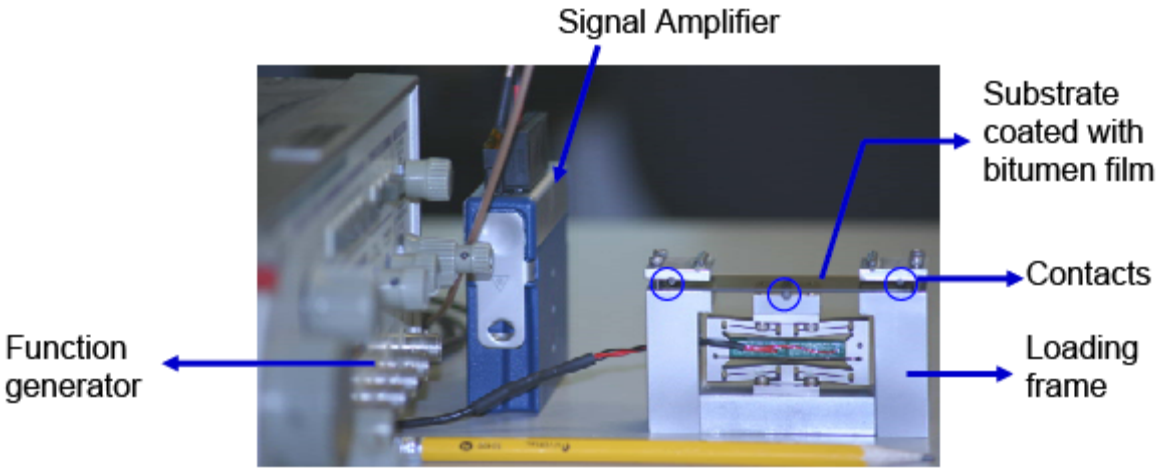

Figure F2d-1.1. Microstrain loading apparatus.

Work Planned Next Quarter

The loading frame will be calibrated for use and preliminary tests will be conducted. Fatigue loading to thin films of asphalt binder on glass substrate will be applied. The changes in morphology of the asphalt binder and evolution of cracks at different stages of the fatigue test will be examined using an AFM.

Work Element F2e: Verification of the Relationship between DSR Binder Fatigue Tests and Mixture Fatigue Performance

Subtask F2e-1: Evaluate Binder Fatigue Correlation to Mixture Fatigue Data (UWM Year 1 start)
Subtask F2e-2: Selection of Testing Protocols (TAMU, UWM)
Subtask F2e-3: Binder and Mixture Fatigue Testing (TAMU, UWM)
Subtask F2e-4: Verification of Surrogate Fatigue Test (TAMU, UWM)
Subtask F2e-5: Interpretation and Modeling of Data (TAMU, UWM)
Subtask F2e-6: Recommendations for Use in Unified Fatigue Damage Model (TAMU, UWM)

Note: These subtasks will be reported together.

Task Lead: Haifang Wen

Progress This Quarter

Since the start of the Year 1 work plan and during this quarter especially, the team has extensively evaluated two aspects of fatigue for asphalt binder: a surrogate test for fatigue of asphalt binder, and the application of viscoelastic continuum damage mechanics to asphalt binder.

Surrogate test for fatigue of asphalt binder

A surrogate test is desired to substitute the time-consuming time sweep test for rapid characterization of fatigue performance of asphalt binder. The team developed a monotonic shear test using the Dynamic Shear Rheometer (DSR). A constant strain-rate, 45% per minute in this case, was applied to the specimen until the stress reaches the peak level and drops. The fracture energy was calculated under the stress-strain curve up to the peak stress level. It was found that fracture energies of ALF asphalt binders (three replicates for each binder) were highly correlated with the field performance of these binders at ALF site, as shown in figure F2e.1.

This observation indicates that constant strain-rate test has the potential to be a surrogate test for fatigue of asphalt binder. The fracture energy from the constant strain-rate test of asphalt binder could be a good indicator to fatigue performance of asphalt binder. The team will further evaluate the repeatability and ruggedness of this test.

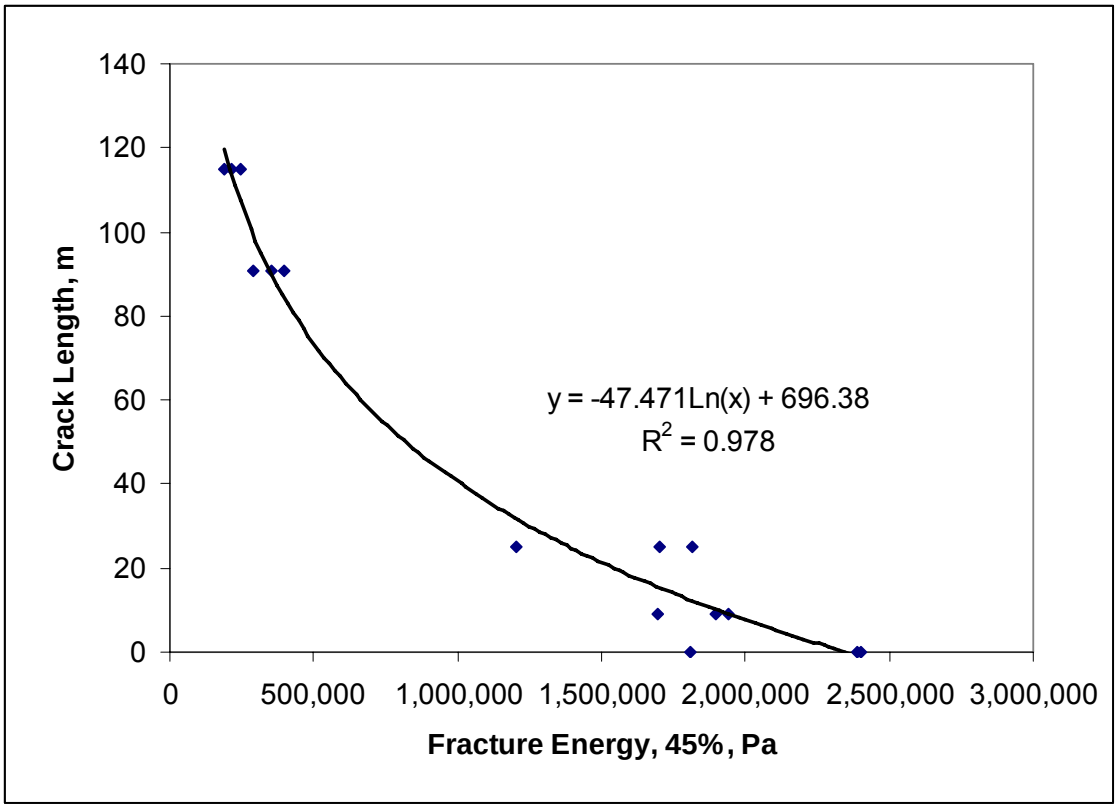

Figure F2e.1. Correlation of fracture energy and field performance of asphalt binders.

Applicability of Viscoelastic Continuum Damage (VECD) Mechanics

Viscoelastic continuum damage mechanics were employed to characterize the asphalt binders. Frequency sweep and monotonic constant-strain rate tests were conducted using DSR. The complex moduli of asphalt binders were obtained from frequency sweep testing, and converted to the time domain to obtain the relaxation modulus master curve. In order to validate this method for calculating relaxation modulus, a stress relaxation test was performed in the DSR. Using the same 8-mm geometry as used for the monotonic test, the binder samples were subjected to a constant 2% strain with a rise time of 0.1 sec. Common convention dictates that relaxation data between zero and ten times the rise time not be used for analysis in order to avoid inertial effects of the sudden ramp in strain level (Lakes 1999). For this research, a conservative approach of 20 to 30 times the rise time was used. Typical results are shown below.

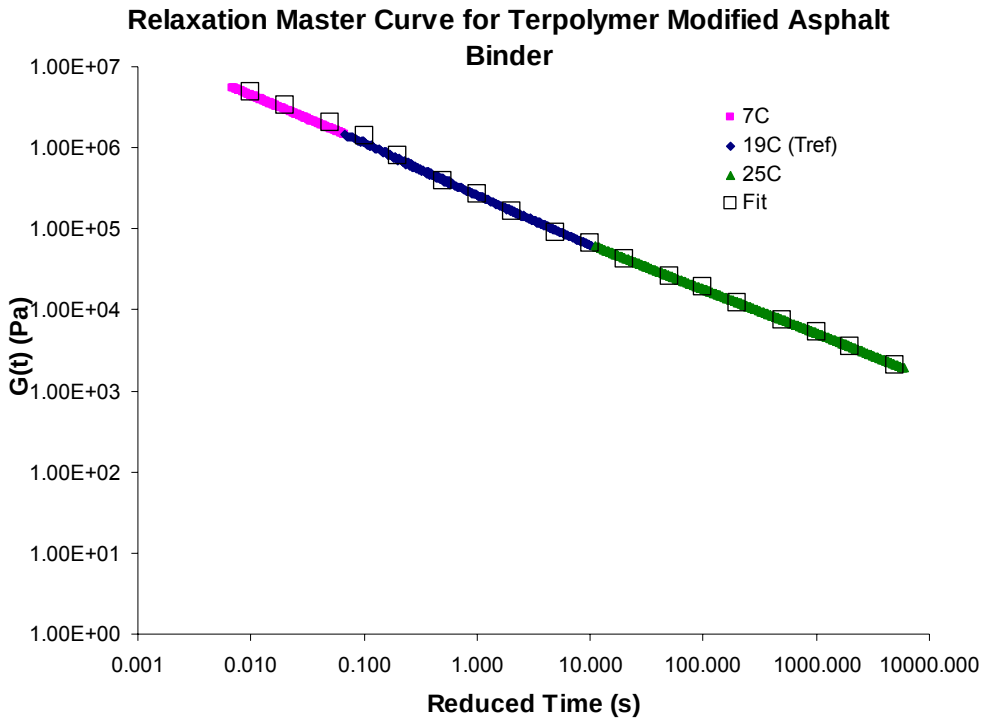

Figure F2e.2. Shifted relaxation curves plotted with the Prony series fit.

The relaxation moduli were fitted using the Prony series and used for pseudo strain calculation. The pseudo strain was then used to obtain pseudo stiffness, C, and damage parameter, S. Three strain rates were used for each asphalt binder. It was found that the VECD approach eliminated the effects of different strain rate. The C vs. S curves for three strain rates collapsed, as shown in figure F2e.3. The C vs. S relationship could possibly be used to predict the fatigue life of asphalt binders if it follows the same characteristic curve for time sweep testing, as suggested by previous studies performed with mixtures by Kim et al.

This demonstrates that VECD has the potential to be used for asphalt binder, as well as asphalt mixtures. The cyclic fatigue test data for these binders will be analyzed to evaluate of the effectiveness of VECD on the time sweep test for binders.

The project team also met with Dr. M. Emin Kutay with TFHRC to discuss his work on VECD concepts on mixtures using the same binders from this research. Dr. Kutay showed the ability of the C(S) curve calculated from cyclic data to accurately predict number of cycles to failure using test conditions other than those used to originally determine the C(S) curve, validating that this approach is independent of test conditions. It is the goal of the UW team that this can eventually be applied to binders as well, and a possible collaborative effort between Dr. Kutay and the UW ARC research team is currently being explored. One goal of the collaboration would be to establish the significance of the viscoelastic phase angle on VECD mechanics, as it is a critical parameter in binder characterization, and also since current VECD research on mixtures has not fully explored this material property.

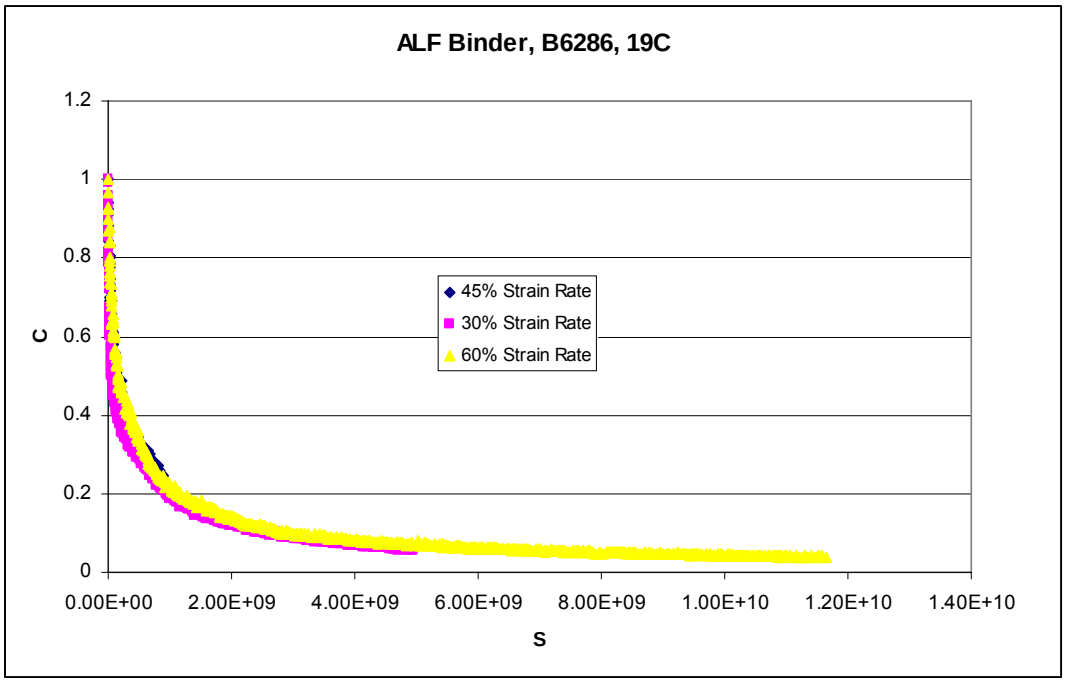

Figure F2e.3. C vs. S curves for asphalt binder.

Work Planned Next Quarter

Further analysis of the monotonic data to establish the repeatability of the test method will be performed. Also, test results from the monotonic testing of binders used for a previous study on mixture fatigue will be analyzed to investigate the possible correlation between mixture fatigue and binder monotonic testing. The goal for next quarter's work in this area will be to establish the ability of the monotonic binder test to predict number of cycles to failure for binder time sweep testing.

CATEGORY F3: MODELING

Work Element F3a: Asphalt Microstructural Model (WRI Year 2 start)

Progress This Quarter

No activity this quarter.

Work Planned Next Quarter

No work planned.

Work Element F3b: Micromechanics Model

Subtask F3b-1: Model Development (TAMU)

Progress This Quarter

A summary of the activities conducted by the researchers at the University of Nebraska during this quarter are as follows:

- Revisit to the concepts of micromechanics-based computational modeling,
- Review and summary of historical approaches of cohesive zone modeling which is the model to simulate damage initiation and propagation,
- A numerical convergence study of the cohesive zone model to determine an appropriate size of the cohesive zone.

A more detailed description of the findings from the review of topics described above are presented below.

Concepts: micromechanics-based computational modeling

As shown in figure F3b-1.1, the microstructure of a general asphalt mixture in the pavement surface layer exhibits two distinct phases: a portion of relatively coarse aggregate particles (in white) and an asphalt matrix phase (in black), comprised of asphalt cement, fine aggregates (smaller than about 0.28mm), and entrained air voids. At room temperature or higher, the coarse aggregate particles typically demonstrate linear elastic behavior, while the asphalt matrix phase is subjected to significant damage resulting in nonlinear-inelastic performance of the overall asphalt mixture. Due to the significant geometric complexity and nonlinear-inelastic material response, computational approaches based on the micromechanics concepts have been considered the best option for a realistic simulation of small scale damage and interactions among mixture constituents and their impact on overall structural failure of asphalt mixtures.

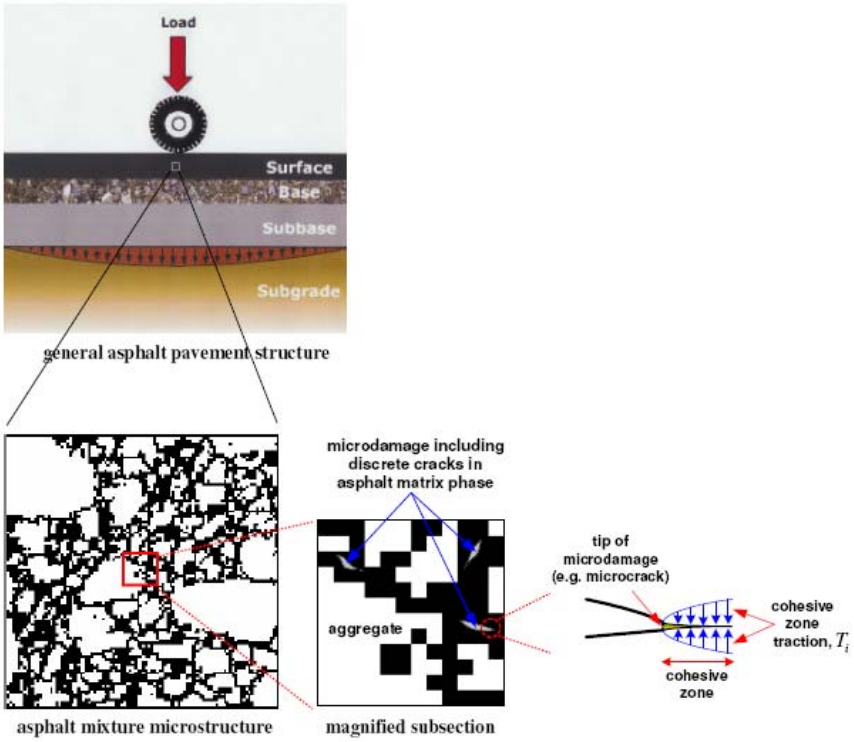

Figure F3b-1.1. Microstructure of an asphalt mixture and its modeling concepts based on micromechanics.

Elastic Model for Aggregates

The linear elastic constitutive relationship for the aggregate phase can be expressed as:

$$\sigma_{ij}(x_k,t) = C_{ijkl,E}\,\varepsilon_{kl}(x_k,t) \qquad \text{(F3b-1.1)}$$

where $\sigma_{ij}(x_k,t)$ = stress as a function of space and time,
$\varepsilon_{kl}(x_k,t)$ = strain as a function of space and time,
$C_{ijkl,E}$ = elastic modulus which is not time-dependent,
x_k = spatial coordinates, and
t = time of interest.

The time-independent elastic modulus consists of elastic material properties. If the individual particle of aggregates is assumed to follow simply isotropic linear elastic behavior, only two independent material constants among Young's modulus (E), shear modulus (G), and Poisson's ratio (ν) are required.

Viscoelastic Model for Asphalt Phase

The constitutive behavior of the asphalt matrix phase can often be represented by the following linear viscoelastic convolution integral:

$$\sigma_{ij}(x_k,t) = \int_0^t C_{ijkl,VE}(t-\tau)\frac{\partial \varepsilon_{kl}(x_k,\tau)}{\partial \tau} d\tau \qquad \text{(F3b-1.2)}$$

where $C_{ijkl,VE}(t)$ = linear viscoelastic time-dependent stress relaxation modulus, and
τ = time-history integration variable.

The linear viscoelastic relaxation modulus of the asphalt phase is determined by performing laboratory constitutive tests such as static creep/relaxation tests or dynamic frequency sweep tests within theory of linear viscoelasticity. Testing results can be represented by a mathematical form such as a Prony series based on the generalized Maxwell model. The linear viscoelastic stress relaxation modulus by a Prony series can be expressed as:

$$C_{ijkl,VE}(t) = C_{ijkl,\inf} + \sum_{p=1}^{M} C_{ijkl,p} \exp\left(-\frac{C_{ijkl,p}}{\eta_{ijkl,p}} t\right) \qquad \text{(F3b-1.3)}$$

where $C_{ijkl,\inf}$ and $C_{ijkl,p}$ = spring constants in the generalized Maxwell model,
$\eta_{ijkl,p}$ = dashpot constants in the generalized Maxwell model, and
M = the number of dashpots.

Nonlinear Viscoelastic Model for Fracture-Damage of Asphalt Phase

Modeling of fracture-damage zone is complex subject particularly for inelastic materials such as asphalt mixtures. The fracture-damage behavior can be modeled in many different ways, and one of the well-known approaches is to implement a cohesive zone as illustrated in figure 1. The cohesive zone models are well-established tools in classical fracture mechanics developed to remove stress singularities ahead of crack tips. The cohesive zone modeling concept has been receiving increasing attention from the asphalt mechanics community.

At the tip of damage (such as crack) the cohesive zones have constitutive behavior that may be expressed by the general traction-displacement relationship as follows:

$$T_i(x_k,t) = T_i\{u_k, \alpha(t)\} \qquad \text{(F3b-1.4)}$$

where T_i = cohesive zone traction vector,
u_k = cohesive zone displacement vector, and
$\alpha(t)$ = a function representing damage evolution characteristics, and
{ } = implies history dependence for damaged zones.

Fine-Mesh Finite Element Method (FEM)

As illustrated in figure F3b-1.2, the finite element method with fine meshes that are constructed from a real digital image of asphalt concrete microstructure can be employed to deal with

mixture heterogeneity. Figure F3b-1.2 shows a binary digital image, its magnified subsection, and finite element meshes.

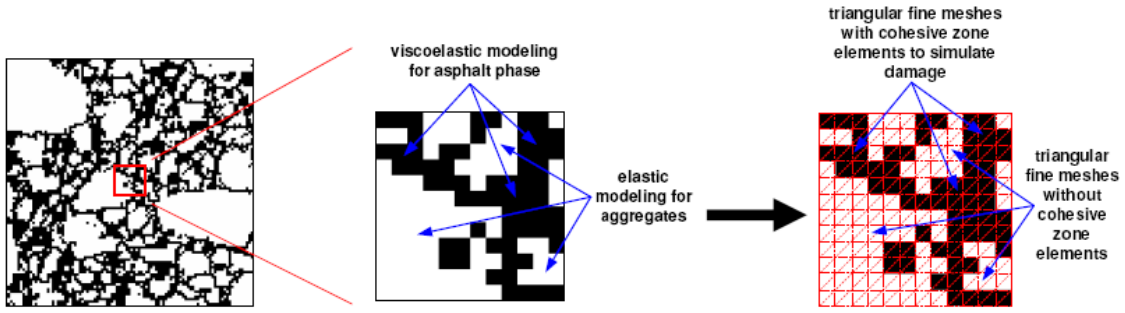

Figure F3b-1.2. Fine-mesh finite element method based on micromechanics concepts.

The cohesive zones which are subjected to initiation of microscale fracture-damage and its propagation have been simulated by employing regularly oriented interface elements based on a pixel grid from the digital image processing. Digital pixel information during image processing has been translated into triangular solid elements and interface elements (see figure 2) between solid elements within the matrix phase to simulate damage. As an example, the binary digital image shown in figure F3b-1.2 is 0.028m by 0.028m, which has been regularly digitized to 200 by 200 triangular elements. This results in a 280μm/element, which infers that the finite element analysis can allow one to successfully simulate microscale damage of 280μm.

Review: cohesive zone models

The classical theory of fracture mechanics, as described by Griffith (1920), assumes that there is no plastic deformation in the material, or such deformation is negligible (linear elastic fracture mechanics - LEFM). This methodology also assumes that crack growth occurs whenever the energy release rate exceeds the critical energy release rate, which is considered to be a material property.

However, for materials that exhibit subcritical crack propagation (Paris and Erdogan 1963; Frost and Dixon 1967), the LEFM cannot be used without a modification. Dugdale (1960) and Barenblatt (1962) were the first to develop a so-called cohesive zone models for elastic materials. The model is considered to be cohesive because it assumes the existence of cohesive tractions acting in the fracture process zone at the crack tips. The cohesive zone model allows crack growth analysis from pre-existing cracks as well as from plain surfaces. Such a model has been used for modeling a multitude of ductile materials, including asphaltic mixtures (Jenq and Perng 1991).

Figure F3b-1.3 illustrates a cohesive zone in mode I fracture (opening of the crack faces). Separation starts at a tensile stress σ_{max}, originally defined by Barenblatt (1962) as a theoretical strength generally several orders of magnitude higher than the actual strength. Crack evolution is modeled considering stress transferring through the cohesive zone to be dependent on the relative displacements of the cohesive zone faces. In mode I, the constitutive relation between

the cohesive stress σ and the separation distance w has been assumed to be a material property. Some examples of $\sigma(w)$ are illustrated in figures 4(a)-4(c). The area under the curve $\sigma(w)$ is the energy absorbed per unit area of crack when the cohesive zone opens from zero to the maximum displacement w_c. The parameters σ_{max}, w_c and $\sigma(w)$ are the material properties in the model.

Needleman (1987), in his investigation of the debonding of an inclusion from a metal matrix, first presented a cohesive zone model in terms of an interface potential that specifies the dependence of the tractions on the displacements. Just like the original model by Barenblatt (1962), in Needleman's model, as the crack surfaces separate, tractions increase up to a maximum and decrease to zero when full separation occurs. As can be seen in figures F3b-1.4(a) and 4(b), the difference between these models is in the fact that for the original model developed for crystals the cohesive stress value is zero for regular intermolecular distances b. With the opening displacement growing to approximately *1.5b*, the cohesive stresses reach a maximum after which it decreases rapidly with further increase in the distance. Another possibility is shown in figure F3b-1.4(c). Note that in all cases, the traction eventually decays to zero, the point at which decohesion leads to crack propagation.

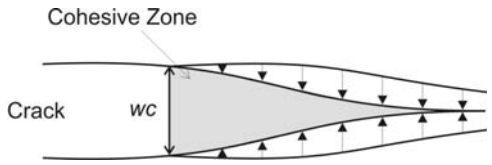

Figure F3b-1.3. Illustration of a cohesive zone in mode I fracture.

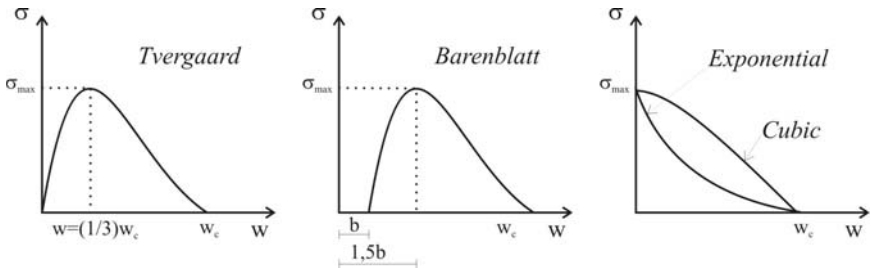

Figure F3b-1.4. Constitutive models for the cohesive zone.

Tvergaard (1990) further developed the model considering normal and tangential separation, and the tractions are coupled to normal opening [$u_n = w$] and tangential displacements, [u_t] and [u_s]. In a two-dimensional analysis, besides the normal displacement [u_n], only one tangential displacement needs to be considered [u_t]. The extension to the three-dimensional case is straightforward (Foulk 1997). Tvergaard describes a nondimensional parameter, λ, that is used to couple the normal and tangential behavior such as:

$$\lambda = \left[\left(\frac{u_n}{w_n} \right)^2 + \left(\frac{u_t}{w_t} \right)^2 \right]^{1/2} \qquad \text{(F3b-1.5)}$$

where $[w_n]$ and $[w_t]$ = maximum values of $[u_n]$ and $[u_t]$, respectively.

When $\lambda \geq 1$, separation occurs, that is, the cohesive stress vanishes. The tractions are defined to be a function of the displacements as follows:

$$T_n = \frac{u_n}{w_n} F(\lambda); \quad T_t = \beta \frac{u_t}{w_t} F(\lambda) \qquad \text{(F3b-1.6)}$$

where β = a material property relating shear to normal strength,
T_n and T_t = the normal and tangential cohesive tractions within the cohesive zone.

T instead of σ is used to represent the cohesive stresses in mixed mode fracture (mode I and II). The model is sufficiently generic such that any constitutive relation $T = T(\lambda)$ can be used. Tvergaard (1990), for example, assumed a cubic model, $T = 27/4\ \sigma_{max}\ (\lambda - 2\lambda^2 + \lambda^3)$.

Not many approaches had taken into account time-dependent behavior so far. Knauss (1969, 1970) was one of the first to investigate the effects of the rate on crack growth behavior of rubbery materials. Constanzo and Allen (1993) observed that a void nucleation and decohesion ahead of the crack tip could be modeled using a nonlinear viscoelastic cohesive zone model (Schapery 1975a, 1975b, 1975c). Yoon and Allen (1999) used the continuum thermo-viscoelasticity and developed a damage evolution relation for a nonlinear viscoelastic cohesive zone model, and later this evolution relation was re-constructed based on the micromechanics theory and incrementalized into a finite element code (Allen and Searcy 2000, 2001a, 2001b). The two-dimensional traction-displacement relationship for the nonlinear viscoelastic cohesive zone model (Yoon and Allen 1999; Allen and Searcy 2000) is as follows:

$$T_i(t) = \left[1 - \alpha(t)\right] \cdot \left[\sigma_i^f + \frac{1}{\delta_i} \int_0^t E_{CZ}(t-\tau) \frac{\partial u_i(\tau)}{\partial \tau} d\tau \right] \qquad \text{(F3b-1.7)}$$

where $T_i(t)$ = cohesive zone traction,
$u_i(t)$ = cohesive zone displacement,
δ_i = cohesive zone length parameter,
σ_i^f = requisite stress level to initiate cohesive zone,
$\alpha(t)$ = damage evolution function,
$E_{CZ}(t)$ = linear viscoelastic relaxation modulus of the cohesive zone, and
$i = n$ (normal direction) or t (tangential direction).

Viscoelastic stress relaxation modulus of the cohesive zone is determined by performing laboratory constitutive tests, the results of which can also be represented by a Prony series form (in equation 3) to be implemented in the model. In addition to the stress relaxation modulus of the cohesive zone, laboratory testing to define the cohesive zone length parameter, δ_i and the

damage evolution function, $\alpha(t)$ also needs to be performed. The directly measured damage characteristics can then be incorporated into an analytical equation which should be appropriate for simulating rate-dependent damage growth that is typical in viscoelastic asphalt mixtures.

Equation (8) is one example of the damage evolution function including two damage evolution parameters (α_1 and m).

$$\frac{d\alpha}{dt} = \begin{cases} \alpha_1 \left[\dfrac{u_i(t)}{\delta_i} \right]^m, & \dfrac{1}{\delta_i}\dfrac{du_i(t)}{dt} > 0 \text{ and } \alpha < 1 \\ 0, & \dfrac{1}{\delta_i}\dfrac{du_i(t)}{dt} \le 0 \text{ or } \alpha = 1 \end{cases} \tag{8}$$

Numerical convergence study of cohesive zone model

In order to properly capture the physics of failing material with the aid of numerical techniques such as the finite element method, it is important that the finite element mesh size be smaller than the length of single cohesive zone. To this end, a numerical convergence study of the damage evolution via cohesive zones was performed by employing a double cantilever beam (DCB) specimen (in figure F3b-1.5) with a set of ten different finite element meshes. The DCB specimen (10 inch long and 0.5 inch height) is composed of two linear elastic beams connect with a viscoelastic cohesive zone. Although the viscoelastic cohesive zone has zero thickness, it was schematically drawn incorrectly on figure 8 just for illustrative purpose. The DCB specimen with a 2 inch long pre-crack is subjected to monotonically increasing displacements u_y. The results for each finite element mesh are compared to determine the characteristic length scale of the single cohesive zone element that presents mesh convergence.

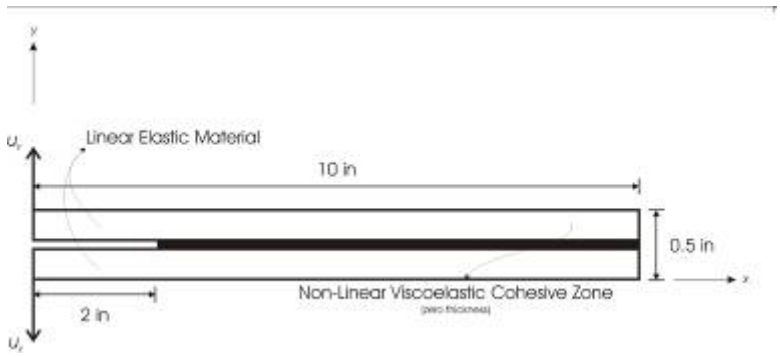

Figure F3b-1.5. DCB specimen.

Ten different finite element meshes were constructed. All the meshes are composed of constant strain triangle solid elements with cohesive zone interface elements (double nodes), but they differ in number of nodes, number of elements, and, consequently, number of interface elements. Mesh 01 is the coarser mesh (252 nodes, 400 elements and 16 interface elements), and Mesh 10 (shown in figure 6) is the finest one (2412 nodes, 4000 and 160 interface elements). Figure 6

also shows the displacement boundary conditions imposed. Table F3b-1.1 presents the properties for each finite element mesh.

Figure F3b-1.6. Finite element Mesh 10 and its boundary conditions.

Material properties were chosen arbitrarily. No reference was made to any real material because the purpose of this work is to perform a convergence study of the method and not to simulate any material in particular. Table F3b-1.2 shows the material properties used. For the DCB only elastic constants (elastic modulus E and Poisson's ratio ν) were adopted, while for the viscoelastic cohesive zone, the relaxation modulus is described by a Prony series form. Damage parameters for the cohesive zone are also presented in the table.

Table F3b-1.1. Finite element mesh properties.

Mesh	No. of Nodes	No. of Elements	No. of Interface Elements	Interface Element Size (in)
Mesh 01	252	400	16	0.5000
Mesh 02	492	800	32	0.2500
Mesh 03	732	1200	48	0.1667
Mesh 04	972	1600	64	0.1250
Mesh 05	1212	2000	80	0.1000
Mesh 06	1452	2400	96	0.0833
Mesh 07	1692	2800	112	0.0714
Mesh 08	1932	3200	128	0.0625
Mesh 09	2172	3600	144	0.0555
Mesh 10	2412	4000	160	0.0500

Table F3b-1.2. Material properties.

Location	E (psi)		ν	η_i		Damage Parameters	
Beam	0.5E+08		0.3	-	-	-	-
Cohesive Zone	∞	0.5E+03	-	-	-		
	1	0.1E+03	-	1	0.1E+01	σ_n^f	0
	2	0.1E+03	-	2	0.1E+02	σ_t^f	0
	3	0.1E+03	-	3	0.1E+03	δ_n	0.1E+01
	4	0.1E+03	-	4	0.1E+04	δ_t	0.1E+01
	5	0.1E+03	-	5	0.1E+05	α_1	0.5
	6	0.1E+03	-	6	0.1E+06	m	0.5
	7	0.1E+03	-	7	0.1E+07		

Figures F3b-1.7-9 demonstrate simulation results from all meshes. Figure F3b-1.7 plots the averaged normal traction along the cohesive zone for each time step versus the tip opening displacement (0.0001/sec). Mesh convergence can be determined by calculating the area under each graph in figure F3b-1.7. The area for Meshes 09 and 10 are equal up to four significant digits. Figure 8 shows the area difference for each consecutive mesh.

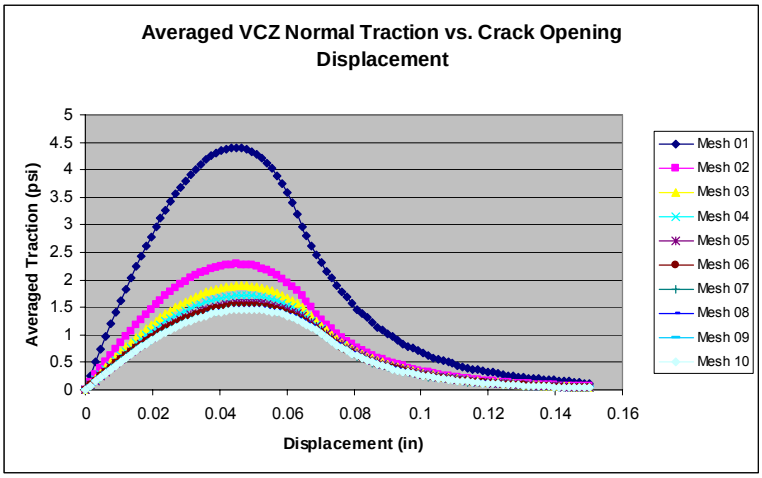

Figure F3b-1.7. Averaged VCZ normal traction per second versus tip opening displacement.

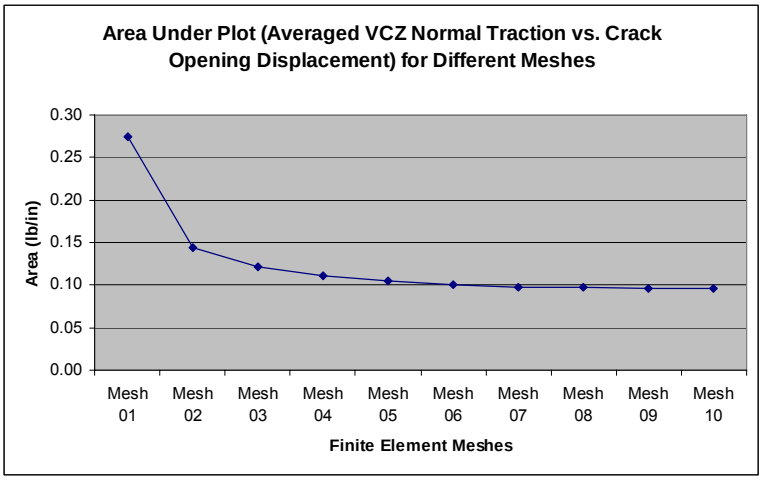

Figure F3b-1.8. Area under plot (traction vs. crack opening displacement) for all finite element meshes.

Figure F3b-1.9 illustrates the total crack tip advancement versus time. It can be seen that crack growth for Mesh 09 follows practically the same path as Mesh 10.

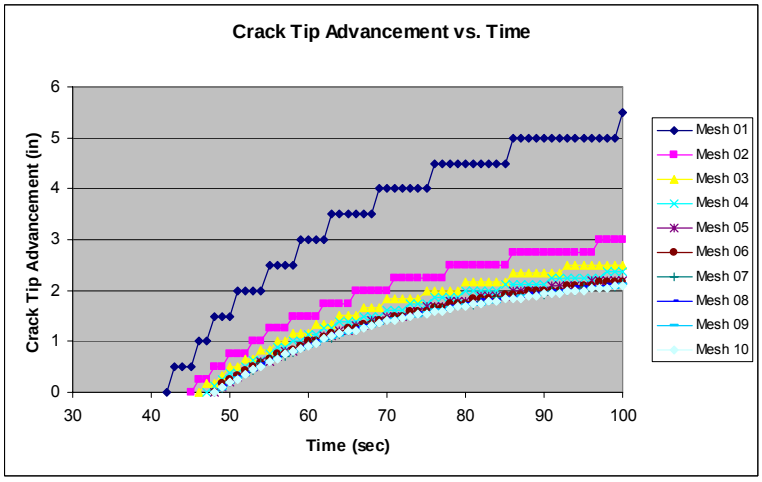

Figure F3b-1.9. Crack tip advancement versus time.

Work Planned Next Quarter

The planned activities for the next quarter are

- To continue the review of literature related to the micromechanics-based computational modeling techniques and the cohesive zone modeling approaches,

- To integrate microstructural characterization of mixtures with fundamental materials/mixture properties that will be incorporated with this modeling effort in coordination with other researcher groups (Texas A&M Univ. and Univ. of Wisconsin-Madison) in order to,
- To study the representative volume elements (RVE) of various asphalt mixtures to facilitate the computational modeling within the micromechanics concept.

Subtask F3b-2: Account for Material Microstructure and Fundamental Material Properties (TAMU)

Progress This Quarter

No work this quarter.

Work Planned Next Quarter

No work planned.

References

Allen, D. H. and C. R. Searcy, 2000, Numerical Aspects of a Micromechanical Model of a Cohesive Zone. *Journal of Reinforced Plastics and Composites*, 19(3): 240-248.

Allen, D. H. and C. R. Searcy, 2001a, A Micromechanical Model for a Viscoelastic Cohesive Zone. *International Journal of Fracture*, 107: 159-176.

Allen, D. H. and C. R. Searcy, 2001b, A Micromechanically Based Model for Predicting Dynamic Damage Evolution in Ductile Polymers. *Mechanics of Materials***,** 33: 177-184.

Barenblatt, G. I., 1962, Mathematical Theory of Equilibrium Cracks in Brittle Fracture. *Advances in Applied Mechanics*, v.7, p. 55-129, Academic Press, New York.

Constanzo, F., and D. H. Allen, 1993, A Continuum Mechanics Approach to Some Problems in Subcritical Crack Propagation. *International Journal of Fracture*, 63: 27-57.

Dugdale, D., 1960, Yielding of Steel Sheets Containing Slits". *Journal of Mechanics and Physics of Solids*, 8: 100-104.

Foulk, J. W., 1997, "A Model for Predicting the Damage and Oxidation Dependent Life of SCS-6/TI-β21S[O]$_4$ Metal Matrix Composite". Master´s Thesis, Texas A&M University, College Station, TX.

Frost, N. E., and J. R. Dixon, 1967, A Theory of Fatigue Crack Growth. *International Journal of Fracture Mechanics*, 3(4): 301-316.

Griffith, A. A., 1921, The Phenomena of Rupture and Flow in Solids. *Philosophical Transactions of the Royal Society of London*, Series A 221, p. 163-198.

Jeng, Y. S. and J. D. Perng, 1991, Analysis of Crack Propagation in Asphalt Concrete Using Cohesive Crack Model. *Transportation Research Record*, 1317: 90-99.

Knauss, W. G., 1969, Stable and Unstable Crack Growth in Viscoelastic Media. *Transaction of the Society of Reology*, 13:3, 291-313.

Knauss, W. G., 1970, Delayed Failure - The Griffith Problem for Linearly Viscoelastic Materials. *International Journal of Fracture Mechanics*, 1: 7-20.

Needleman, A., 1987, A Continuum Model for Void Nucleation by Inclusion Debonding. *Journal of Applied Mechanics*, 54: 525-531.

Paris, P. C., and Erdogan, F., 1963, A Critical Analysis of Crack Propagation Laws. *Journal of Basic Engineering*, 85: 528-534.

Schapery, R. A., 1975a, A Theory of Crack Initiation and Growth in Viscoelastic Media; Part I: Theoretical Development. *International Journal of Fracture*, 11(1):141-159.

Schapery, R. A., 1975b, A Theory of Crack Initiation and Growth in Viscoelastic Media; Part II: Approximate Methods of Analysis. *International Journal of Fracture*, 11(3): 369-387.

Schapery, R. A., 1975c, A Theory of Crack Initiation and Growth in Viscoelastic Media; Part III: Analysis of Continuous Growth. *International Journal of Fracture*, 11(4): 549-562.

Tvergaard, V., 1990, Effect of Fiber Debonding in a Whisker-Reinforced Metal. *Materials Science & Engineering A: Structural Materials: Properties, Microstructure, and Processing*, A125(2): 203-213.

Yoon, C., and D. H. Allen, 1999, Damage Dependent Constitutive Behavior and Energy Release Rate for a Cohesive Zone in a Thermoviscoelastic Solid. *International Journal of Fracture*, 96: 56-74.

Work Element F3c: Development of Unified Continuum Model

Subtask F3c-1: Analytical Fatigue Model for Mixture Design (TAMU)

Progress This Quarter

The model was significantly developed during this quarter. We have put together an experiment using the Dynamic Mechanical Analyzer to test the fatigue of various asphalt-aggregate combinations at different temperatures, frequencies and stress amplitudes. However, we experienced technical problems with the DMA which delayed conducting these experiments. We will complete these experiments during the coming quarter.

Work Planned Next Quarter

We will complete the DMA testing of various asphalt-aggregate combinations at different frequencies, temperatures and stress levels.

Subtask F3c-2: Unified Continuum Model (TAMU)

Progress This Quarter

The development of the unified continuum model was further advanced. A summary of the damage model and its numerical implementation is presented below.

The total response of viscous material includes recoverable and irrecoverable parts. The recoverable strain can be represented as elastic and viscoelastic strain; while the irrecoverable strain includes plastic and viscoplastic strain. The recoverable strain can be linear or nonlinear behavior. The linear viscoelastic is the material behavior is independent of stress or strain status, and the nonlinear viscoelastic is function of stress or strain. In this research, the recoverable strain is assumed to be distributed by viscoplasticity only, and all of recoverable strain is nonlinear viscoelastic. The total strain can be shown in equation (1)

$$\varepsilon_{ij}^{total} = \varepsilon_{ij}^{NVE} + \varepsilon_{ij}^{vp} \tag{1}$$

Where ε_{ij}^{total} is total strain, ε_{ij}^{NVE} is nonlinear viscoelastic strain, and ε_{ij}^{vp} is viscoplastic strain.

From Eq. (1), the total strain rate can be shown as Eq. (2)

$$\dot{\varepsilon}_{ij}^{total} = \dot{\varepsilon}_{ij}^{NVE} + \dot{\varepsilon}_{ij}^{vp} \tag{2}$$

The viscoplastic strain rate can be defined by flow rule. This research uses the nonassociative flow rule to represent the viscoplastic strain rate. Applying Perzyna's theory with nonassociative flow rule, the viscoplastic strain rate can be shown as:

$$\dot{\varepsilon}_{ij}^{vp} = \Gamma\langle\phi(f)\rangle\frac{\partial g}{\partial \sigma_{ij}} \tag{3}$$

where, $\Gamma\langle\phi(f)\rangle$ determines the magnitude of viscoplastic strain rate $\dot{\varepsilon}_{ij}^{vp}$; while $\frac{\partial g}{\partial \sigma_{ij}}$ controls the direction of $\dot{\varepsilon}_{ij}^{vp}$. g is viscoplastic potential energy. Γ is viscosity parameter and ϕ is overstress function which can be express as:

$$\langle\phi(f)\rangle = \begin{cases} 0 & \phi(f) \le 0 \\ f & \phi(f) > 0 \end{cases} \tag{4}$$

where, f is yield surface function. Eq. (3) and (4) show that the viscoplastic happens only when the overstress function exceeds zero.

Yield Surface Function

This research employs Extended Drucker-Prager yield surface which can be shown as:

$$f = F(\sigma_{ij}) - \kappa(\varepsilon_e^{vp}) = \tau - \alpha I_1 - \kappa(\varepsilon_e^{vp}) \tag{5}$$

where α is material parameter, $\kappa(\varepsilon_e^{vp})$ is the hardening function which is the function of effective viscoplastic strain. τ and I_1 are the deviatoric shear stress and first invariant stress, respectively shown as Eq. (6).

$$I_1 = \frac{1}{3}\sigma_{ii}; \qquad \tau = \frac{\sqrt{J_2}}{2}\left[1 + \frac{1}{d} - \left(1 - \frac{1}{d}\right)\frac{J_3}{\sqrt{J_2^3}}\right] \tag{6}$$

where J_2 and J_3 are second and third deviator stress invariants which can be shown as:

$$J_2 = \frac{3}{2}S_{ij}S_{ij}; \qquad J_3 = \frac{9}{2}S_{ij}S_{jk}S_{ki} \tag{7}$$

where S_{ij} is deviator stress .

Viscoplastic Potential Energy Function

The viscoplastic potential energy can be shown as:

$$g = \tau - \beta I_1 \tag{8}$$

where β is material parameter.

In Eq. (3), the $\frac{\partial g}{\partial \sigma_{ij}}$ has to be determined to calculated viscoplastic strain rate. From Eq. (8),

$\frac{\partial g}{\partial \sigma_{ij}}$ can be shown as:

$$\frac{\partial g}{\partial \sigma_{ij}} = \frac{\partial \tau}{\partial \sigma_{ij}} - \beta \frac{\partial I_1}{\partial \sigma_{ij}}$$
$$= \frac{1}{2}\left[\frac{3S_{ij}}{2\sqrt{J_2}}\left(1+\frac{1}{d}\right) - \left(\frac{\left(\frac{27}{2}S_{ik}S_{kj} - 3J_2 S_{ij}\right)J_2 - 3S_{ij}J_3}{J_2^2} \right)\left(1-\frac{1}{d}\right) - \frac{2\beta}{3}\delta_{ij} \right] \tag{9}$$

Numerical Implementation

In finite element method, the stress and strain should be present as increment formulation which can be express as:

$$\begin{aligned} \left(\sigma_{ij}\right)^{n+1} &= \left(D_{ijkl}^{NVE}\right)^n \left(\left(\varepsilon_{kl}^{total}\right)^{n+1} - \left(\varepsilon_{kl}^{vp}\right)^{n+1}\right) \\ &= \left(D_{ijkl}^{NVE}\right)^n \left(\left(\varepsilon_{kl}^{total}\right)^{n} + \left(\Delta\varepsilon_{kl}^{total}\right)^{n+1} - \left(\varepsilon_{kl}^{vp}\right)^{n} - \left(\Delta\varepsilon_{kl}^{vp}\right)^{n+1}\right) \\ &= \left(\sigma_{ij}\right)^n + \left(D_{ijkl}^{NVE}\right)^n \left(\left(\Delta\varepsilon_{kl}^{total}\right)^{n+1} - \left(\Delta\varepsilon_{kl}^{vp}\right)^{n+1}\right) \end{aligned} \tag{10}$$

In Eq. (10), the viscoplastic strain increment can be defined using Perzyna's model and it can be shown as:

$$\Delta\varepsilon^{vp} = \Gamma\left\langle\phi(f)\right\rangle \frac{\partial g}{\partial \sigma}\Delta t = \Delta\gamma^{vp}\frac{\partial g}{\partial \sigma} \tag{11}$$

Substituting Eq. (11) into (10), the current stress can be shown as:

$$\left(\sigma_{ij}\right)^{n+1} = \left(\sigma_{ij}\right)^n + \left(D_{ijkl}^{NVE}\right)^n \left(\left(\Delta\varepsilon_{kl}^{total}\right)^{n+1} - \Delta\gamma^{vp}\frac{\partial g}{\partial \sigma}\right) \tag{12}$$

The assuming trial stress shown as:

$$\sigma_{ij}^{tr} = \left(\sigma_{ij}\right)^n + \left(D_{ijkl}^{NVE}\right)^n \left(\Delta\varepsilon_{kl}^{total}\right)^{n+1} \tag{13}$$

Then, the trial yield surface can be shown as:

$$f^{tr} = \tau^{tr} - \alpha I_1^{tr} - \kappa\left(\left(\varepsilon_e^{vp}\right)^n\right) \tag{14}$$

Checking the trial stress status, if the stress status exceeds the yield surface, the viscoplastic happened and the stress correction procedure should be applied. If the viscoplastic happens, in order to obtain the viscoplastic strain increment, this research uses the Newton-Raphson scheme. In Eq. (14) the viscoplastic multiplier can be shown as:

$$\Delta\gamma^{vp} = \Delta t\Gamma\langle\phi(f)\rangle = \Delta t\Gamma f \tag{15}$$

Defining a function χ which can be shown as:

$$\chi = \tau^{tr} - \alpha I_1^{tr} - \kappa\left(\left(\varepsilon_e^{vp}\right)^n\right) - \left(\frac{\Delta\gamma^{vp}}{\Delta t\Gamma}\right) \tag{16}$$

Using Newton-Raphson scheme to let $\chi \cong 0$ to obtain $\Delta\gamma^{vp}$. The Newton-Raphson scheme needs the differential of $\Delta\gamma^{vp}$ which can be shown as:

$$\frac{\partial\chi}{\partial\Delta\gamma^{vp}} = -\frac{\partial\kappa}{\partial\varepsilon_e^{vp}}\frac{\partial\varepsilon_e^{vp}}{\partial\gamma^{vp}} - \frac{1}{\Delta\gamma^{vp}}\left(\frac{\Delta\gamma^{vp}}{\Delta t\Gamma}\right) \tag{17}$$

In equation (17) $\dfrac{\partial\varepsilon_e^{vp}}{\partial\gamma^{vp}}$ can be derived as:

$$\frac{\partial\varepsilon_e^{vp}}{\partial\gamma^{vp}} = \frac{1}{\sqrt{1+2\left(\dfrac{\dfrac{1}{2d}+\dfrac{\beta}{3}}{\dfrac{1}{d}-\dfrac{\beta}{3}}\right)^2}}\sqrt{\frac{\partial g}{\partial\sigma_{ij}}\frac{\partial g}{\partial\sigma_{ij}}} \tag{18}$$

After obtaining $\Delta\gamma^{vp}$, the viscoplastic strain increment can be calculated and the total stress also can be determined.

Work Planned Next Quarter

We will continue the further development and refinement of the unified continuum model.

Subtask F3c-3: Multi-Scale Modeling (TAMU)

Progress This Quarter

No activity this quarter.

Work Planned Next Quarter

No work planned.

Work Element F3d: Calibration and Validation (TAMU, UNR, UWM, WRI)

Progress This Quarter

No activity this quarter.

Work Planned Next Quarter

No work planned.

PROGRAM AREA: ENGINEERED MATERIALS

CATEGORY E1: MODELING

Work element E1a: Analytical and Micro-mechanics Models for Mechanical Behavior of Mixtures (Year 1 start)

Subtask E1a-1: Analytical Micro-mechanical Models of Binder Properties (TAMU)

Progress This Quarter

A self-consistent micromechanics model has been developed to determine the bulk moduli and shear moduli of different types of aggregates. The theory of composite materials was used to obtain the upper bound and lower bounds of the fundamental properties of aggregates. Based on the upper and lower bounds of the aggregate moduli, self-consistent formulae were established for the three components of mixes, namely, aggregates, bitumen and air. In order to compute the bulk moduli and shear moduli of aggregates, the self-consistent formulae were programmed using the System Identification Method in the computer program MATLAB. The system identification process, which was modeled with a mathematical representation (self-consistent micromechanics model), was capable of calculating the bulk moduli and shear moduli of aggregates from resilient modulus tests made on mixes. A catalog of aggregate fundamental properties is under development; this catalog will address the bulk moduli and shear moduli of a variety of aggregates with different measures of shape, texture, angularity and gradation.

Work Planned Next Quarter

The planned activity for the next quarter is to continue developing the catalog of fundamental properties of a wide range of aggregates. Moduli data of mixes and binders will be collected from laboratory experiments that were made in related research projects. A series of experiments will be conducted to measure the properties of more mixes in order to include more types of aggregates in the catalog. This catalog will serve to determine the shear moduli and bulk moduli of mixes also using system identification method but in a forward approach.

Subtask E1a-2: Analytical Micro-mechanical Models of Modified Mastic Systems (TAMU)

Progress This Quarter

No activity this quarter.

Work Planned Next Quarter

No work planned.

Subtask E1a-3: Analytical Models of Mechanical Properties of Asphalt Mixtures (TAMU Year 2 start)

Progress This Quarter

No activity this quarter.

Work Planned Next Quarter

No work planned.

Subtask E1a-4: Analytical Model of Asphalt Mixture Response and Damage (TAMU Year 3 start)

Progress This Quarter

No activity this quarter.

Work Planned Next Quarter

No work planned.

Work element E1b: Binder Damage Resistance Characterization (DRC)

Subtask E1b-1: Rutting of Asphalt Binders (UWM)

Task Lead: Haifang Wen

Progress This Quarter

The team has extensively evaluated aspects of rutting for asphalt binder: (a) tertiary flow for asphalt binder, and (b) power law modeling of asphalt binders and asphaltic mixtures. The major findings are briefed here.

(a) Tertiary flow of asphalt binder.

Repeated creep and recovered tests were conducted on asphalt binders, using the parallel plate in Dynamic Shear Rheometer (DSR). Tertiary flow was clearly observed. However, when the parallel plate was replaced with cone plate, the tertiary flow disappeared. Figure E1b-1.1 shows the tests results on the same binder when parallel plate and cone plate were used, respectively. It can be seen that the creep strains from parallel plate test exhibited tertiary flow and diverted from the strains of cone plate tests in which no tertiary flow happened. Digital pictures were taken for both parallel plate and cone plate tests, as shown in figure E1b-1.2. It was found that material loss was severe when the parallel plate was used. The opposite was true for cone plate tests. For parallel tests, the cross section of asphalt binder specimens was reduced as the material flowed

away from the plate. It seems that the tertiary flow is partially a result of the change of geometry.

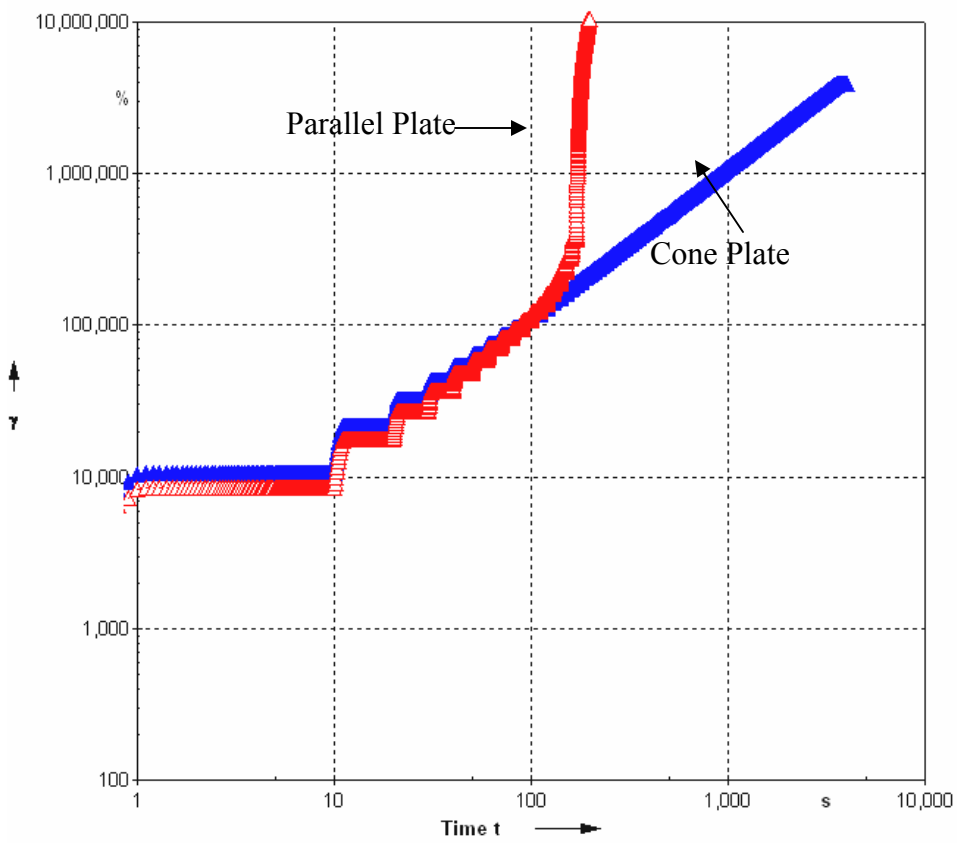

Figure E1b-1.1. Chart. Discrepancy of shear strains between parallel and cone plate under creep test.

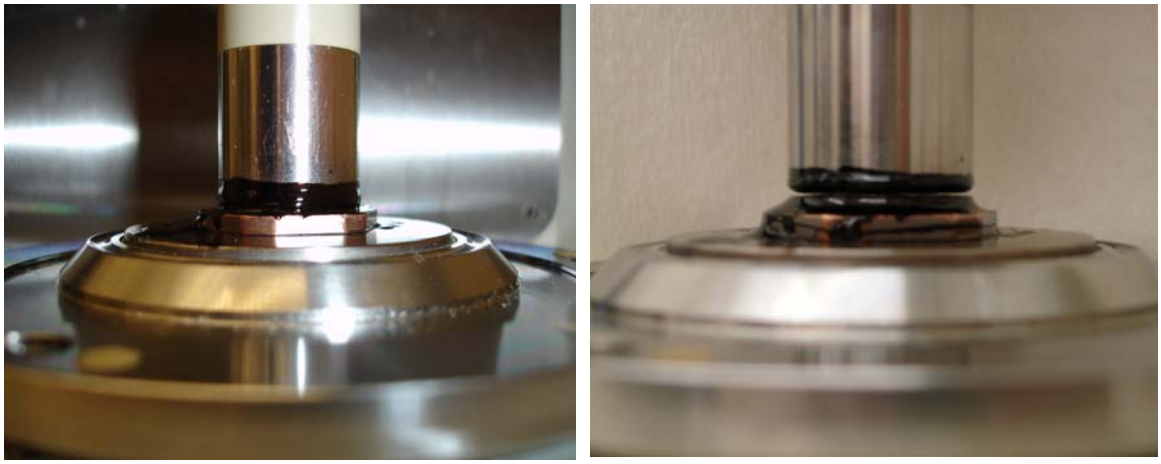

Figure E1b-1.2. Photos. Specimen before and after parallel plate tests.

(b) Power Law Modeling of Rutting of Asphalt Binder

Considering the linear shape of the curves in the log-log scale, nonlinear power representation seems to be the best fit for the behavior of the material. Nonlinear power representation is given by the following equation (Delgadillo 2007):

$$\gamma(t,\tau) = \sum_{i=1}^{m} k_i \cdot t^{n_i} \cdot \tau^{p_i}$$

Where: γ = shear strain
t = time
τ = shear stress
ki, ni, pi = constants

The number of arguments *m* to be used depends on the material. For the polymer modified binder, a value of *m* equals to two was found to be enough to describe the shape of the curves. This is logical considering that the curves show a linear shape with two different slopes.

Nonlinear fitting using was used to determine the parameters of the model. In order to give the same importance to the low strain/time range as to the high strain/time range, the fitting was weighed using the strain as the weighing variable. The fitting showed to be very good, with an R value of 0.998. The following equation shows the results of the nonlinear power law fitting.

$$\gamma = 2.3668 \cdot 10^{-4} \cdot t^{0.58717} \cdot \tau^{0.99412} + 1.8484 \cdot 10^{-19} \cdot t^{2.0019} \cdot \tau^{4.0265}$$

The first argument on the right side of the equation represents the behavior at low stress levels and shorter times. The power parameter on the stress variable is almost equal to one, which confirms the linear behavior on this region. The second argument on the right side of the equation represents the nonlinear behavior at higher stresses and longer loading times. Figure E1b-1.3 shows the results of the fitting of the shear strain using power law model.

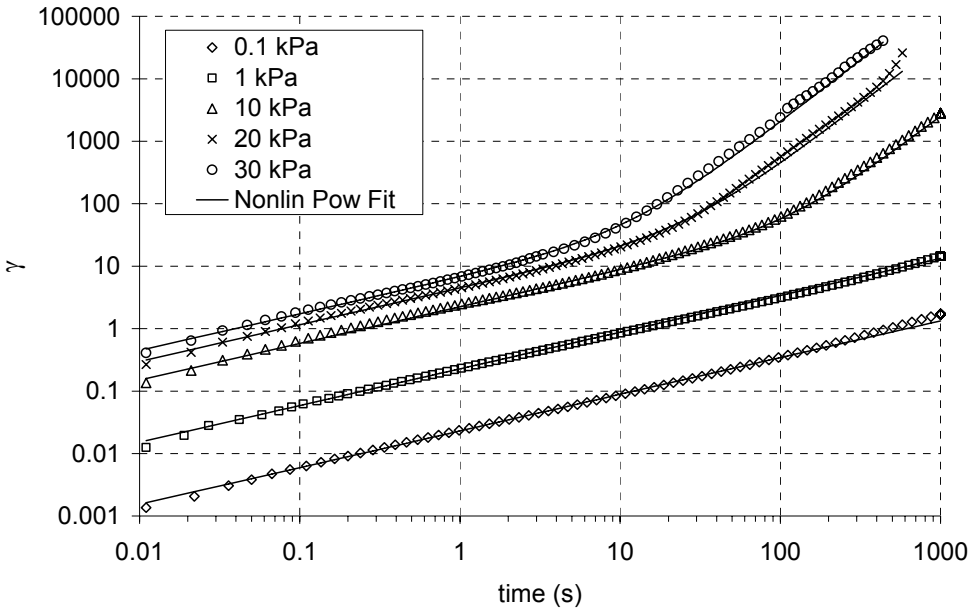

Figure E1b-1.3. Nonlinear Power Fitting, Creep Phase, Pg64-34 Binder, 1000 s Loading.

The creep compliance of the material can be obtained by dividing the shear strain by the shear stress, as follows:

$$J(t) = 2.3668 \cdot 10^{-4} \cdot t^{0.58717} \cdot \tau^{0.00588} + 1.8484 \cdot 10^{-19} \cdot t^{2.0019} \cdot \tau^{3.0265}$$

$$J(t) \approx 2.3668 \cdot 10^{-4} \cdot t^{0.58717} + 1.8484 \cdot 10^{-19} \cdot t^{2.0019} \cdot \tau^{3.0265}$$

Work Planned Next Quarter

The team will continue the experiments to include different binders and loading patterns for asphalt binders. In addition, analysis and modeling of rutting behavior will continue. The imaging analysis of the strain distribution will be obtained.

References

Delgadillo R.,2007, "Nonlinearity of Asphalt Binders and The Relationship with Asphalt Mixture Permanent Deformation," A preliminary document submitted in partial fulfillment of the requirement for the degree of Doctor of Philosophy (Civil and Environmental Engineering) at the University of Wisconsin – Madison, 2007.

Subtask E1b-2: Feasibility of Determining Rheological and Fracture Properties of Thin Films of Asphalt Binders and Mastics using Nano-indentation (UWM Year 2 start)

Task Lead: Dante Fratta

The behavior of asphalt mixtures is highly affected by the rheological and fracture properties of the asphalt mastic, the glue that holds together the aggregate skeleton in the composite asphalt mixture. The current asphalt binder specifications are based on mechanical tests performed on specimens with dimensions that are not representative of the scale of asphalt films found in a typical asphalt mixture, which is in the range of 13.5 μm to 600 μm (with 30 to 50% in the range of 13.5 to 17 μm). Presently, there are no standard nondestructive methodologies that address the determination of mechanical properties of asphalt thin films in an asphalt mixture.

The purpose of this study is to evaluate the usefulness of nano-indentation devices to measure asphalt binder or mastic properties. This work element will be conducted in collaboration with the University of Minnesota and it will focus on utilizing nano-indentation equipment available at the University of Minnesota or other research establishments for exploratory measurements. These measurements will be compared to measurements collected with conventional methods used today in the PG grading such as the DSR, BBR and the Direct Tension. The proposed nano-indentation methodology applied to binders could greatly improve QC/QA methods of accepting pavement materials after construction is complete. It will also simplify changing monitoring evaluation caused by aging or repeated loading while eliminating needs for expensive and destructive methods.

The proposed study has the following objectives:

- Determine the rheological and fracture properties of asphalt binders and mastics using nano-indentation measurements.
- Compare the rheological and fracture properties of asphalt mastics determined with the current PG grading test methods to the similar properties determined using nano-indentation.
- Develop a methodology for the systematic evaluation of viscoelastic properties of binders using the nanoindentation technique.

Activities This Quarter

The University of Wisconsin-Madison research team contacted the University of Minnesota to evaluate the potential of nano-indentation measurements to evaluate the rheological and fracture properties of binders. In a set of exploratory tests at 5 and 10 μm indentation, the results show a great amount of creep and stress relaxation (figures E1b-2.1 and E1b-2.2). The analysis of the curves yields the hardness H of the binder as (Li and Bhushan 2002; Pichler et al. 2005):

$$H = \frac{P}{A_c} = \frac{P}{\pi h_c^2 \tan^2(\theta)} \quad (1)$$

where P is the indenter normal force, A_c is the indenter projected horizontal area, h_c is the contact depth, and θ is the indenter half angle. The Young's modulus E is obtained from the initial part of the unloading part of the indentation curve $S=dP/dh_c$:

$$S = \beta \frac{2}{\sqrt{\pi}} \frac{E}{1-\nu^2} \sqrt{A_c} = \beta \frac{2}{\sqrt{\pi}} \frac{E}{1-\nu^2} \sqrt{\pi h_c^2 \tan^2(\theta)} \quad (2)$$

where β is constant that depends on the geometry of the intender and ν is the Poisson's ratio.

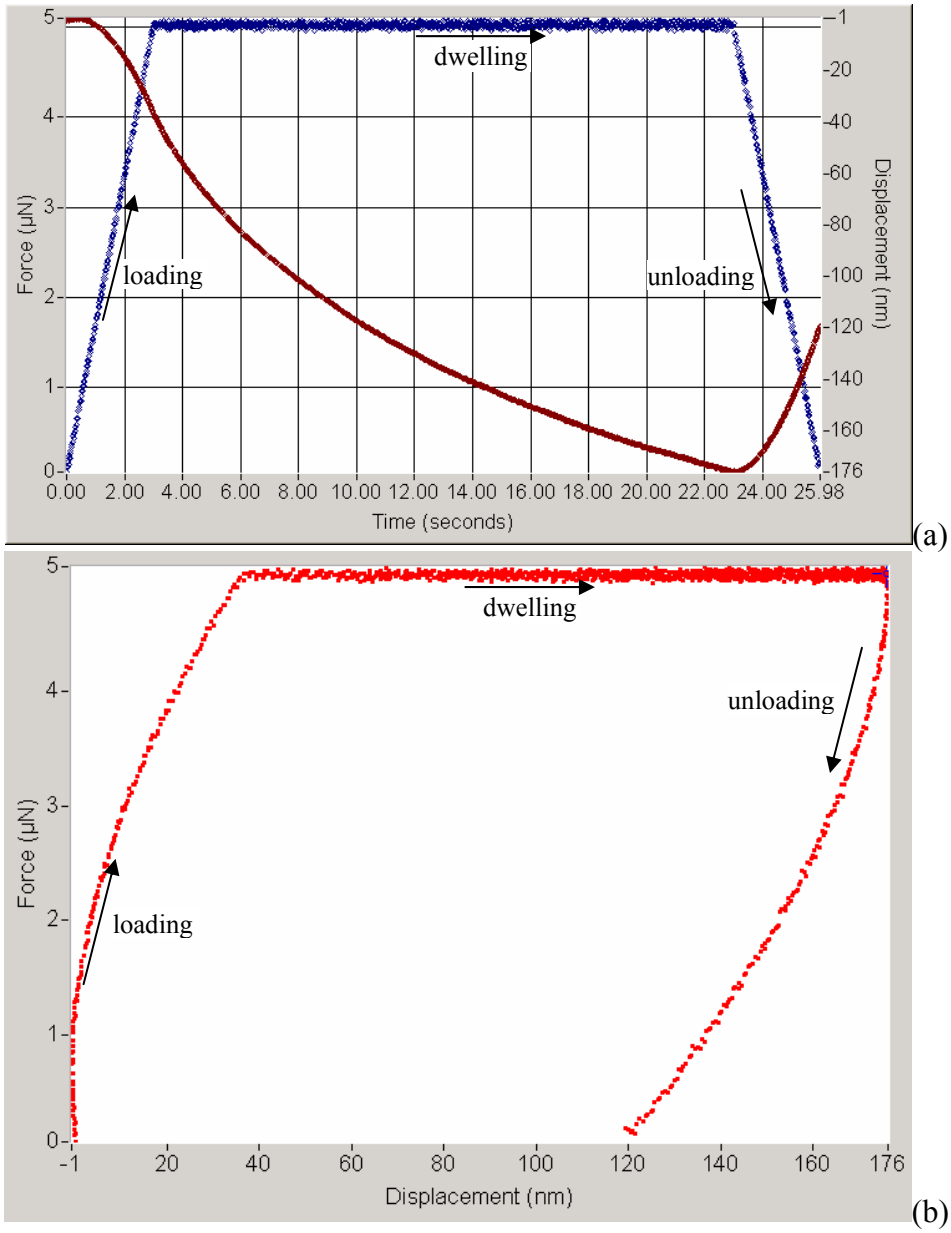

Figure E1b-2.1. Graph. 5 μN indentation results on BAY+filler with a 500 μm flat punch probe. (a) Force and displacement versus time and (b) force versus displacement.

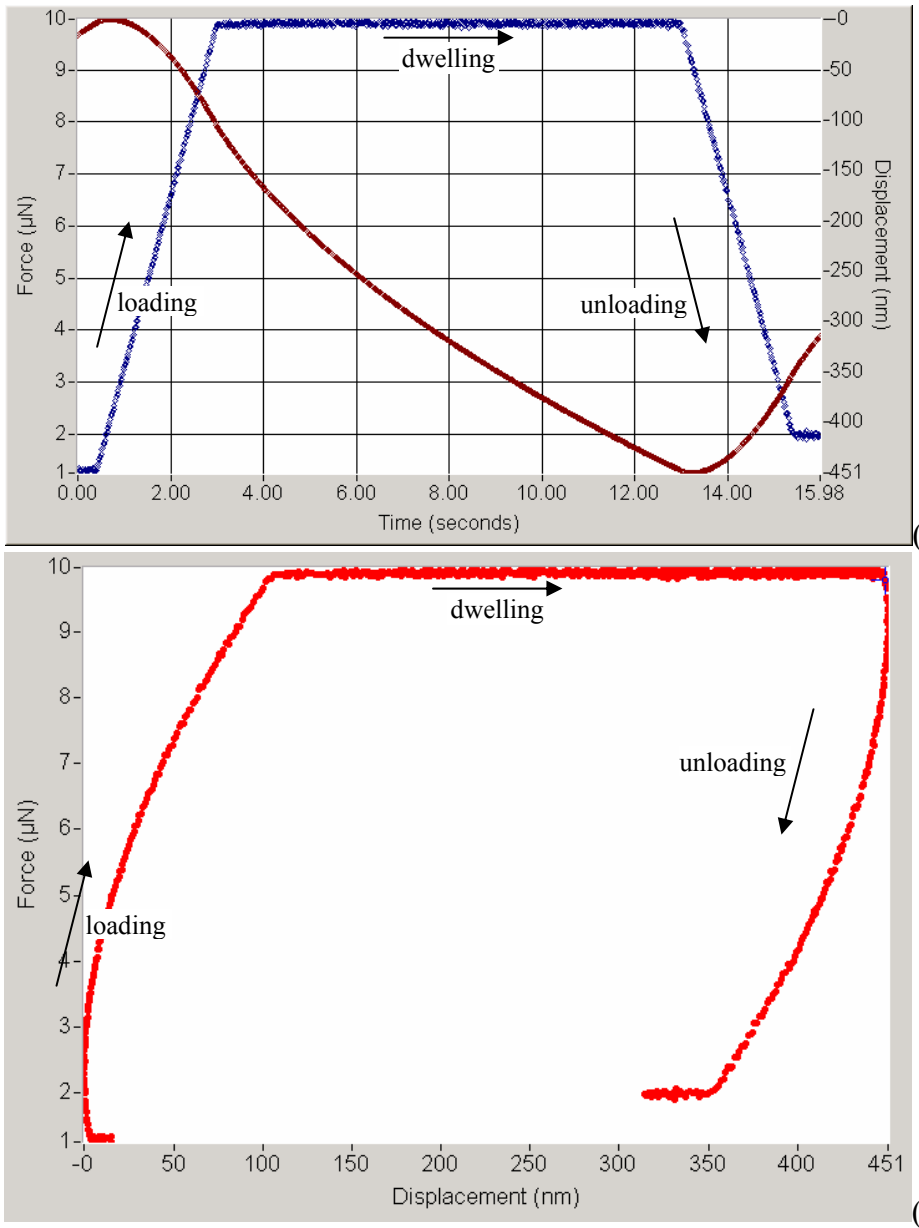

Figure E1b-2.2. Graph. 10 µN indentation results on BAY+filler with a 500 µN flat punch probe. (a) Force and displacement versus time and (b) force versus displacement

The viscosity η of the binder is obtained from fitting a three-parameter Kelvin-Voight model to the dwelling part of the nanoindentation curve (figure E1b-2.3 - Pichler et al. 2005) or alternatively by fitting a log of time model to the constant rate of loading part of the curve (Beake 2006). That is, the nanoindentation data can then be used to calculate the elastic stiffness along the unloading part of the curve, and the viscosity along the loading or dwelling parts of the curve (Li and Bhushan 2002; Pichler et al. 2005; Beake 2006). That is, the results can then be compared with data from DSR testing.

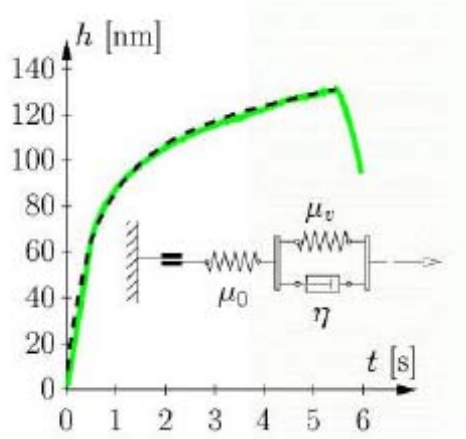

Figure E1b-2.3. Graph. Three-element Kelvin-Voigt model for the evaluation of the viscosity η of a binder during the constant load part of the nano-indentation curve (Pichlet et al. 2005).

One problem the technicians faced during testing was large adhesion between the binder sample and the indenter probe. To reduce/control the effect of adhesion on the probe, a drop of water was added to the surface of the binder sample.

These results seem to show some potential for the use of the nanoindentation technique to evaluate rheological properties of asphalt binder. Several more tests, including a small parametric study, will be run to further the evaluate potential of the nanoindentation technique for the evaluation of the viscoelastic and fracture properties of asphalt binders.

Problems Encountered and Solutions

The greatest problem faced during preliminary testing was the adhesion of the nanoindenter to the binder during testing. The technicians try to control this by adding a thin film of water between the binder and the indenter. The researchers will try to keep using this solution while evaluating possible effects of the water film on the measurements.

Work Next Quarter

During the first quarter of 2008, the research team will continue exploring nanoindentation and DSR testing for the evaluation and correlation rheological properties of binders at two different temperatures. As the nanoindentation and DSR methodologies do not measure the exact same material parameters (e.g., different size scales, different deformation modes, etc.), the research team will evaluate the differences in boundary condition, loading rates, and scales (McGennis et al. 1994; Lin et al. 2006). The Kelvin-Voigt model and logarithm of time method will be used to evaluate the rheological properties (Ashby and Jones 1996; Roberts et al. 1996; Li and Bhushan 2002; Pichler et al. 2005; Beake 2006).

References

Ashby, M. F., and D. R. H. Jones, 1995, *Engineering Materials 1*. Butterworth-Heinemann, 306 pp.

Beake, B., 2006, Modelling indentation creep of polymers: a phenomenological approach. *J. Phys. D: Appl. Phys.*, 39: 4478–4485.

Li, X., and B. Bhushan, 2002, A review of nanoindentation continuous stiffness measurement technique and its applications. *Materials Characterization*, 48(5): 11–36.

Lin, D. C., E. K. Dimitriadis, and F. Horkay, F., 2006, Advances in the mechanical characterization of soft materials by nanoindentation. *Recent Res. Devel. Biophys.*, 5(2006): ISBN: 81-7895-215-7.

McGennis, R. B., S. Shuler, and H. U. Bahia, 1994, *Background of SUPERPAVE Asphalt Binder Test Methods*. Federal Highway Administration Report No. FHWA-SA-94-069.

Pichler, C., A. Jager, R. Lackner, and J. Eberhardsteiner, 2005, Identification of Material Properties from Nanoindentation: Application to Bitumen and Cement Paste. *Proc.*, 22nd Danubia-Adria Symposium on Experimental Methods in Solid Mechanics, Sept. 28-Oct. 1, 2005, Moniticellu Terme, Parma, Italy.

Roberts, F. L., P. S. Kandhal, E. R. Brown, D.-T. Lee, and T. W. Kennedy, 1996, *Hot Mix Asphalt Materials, Mixtures, and Construction*. National Asphalt Pavement Association – Research and Education Foundation, Lanham, MD, 585 pp.

Work element E1c: Warm and Cold Mixes

Subtask E1c-1: Warm Mixtures (UWM)

Task Lead: Andrew Hanz

Progress This Quarter

Activities in the past quarter focused on the effects of both wax based (Sasobit) and a proprietary mineral based warm mix additives on asphalt binder properties. The preliminary study focused on the effects of both additives on mixing and compaction temperatures as measured in the Brookfield Viscometer. Furthermore, the effects of Sasobit on physical hardening and mineral based additives on binder rutting performance and mixture workability were investigated. The following is summary of the findings of each of these efforts.

Effects of Sasobit on Binder Viscosity and Mixing and Compaction Temperatures

The effects of Sasobit on binder viscosity were evaluated through assessment of the binder viscosity profiles for two different binder grades (PG 70-22) and concentrations (1% and 3%). Viscosity profiles were created for three temperatures: 105 ºC, 135 ºC, and 165 ºC. Figures E1c-1.1 and E1c-1.2 provide the viscosity profiles at the aforementioned testing temperatures for PG 70-22 and PG 70-28, respectively.

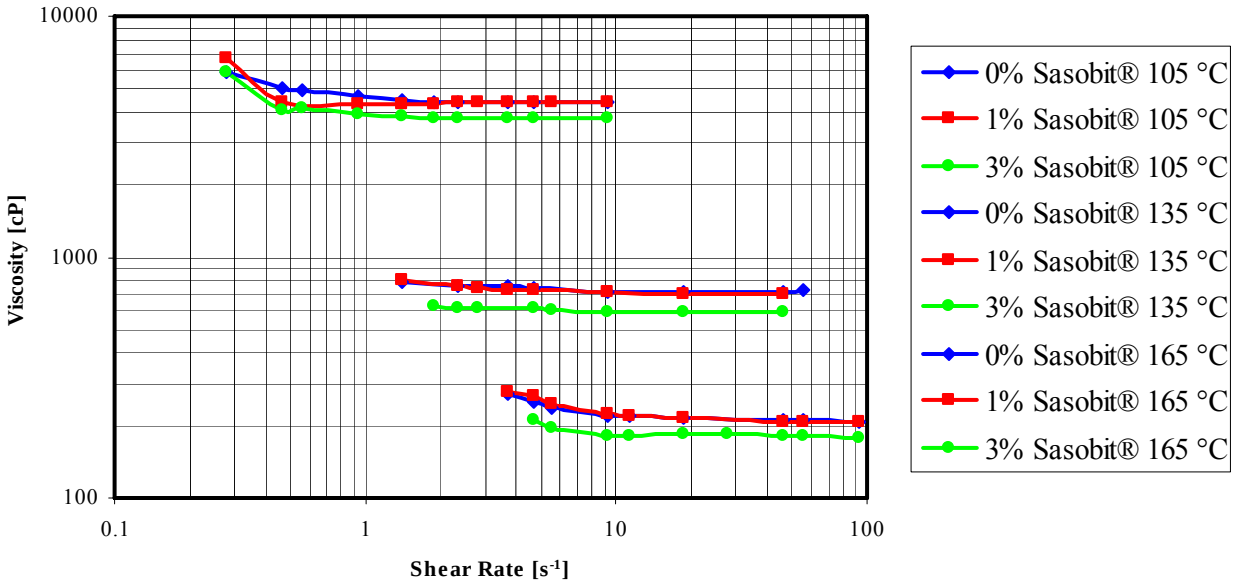

Figure E1c-1.1. Chart. Viscosity profile for PG 70-22.

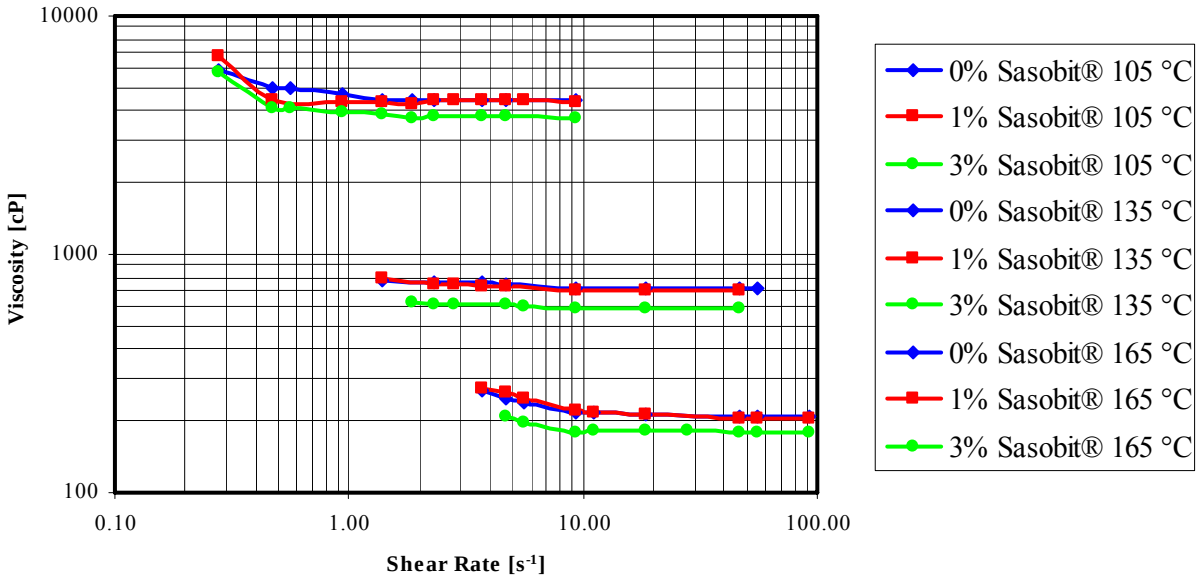

Figure E1c-1.2. Chart. Viscosity profile for PG 70-28 binder.

The viscosity profiles for both binder grades show virtually no effect of the addition of Sasobit on binder viscosity for all shear rates at concentrations lower than 3%. To investigate the relationship between the measured viscosity profiles and mixing and compaction temperatures, the methodology developed in NCHRP Project 9-10, which uses measurements of zero shear viscosity and curve fitting using the Cross Williamson Model, was applied. Table E1c-1.1 provides a summary of the mixing and compaction temperatures determined for a given Sasobit concentration and binder type.

Table E1c-1.1. Summary of estimated mixing and compaction temperatures for Sasobit.

		Sasobit Concentration		
Binder	**Temperature (C)**	**0%**	**1%**	**3%**
PG 70-22	Mixing	144.3	---	140.4
	Compaction	132	---	128.7
PG 70-28	Mixing	152.3	152.9	145.9
	Compaction	137	137.3	132.4

The data provided in Table E1c-1.1 shows only an approximately 4 ºC reduction in mixing and compaction temperatures for 3% Sasobit. Based on the extra cost of the additive and the potential reduction in low temperature binder performance, this reduction is not significant enough to justify the use of Sasobit. However, further work needs to be done to verify these results and investigate the effect of binder grade on the ability of Sasobit to reduce mixing and compaction temperatures.

Effects of Sasobit on Physical Hardening

The same binders and concentrations of Sasobit previously discussed were used to examine the effects of Sasobit on the physical hardening of asphalts. The conclusions of the study are as follows:

- The addition of Sasobit to the binder produces a significant increase of the stiffness, and a reduction of the m-value. The magnitude of this effect is almost identical for both RTFO and PAV aged samples, thus indicating a minor susceptibility of Sasobit to aging.
- BBR and glass transition tests show that Sasobit has a negligible influence on rate and magnitude of physical hardening. Specifically, the phenomenon is slightly intensified for PAV aged binders, while it is vaguely weaker for RTFO aged ones. This tendency is somehow more marked for the PG 70-22 asphalt.

- For the PG 70-28, the T_g of the Sasobit-modified binder is higher than the one of the original binder. The explanation could be that with the addition of the FT-wax (a glasslike material) the glassy region of the material is extended. On the other hand, the PG 70-22 shows an opposite behavior, proving (besides the non-optimal dispersion of the experimental data) the strong dependency on asphalt.
- Both asphalts exhibit clearly the occurrence of physical hardening, through the different T_g measured during cooling and heating processes. Furthermore, the free volume estimated during heating is always bigger than the one during cooling, revealing the free volume fraction which is lost in the isothermal conditioning period of 10 minutes.
- Future research should be focused on the dependency of physical hardening on the PG grade of the binder, the possible interference of Sasobit with previous modifying agents and the occurrence of physical hardening in WMA mixtures.

Mineral Based Additives Effects on Binder Viscosity

The effect of a proprietary mineral additive on binder mixing temperatures and the duration for which the effect is realized in the binder was measured through evaluation of binder viscosity at three prescribed shear rates (0.68, 2.04, and 6.80/s) at mixing times of 1 and 6 hours. Temperature was also varied (150 ºC, 115 ºC, and 90 ºC) to capture the temperature dependence on the rate of release of the water from the hydrated compound and its effects on reduction in binder viscosity. All tests were conducted using a PG 64-22 binder. Furthermore, anhydrous molecules of the mineral additives investigated were acquired to provide a control. The effect of the WAM additives on binder viscosity is communicated in figure E1c-1.3 as a plot of the ratio of Vneat/Vadditive for a given shear rate.

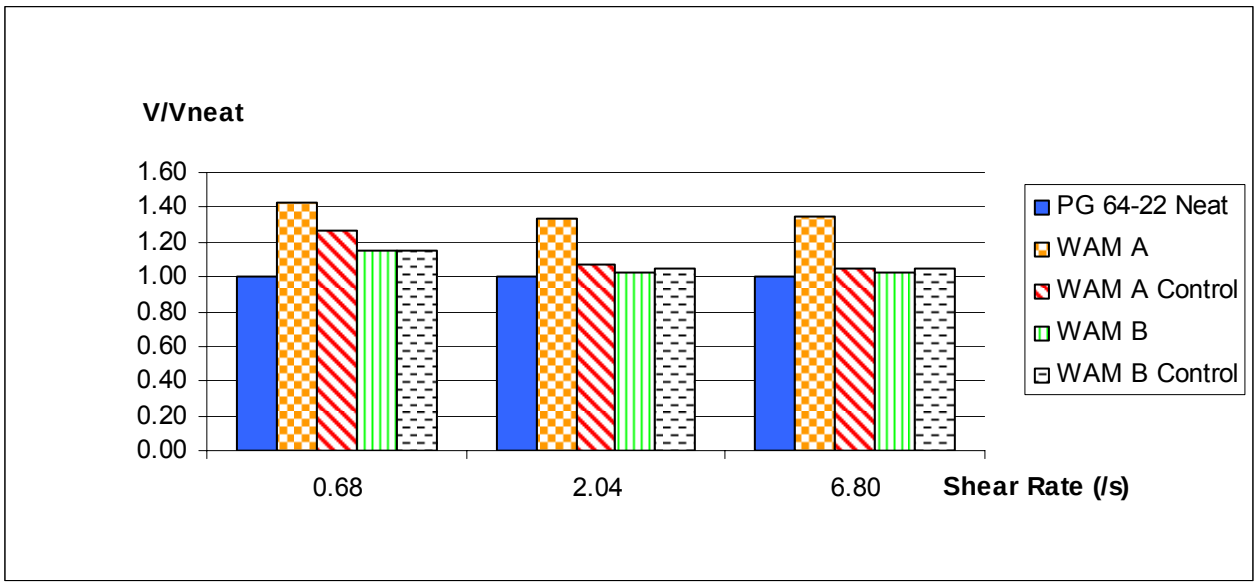

Figure E1c.1-3. Chart. Plot of viscosity ratio for 115 ºC mixing temperature and 1 hour conditioning time.

For all shear rates, addition of the warm mix additive did not result in a reduction in viscosity. In fact, in most cases viscosity increased, possibly due to the effect of the mineral filler used as a delivery system for the hydrated compound. As expected, reduction in viscosity was also not realized after 6 hours conditioning time. The main finding from this investigation is that other test methods for quantifying the effect of water based warm mix additives on mixing and compaction temperatures must be researched as part of this work plan. New potential methods are being developed in NCHRP Project 9-39, and the applicability of these methods to water based warm mix additives will be developed upon delivery of the final report, which is due June 30, 2008.

Mineral Based Additives – Effect on Binder Rutting Performance

The effect of mineral based warm mix additives on binder performance was evaluated through a frequency sweep (0.5 to 20 Hz) at testing temperatures of 40 ºC, 52 ºC, 64 ºC, and 76 ºC using 40 mm parallel plate geometry in the Dynamic Shear Rheometer. The frequency sweep was chosen as an evaluation tool for binder performance over the conventional rutting parameter of G*/sind because it allows for more comprehensive characterization of binder performance through development of master curves using time temperature superposition, while still allowing for determination of the Superpave rutting parameter. An example of master curves generated using this testing procedure is provided in figure E1c-1.5.

Master curve data generated in figure E1c-1.5 shows that the warm mix additive as no significant effect on binder performance. The significant finding from this aspect of the research is the development of a test method that has the ability to characterize binder performance that can be used to for both wax based and water based warm mix additives as the study moves forward.

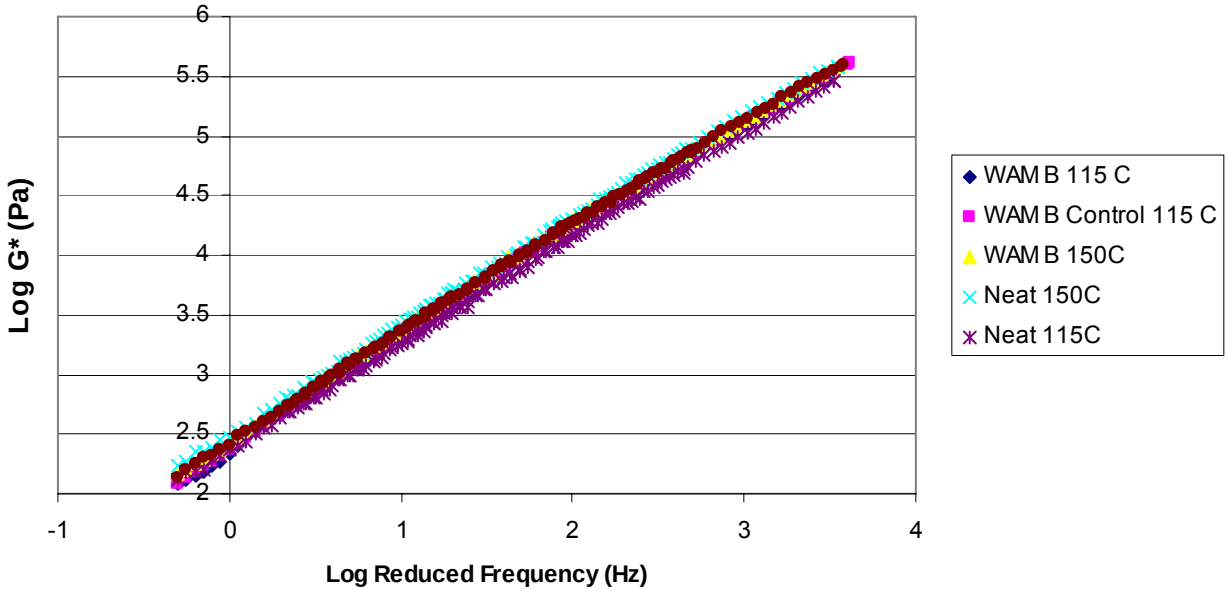

Figure E1c-1.5. Chart. Master curve comparison of neat binder and WAM B at 115 ºC and 150 ºC mixing temperatures.

The lack of effect of the proprietary warm mix additive on binder performance is further verified through analysis of the Superpave rutting parameter (G*/sind) and phase angle (d) at a frequency of 10 rad/s at the previously mentioned testing temperatures. Figures E1c-1.6 and E1c-1.7 provide the change in the rutting parameter and phase angle at 150 ºC, respectively.

Both figures show no significant effects of the mineral based warm mix additive on binder performance in terms of phase angle or the Superpave rutting parameters. Similar results for 115 ºC and 90 ºC additive mixing temperatures were found.

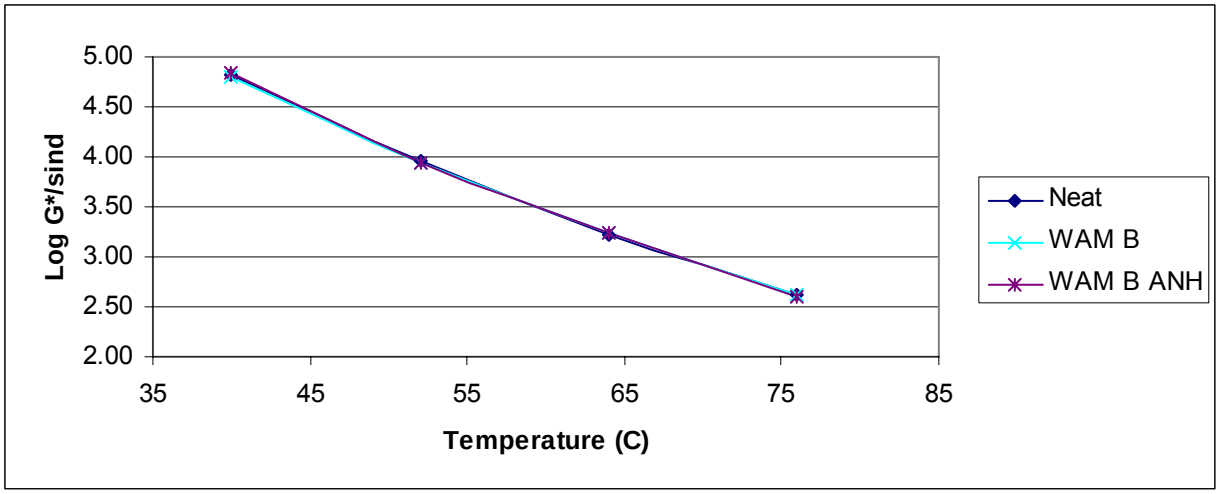

Figure E1c-1.6. Chart. Comparison of G*/sind for neat binder at 150 ºC mixing temperature.

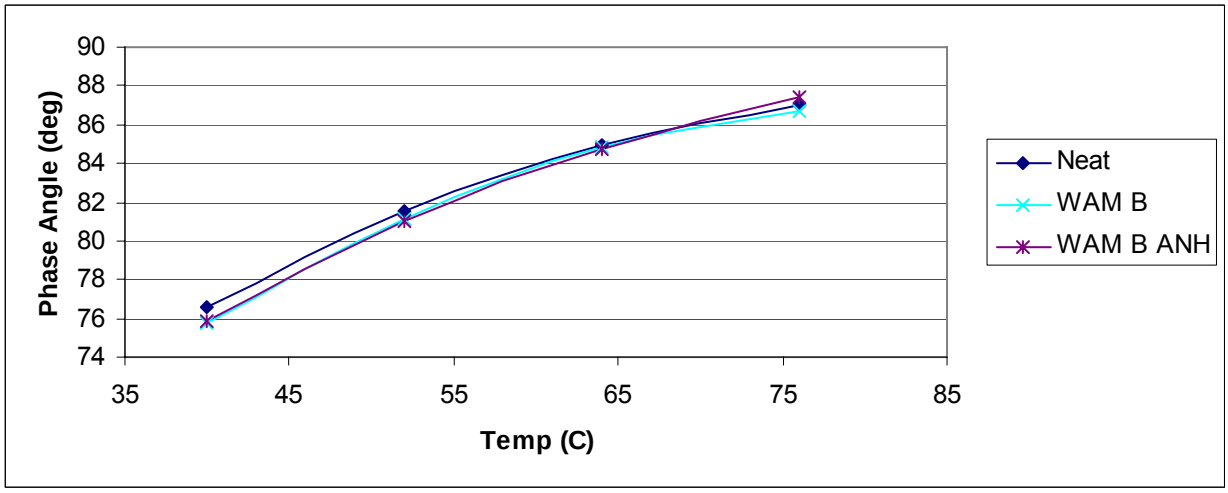

Figure E1c-1.7. Comparison of phase angle for neat binder at 150 ºC mixing temperature.

Effects of Proprietary Warm Mix Additive on Mixture Workability and Performance

The effect of the warm mix additive on mixture workability and performance was investigated through use of the Construction Densification Index (CDI) and Traffic Densification Index (TDI). These indices use the area under the compaction curve for different density thresholds to estimate mixture workability during field compaction (88% Gmm – 92% Gmm) and mixture stability (92% Gmm – 98% Gmm). For this initial investigation an 12.5 mm E10 mix design from a granite source in central Wisconsin was used. Mixes were prepared with neat PG64-22 binder, WAM B, and WAM B Anhydrous additives. All mixes were compacted at a temperature of 125 ºC. Mixture workability was measured in terms of air voids at different gyration levels (Nini, Ndes, and Nmax) and CDI. Mixture workability was evaluated through the TDI. Results of the analysis are provided in figures E1c-1.7 through E1c-1.9.

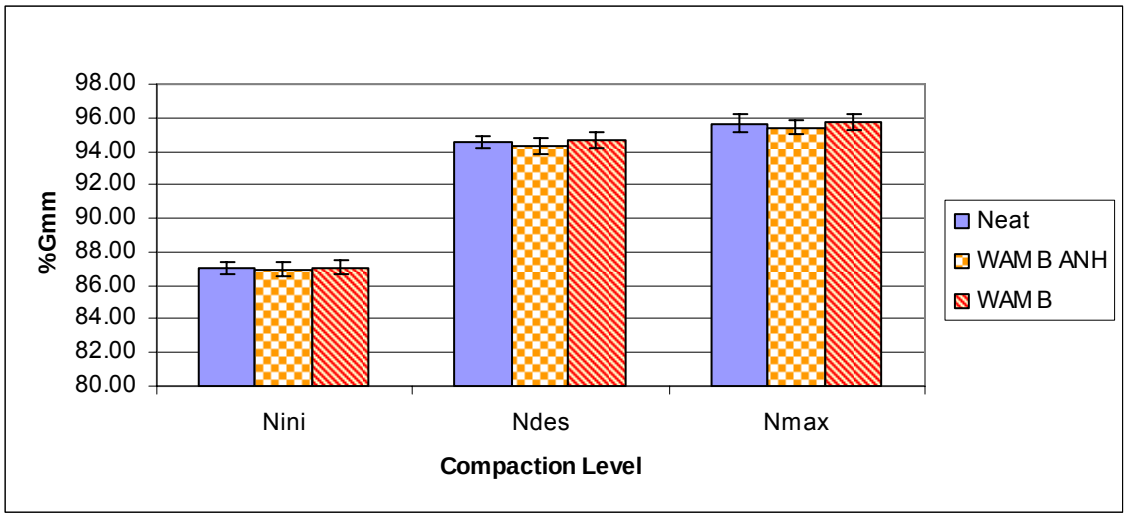

Figure E1c-1.7. Chart. Air voids comparison of warm mix additives at different gyration levels.

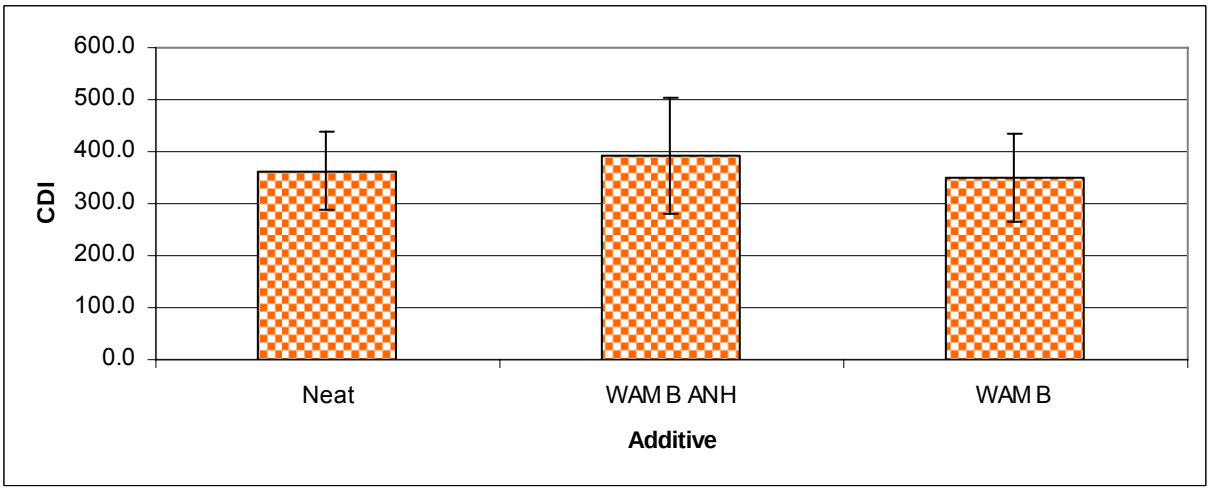

Figure E1c-1.8. Chart. Comparison of CDI for different warm mix additives.

Review of figures E1c-1.7 and E1c-1.8 conclude that the warm mix additives show no significant enhancement to mixture workability during compaction as measured by both air voids and the CDI. Two replicates were compacted for each mix, with the spread between measurements shown in the form of y error bars for all mixes. A wider range of additives and mix designs must be tested for full evaluation of warm mix technologies.

Figure E1c-1.9 uses the traffic densification index (TDI) to investigate the impact of warm mix additives on mixture stability. The TDI was found to correlate well to laboratory measurements of rutting as measured by the Flow Number.

Figure E1c-1.9 found no significant differences in mixture stability as measured by the TDI. Conclusions from this preliminary investigation will be verified through actual mixture Flow Number Testing.

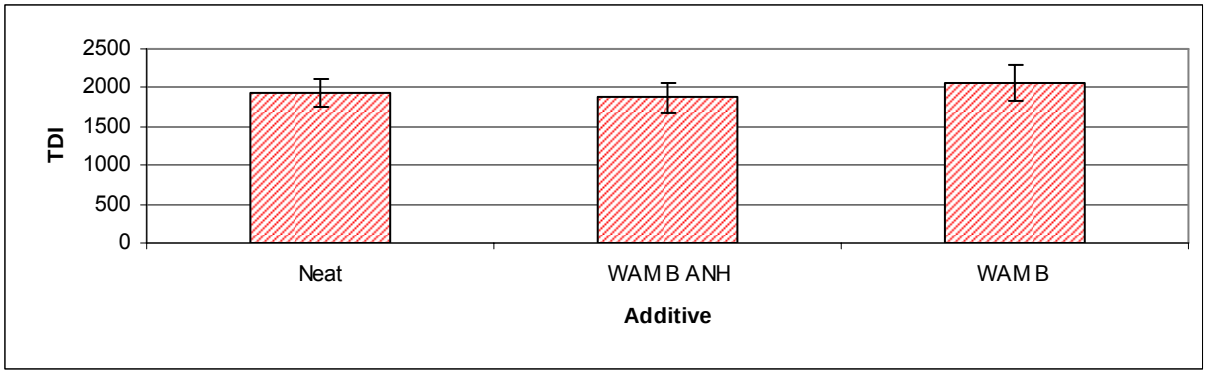

Figure E1c-1.9. Chart. Comparison of TDI for different warm mix additives.

Materials Selection

The UW research team met and identified materials needs in terms of type and quantity to satisfy the requirements of the year 1 work plan. The following is a summary of the materials needs and quantities.

Asphalt Binders (10 Gallons for Each Grade)

- PG 64-22, PG 58-28, PG 58-22, PG 46-28, PG 46-34.

Modifiers

- Polymers (5lbs each)
    - D1101K Linear SBS
    - D1184K Radial SBS
    - Elvaloy AM
    - Elvaloy 4170

- Polyphosphoric Acid (0.2 lbs each)
    - 85% PPA
    - 105% PPA
    - 115% PPA

Warm Mix Additives (20 Kg Each)

- Sasobit and Sasoflex
- Asphaltan B
- Proprietary Warm mix Additive (previously investigated)
- Asphamin

Aggregate (1 ton of each)

- Granite, Gravel, Limestone

Meetings

On December 12-13, UW attended the FHWA Warm Mix Technical Working Group meeting in Baltimore, MD as a friend of the committee. Recent developments in the available technologies were provided by material suppliers and research updates in terms of both laboratory investigations and field studies were given by AAT, MTE, NCAT, and others. The UW plans to stay involved in this committee to enhance coordination between the efforts in the ARC work plan and other FHWA efforts regarding warm mix technologies.

Year 2 Work Plan Development

The findings of preliminary investigations conducted in year one and the comments from the ETG were considered to develop a work plan for Year 2. The Year 2 work plan includes a detailed experimental design and addresses the need to validate laboratory efforts with field trials.

Problems Encountered and Solutions

Problem/Solution: Discovery and development of a laboratory test method for measurement of mixing and compaction temperatures to mimic the mixing and placement temperature reduction realized in the field. Based on activities in Year 1 it is clear that viscosity alone is not able to quantify the lubrication effects of these additives, thus the following new testing methods will be evaluated.

- Casola Method: Developed as part of NCHRP 9-39. Final report for NCHRP Project is pending. However, the procedure was outlined in a presentation given to the South East Asphalt User Producer Group on November 14, 2007.

- Reinke Test Method: Uses a thin film in the DSR (25 microns) and quantifies lubrication as the change in normal force as the machine rotates at a given frequency.
- Other UW Developments: Investigate the use of aggregate surfaces or mineral fillers to incorporate the aggregate effect into binder measurements.

Problem/Solution: Selection of additives and other warm mix technologies consistent with current industry and agency practice. Attendance at the FHWA Warm Mix Technical Working Group Meeting provided insight to the current state of the practice. Based on information presented at this meeting UW is considering the addition of Advera, a mineral based additive similar to Asphamin and Evotherm to the testing matrix.

Work Planned Next Quarter

Work next quarter will focus on the following tasks:

Evaluation of new testing methods for Measurement of Mixing and Compaction Temperatures

The previously mentioned testing methods will be evaluated using the binders, modifiers, and warm mix additives specified for this study. Results in terms of reduction in mixing and compaction temperatures will be compared to the viscosity measurements specified in Superpave and zero shear viscosity predictions of mixing and compaction temperatures specified in NCHRP Project 9-10.

Further Investigation of Mixture Workability using the Construction Densification and Force Indices

All additives specified in the materials needs list will be used to prepare mixes using the same aggregate blend (E10 12.5 mm granite) used for workability evaluation in the previous quarter. Use of all the additives for the same mix will provide a ranking of additive performance in terms of CDI. If no significant additive effect is found, other methods of workability measurement will be pursued.

Development and Population of Materials Reference Library

Proceedings of the FHWA Warm Mix TWG will be considered in finalizing the materials needs for this project. The final list will be used to obtain, catalog, and store the materials needed to complete the project.

Finalize Year 2 Work Plan

The Year 2 work plan will be finalized and submitted to FHWA for review. It is expected that the ETGs will provide comments on the year two work plans by the end of the quarter. All ETG comments will be addressed in a timely fashion.

References

Bahia, H., D. Hanson, M. Zeng, H. Zhai, M. A. Khatiri, and R. M. Anderson, 2001, Characterization of Modified Binders in SuperPave Mix Design. NCHRP Report No. 459. Transportation Research Boards, Asphalt Institute.

Faheem, A, H. Bahia, and H. Ajideh, 2005, Estimating Results of a Proposed Simple Performance Test for Hot-Mix Asphalt from SuperPave Gyratory Compactor Results. WisDOT Study 0092-01-02, Wisconsin Department of Transportation, Madison, WI.

Subtask E1c-2: Development and Evaluation of a Volumetric Mix Design Process for Cold Mix Asphalt (UWM, UNR)

Task Lead: Andrew Hanz

Progress This Quarter

During Year 1, the focus was put on collecting information on emulsions, surface treatments and cold mixtures. The process for information gathering involved a comprehensive literature search and review, visits and interview of experts in the United States and abroad, and attending various workshops or meetings related to the subject. These efforts have resulted in a concept paper in which a system of performance grading of emulsions is proposed. Also, a tentative list for performance measures has been established. To contribute to these efforts, the research team attended the following meetings in the previous quarter:

- October 8: Meeting at Sem Materials in Tulsa, OK to discuss application of Cold Mix Technologies and research needs.
- October 23: UW/UNR ARC Project Meeting: Discuss project and initial draft of year 2 work plan.
- November 7-8: AEMA Workshop, Las Vegas Nevada. General overview of cold mix technologies and discussion of Year 2 work plan with Sem Materials.
- December 5-6: AEMA Workshop, Industry Hills, CA. Finalize Year 2 work plan in meeting with Dr. Kim Jenkins, UNR, and Sem Materials.

Through these efforts two applications of cold asphalt technologies have been identified: spray and mixing. Based on this concept two types of emulsion grades can be introduced as shown in table E1c-2. The types of application in which each of these two emulsion grades are used are listed in the table.

Table E1c-2.1: Grades and applications of emulsified asphalts.

Grade	Application
Spray	Chip Seals
	Microsurfacing
	Crack Sealing
Mixing	Full Depth Recycling
	Partial Depth Recycling
	Asphalt Stabilized Base Course
	Paving Applications as a Binder or Surface Course

Activities this quarter also allowed for the definition of physical properties of emulsions that are important to the design and construction of the various applications were developed and a tentative list is shown in table E1c-2.1. The definition of the parameter to be used and the proposed test methods to measure these properties are also summarized. The properties are divided into two categories: (1) construction properties, which covers emulsion characteristics related to the construction process, and (2) in-service properties, which are related to performance during traffic.

Discussion of the validity and practicality of these concepts allowed for development of the Year 2 work plan. It was decided to separate evaluation and performance standards based on whether the emulsion was used in a spray or mixing application. Development of the Year 2 work plan also included consideration of ETG comments, a separate memorandum detailing how these comments will be addressed is being developed and will be submitted to FHWA. The entire Year 2 work plan will be submitted in early 2008 for ETG review and comment. It is expected that ETG comments will be received in mid-March.

Table E1c-2.2: Summary of pertinent construction and in-service properties for surface treatments.

Engineering Property	Parameter(s) Measured	Comments
Construction Properties		
Storage Stability (ASTM D6930)	%Stability defined as the difference in residue at the top and bottom of the storage vessel after 24 hours.	Emulsions must remain homegenous and fluid during the transport and construction. Unstable emulsions will result in difficulties spraying, breaking, and wetting of aggregates.
Breaking Rate	Change in binder stiffness (G*) at a given temperature and curing time.	Inert, basic (limestone), and acidic (granite) fillers will be used to evaluate the effects of aggregate mineralogy on breaking rate. Temperature sensitivity will also be investigated.
Spray-ability and Drain Out	Viscosity	Binder must have an optimum range of viscosity which is low enough to allow for application and high enough to prevent drain out off the road.
Wetting of Aggregates	Adhesion	PATTI test will be used to evaluate the adhesion of different emulsion/aggregate combinations.
In-Service Properties		
Resistance to Bleeding	Creep Stiffness Early Adhesion	Binder stiffness and adhesion characteristics during emulsion curing may identify potential bleeding problems.
Restistance to Raveling	Residual Binder Cohesion Wet Adhesion of Residual asphalt to aggregate	Raveling is either caused by binder softness (lack of cohesion) or lack of adhesion. Proposed testing addresses both causes.
Fatigue Cracking	Creep Stiffness Estimated Rate of Creep Stiffness Elongation at Break	Excessive cracking will greatly increase the permeability of the surface treatment leading to premature failures.
Aging	Change in rheological properties due to short and long term aging.	The effects of aging on the performance of the residual binder must be understood and applied to design of surface treatments.

Problems Encountered and Solutions

A major problem encountered was definition and procurement of emulsions representative of materials used in the field. Discussion with industry indicated that there are many different emulsions used, and those emulsions are adjusted based on field conditions. Discussion with Sem Materials allowed for identification of commonly used emulsions for use in evaluation of testing methods for constructability and performance. The emulsions will be produced by Sem Materials to ensure that consistency is maintained between laboratory investigation and application to the field. Arrangements have been made to pick up emulsions from Sem Materials labs to ensure that they do not freeze during shipping.

Another problem encountered was the definition of a research approach to define and evaluate the constructability and in-service properties of emulsions relevant to different applications. To address this problem, laboratory and field evaluation of emulsions will be split into spray grade and mixing grade categories.

Work Planned Next Quarter

The next quarter will focus on completion of review of literature and standards and the creation of an international advisory group.

Review of national and international standards for emulsions, aggregates, and performance evaluation of cold asphalt applications.

There many standard test methods and local specifications that are used all over the world. It is important to collect these standards and analyze similarities and differences in these standards as a starting point to develop rational methods and standards. Because cold asphalt applications vary in components and intended purpose, the review in this task will address three areas:

Subtask: Review testing methods, standards, and specifications related to asphalt emulsions.

Subtask: Review testing methods, standards, and specifications related to aggregates used in cold asphalt applications such as surface treatments and CMA.

Subtask: Review testing methods, standards, and specifications related to performance evaluation of cold mix applications including surface treatments and CMA.

Create an international advisory group for the project

A significant part of emulsion testing and applications are based on experience of various individuals, contractors, and suppliers. Very little is documented in publications. It is thus necessary to create an advisory group to identify the critical gaps in the knowledge and guide the research to change some of the tests that are specified today but have no real relationship to performance. The advisory group could help simplify testing and focus specifications on important and relevant properties. The advisory group will meet twice a year at convenient location and in coordination with annual conferences to review progress and provide feedback. The group will also serve as the link to AEMA, ISSA, and other organizations that have a stake in this field.

Figure E1c-2.1 provides the structure for how the tasks completed next quarter relate to the overall research project. More detail is provided in the Year 2 work plan.

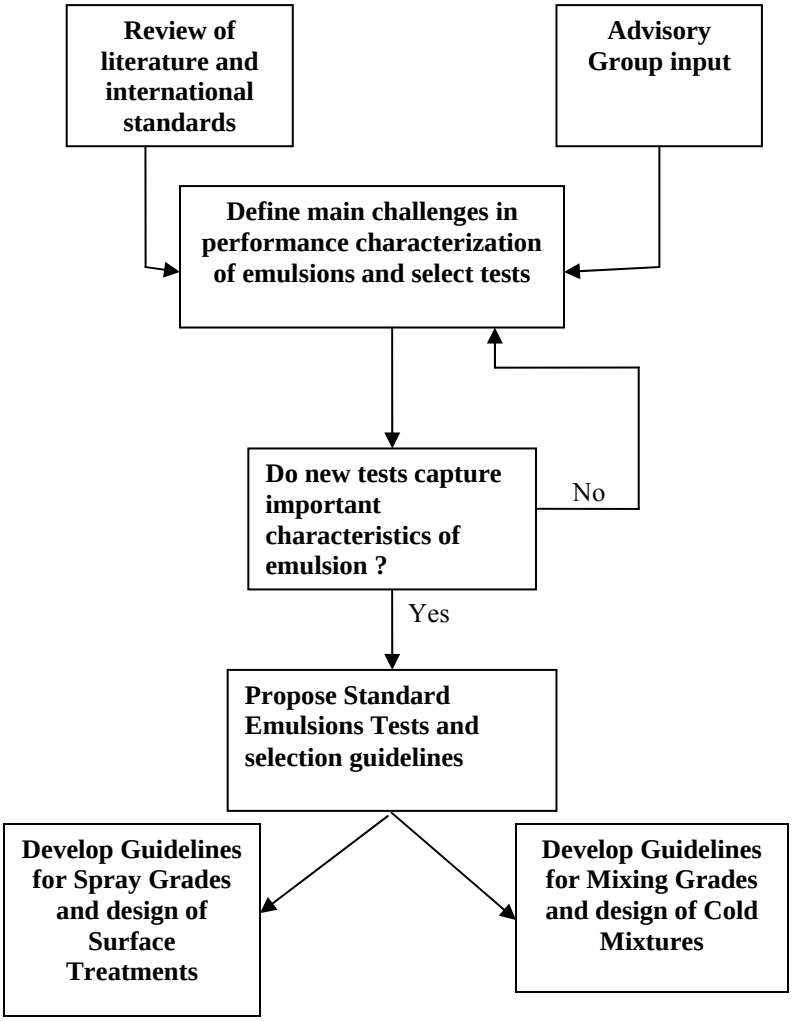

Figure E1c-2.1. Chart. Flow chart of research methodology.

References

Asphalt Institute, 1989, *Asphalt Cold Mix Manual*. Asphalt Institute, Lexington, KY.

ASTM D3628. "Selection and Use of Emulsified Asphalts." Annual Book of ASTM Standards, 2006, American Society for Testing and Materials, Philadelphia, PA.

ASTM D4867. "Standard Test Method for Effect of Moisture on Asphalt Concrete Paving Mixtures." Annual Book of ASTM Standards, Vol. 04.03, American Society for Testing and Materials, Philadelphia, PA.

ASTM D7196. "Standard Test Method for Raveling of Col Mixed Bituminous Emulsion Samples." Annual Book of ASTM Standards, 2006, American Society for Testing and Materials, Philadelphia, PA.

Jenkins K. J., Molenaar, A, de Groot, Van de Ven, 2002, Foamed Asphalt Produced Using Warmed Aggregates. Association of Asphalt Paving Technologists, Colorado Springs, CO 2002.

CATEGORY E2: DESIGN GUIDANCE

Work element E2a: Comparison of Modification Techniques (UWM Year 2 start)

Progress This Quarter

No activity this quarter.

Work Planned Next Quarter

No work planned.

Work element E2b: Design System for HMA Containing a High Percentage of RAP Material (UNR, UWM, WRI, AAT Year 1 Start)

Subtask E2b-1: Develop a System to Evaluate the Properties of RAP Materials

Progress This Quarter

Identify Materials: The following RAP sources were identified and sampled in this quarter:

- One RAP source from South Carolina that fits the category of unmodified-stiff.
- One RAP source from Southern California that fits the category of unmodified-very stiff.

Research Meeting: UNR researchers visited UWM researchers on October 22-23, 2007 and discussed the experimental plan to use the BBR and DSR in evaluating the properties of the RAP binders.

Laboratory Evaluation: In an effort to identify the feasibility of using the BBR for testing RAP mortars, samples were prepared composed of RAP (-#8) material and virgin binder. BBR beam specimens were a challenge to make using the RAP mortar. The -#8 aggregate in the mortar was too large for the standard BBR beam specimen dimensions. Modification of the BBR beam specimen dimensions were made by reconfiguring the standard BBR mold pieces to create a specimen with end cross-sectional dimensions of ~12.7mm x 12.7mm. This configuration involved using 3 of the standard bottom mold pieces and 4 standard mold end pieces. BBR beam specimens were successfully produced using this mold arrangement, which led to the

development of a modified BBR beam specimen mold. The following is the mold shop drawings and also a picture of the finished product.

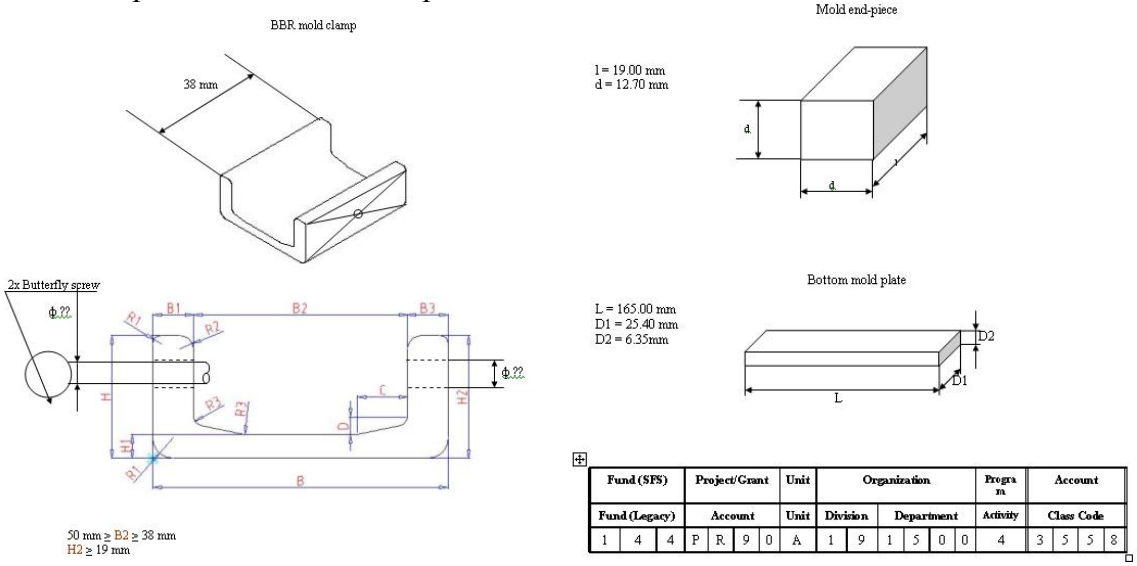

Fund (SFS)			Project/Grant				Unit	Organization						Progra m	Account			
Fund (Legacy)			Account				Unit	Division		Department				Activity	Class Code			
1	4	4	P	R	9	0	A	1	9	1	5	0	0	4	3	5	5	8

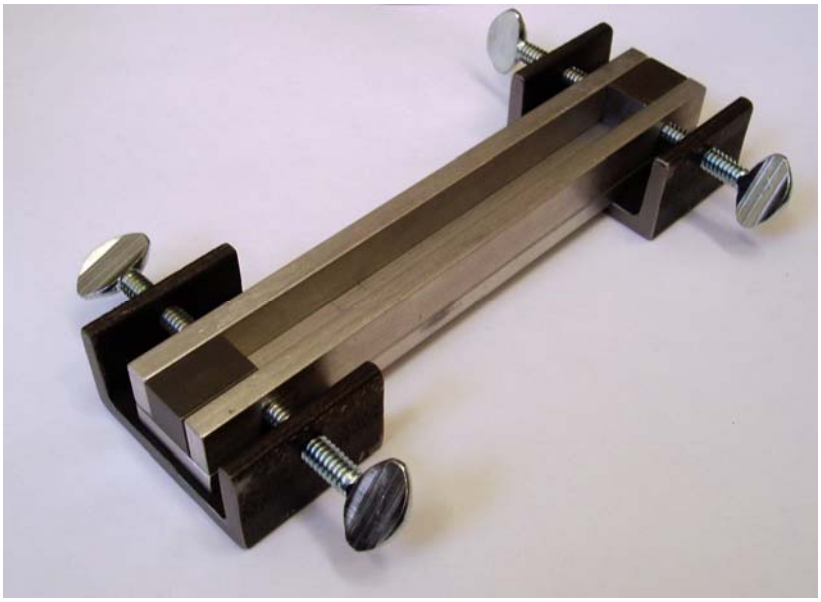

Work Planned Next Quarter

Continue the identification and sampling of the RAP materials. Continue the development of the BBR and DSR testing of RAP materials. Start the experiment on the impact of extraction method on the properties of RAP aggregates.

Subtask E2b-2: Compatibility of RAP and Virgin Binders (WRI Year 2 start)

Progress This Quarter

No activity this quarter.

Work Planned Next Quarter

No work planned.

Subtask E2b-3: Develop a Mix Design Procedure (UNR)

Progress This Quarter

No activity this quarter.

Work Planned Next Quarter

No work planned.

Subtask E2b-4: Impact of RAP Materials on Performance of Mixtures

Progress This Quarter

No activity this quarter.

Work Planned Next Quarter

No work planned.

Subtask E2b-5: Field Trials

Progress This Quarter

Laboratory Evaluation: The objective of this evaluation is to assess the feasibility of designing HMA mixtures containing 20 and 40% RAP without changing the PG grade of the virgin binder. Using a single Wisconsin HMA plant aggregate source, three comparable HMA mixtures were developed that meet WisDOT 12.5 mm E-3 mix design specifications. The four aggregate mixture components were: a 5/8" granite rock, manufactured sand, a natural sand and RAP. The three mixtures that were developed were a "Virgin", 20% RAP, and 40% RAP. Using the same aggregates and blending the mixes so that the final mixture gradations were similar allowed the three mixes to be evaluated based on the percentage of RAP that was incorporated into the mix. The following graphic shows the gradations of the three mixes.

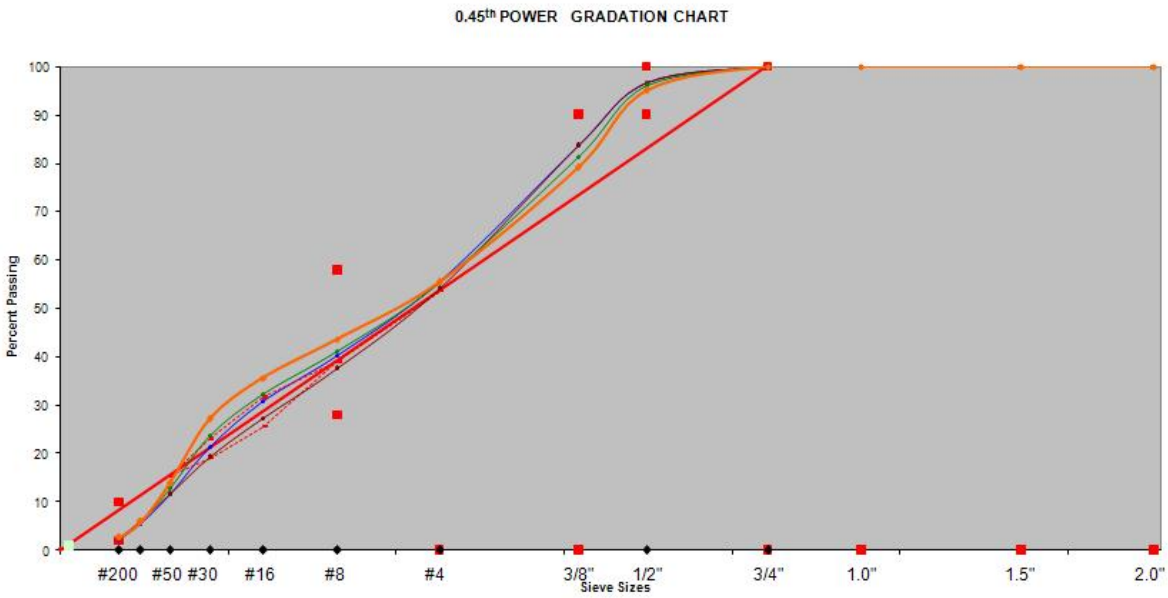

All of the mixtures met WisDOT specifications for an E-3 Superpave mix, showing that it is possible to make a HMA mixture with 40% RAP content. The same virgin binder (PG58-28) was used for all three mixes, e.g., no binder grade adjustments for the RAP contents. After completion of the mix designs, test specimens were made so that the three mixtures could be evaluated based upon moisture damage testing (AASHTO T-283), Superpave gyratory compactor (SGC) compaction data analysis (CDI and TDI), and a low temperature indirect tension testing. The following are the results from the moisture damage testing:

Moisture Damage Analysis

Specimen	Condition	t	D	P	S_t	TSR
Virgin 1	wet	4.83	6	8350	183	
Virgin 2	wet	4.82	6	8900	196	
Virgin 3	dry	4.79	6	8700	193	
Virgin 4	dry	4.79	6	9300	206	95.14
20% RAP a	wet	4.67	6	9600	218	
20% RAP b	wet	4.79	6	8800	195	
20% RAP c	dry	4.72	6	9900	223	
20% RAP d	dry	4.75	6	9350	209	95.74
40% RAP a	wet	4.64	6	8800	201	
40% RAP b	wet	4.66	6	8800	200	
40% RAP c	dry	4.74	6	9200	206	
40% RAP d	dry	4.72	6	9300	209	96.77

This testing shows that all of the mixes pass the moisture damage specification requirements and that there is no significant difference among the mixtures.

The next set of testing utilized the SGC compaction data by analyzing it to compute the compaction densification index (CDI) and the traffic densification index (TDI). This analysis can be done graphically by comparing the SGC compaction curves over the appropriate gyration intervals. The following graphics show the results of the CDI and TDI analysis respectively.

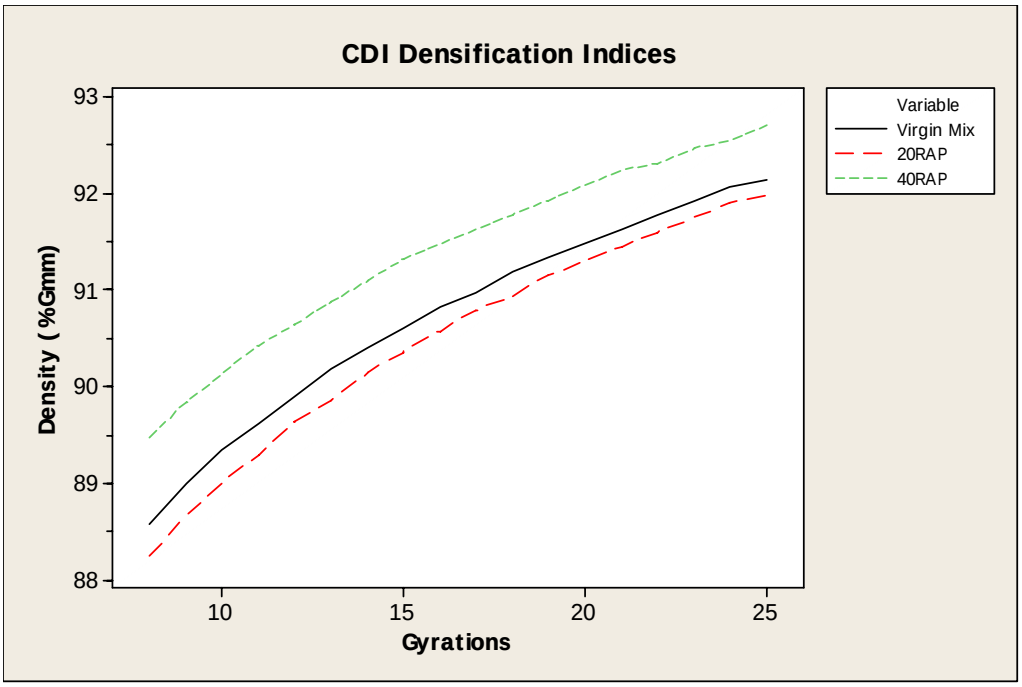

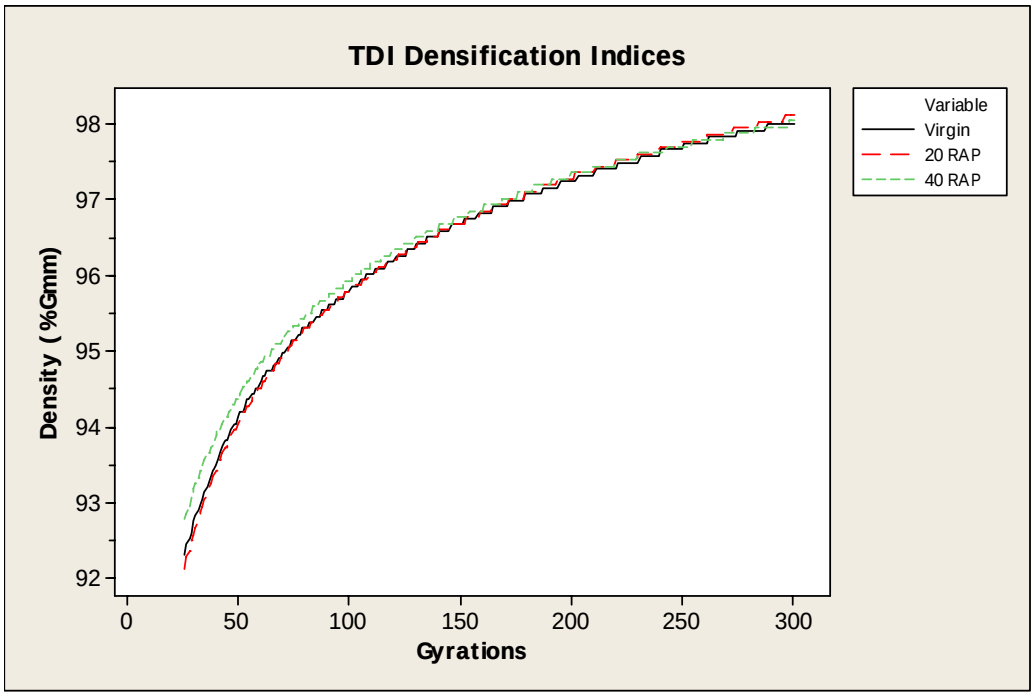

The CDI graphic shows that the area under the 40% RAP curve is the largest, indicating that it would be the most difficult to compact and work with during the paving process. The 20% RAP

and Virgin mixtures are fairly similar, indicating that it would probably be difficult to distinguish between the two mixes in the field. The TDI graphic shows that the area under the 40% RAP curve is slightly larger, indicating that it would be the most resistant to traffic rutting. The SGC compaction data analysis indicates that HMA mixtures with higher amounts of RAP tend to be stiffer than comparable virgin mixes.

A final mixture performance test was conducted on the three mixes. The test involved freezing the test specimens to 0°C for 12 hours and testing their tensile strength using an indirect tension test. The results of the testing are as follows:

Low Temperature IDT Analysis					
Specimen	t	D	P	S_t	Avg S_t
Virgin 1	4.65	6	6700	153	
Virgin 2	4.68	6	8100	184	168
20% RAP 1	4.67	6	8300	189	
20% RAP 2	4.64	6	7300	167	178
40% RAP 1	4.54	6	8300	194	
40% RAP 2	4.6	6	7900	182	188

These testing results indicate that all three mixtures exhibit statistically similar tensile strengths at 0°C temperature.

In summary, the findings from the initial mix design and mixture performance testing that was done indicate that the use of high percentages (up to 40%) of RAP without changing the PG grade of the virgin binder does not appear to have detrimental effects on the performance of the HMA mixture in resisting moisture damage and thermal cracking. However, two facts must be noted on this evaluation; 1) the RAP is from Wisconsin which may not be highly aged, and 2) the fatigue resistance of these mixtures will have to be evaluated.

A cost analysis using these mix designs was also done to identify potential HMA mix material cost savings by utilizing RAP. The costs used in this analysis are representative for Wisconsin at the time of the analysis and are summarized below:

Mixture	Rock	Man Sand	Natural Sand	RAP	Mixture Aggregate Cost	Mixture %AC	Virgin %AC Added	Total Mixture Cost
Virgin	25%	65%	10%	0%	$6.85	4.8%	4.8%	$23.65
20% RAP	25%	50%	5%	20%	$6.35	4.7%	3.9%	$20.00
40% RAP	25%	30%	5%	40%	$5.65	3.8%	2.2%	$13.35

As the table indicates, there is ~15% cost savings between the 20% RAP and the Virgin mixture mainly due to a 0.9% reduction in virgin asphalt usage. However, a 40% RAP mixture was able

to be designed with similar mixture volumetrics as the virgin mix by using 2.6% less virgin asphalt than the virgin mix. This results in an overall savings of ~43% per ton of mixture produced using a virgin asphalt price of $350 per ton. The aggregate savings accounts for ~12% of the total ~43% cost savings.

Work Planned Next Quarter

Evaluate the fatigue resistance of the Wisconsin mixtures with 0, 20, and 40% RAP.

Work element E2c: Critically Designed HMA Mixtures (UNR Year 1 start)

Subtask E2c-1: Identify the Critical Conditions

Progress This Quarter

Load Distribution during Braking of an Eighteen-Wheel Truck: This effort consisted of determining the load distributions on the various axles of tractor-semitrailer (i.e. 18-wheeler) as it travels on any given slope (i.e. downhill, uphill, or level) with the impact of braking. In comparison with a two-axle vehicle, the braking characteristics of a tractor-semitrailer are significantly more complex. For a given two-axle vehicle, the load transfer is only a function of the deceleration rate, whereas for a tractor-semitrailer, the load transfer during braking is dependent not only on the deceleration rate, but also on the braking force of the semitrailer.

Braking decelerates the vehicle, which causes load to transfer to the front of the vehicle. The resulting axle load can be higher or lower than the initial static load, depending on the location of the axle. Figure E2c-1.1 shows the major forces acting on an eighteen-wheel tractor-semitrailer during braking on a sloping pavement. Since Brakes are the primary source of braking deceleration, the aerodynamic drag and rolling resistance are neglected in this study. The various axles include: the tractor steering axle, the tractor tandem axle (i.e. driving axle), and the semitrailer tandem axle (i.e. trailer axle). The tandem axles of the tractor and the semitrailer are considered without equalization, implying that an inter-axle load transfer will take place between the rear and the front axle of the tandem group during the braking period of the truck (Wong 1993).

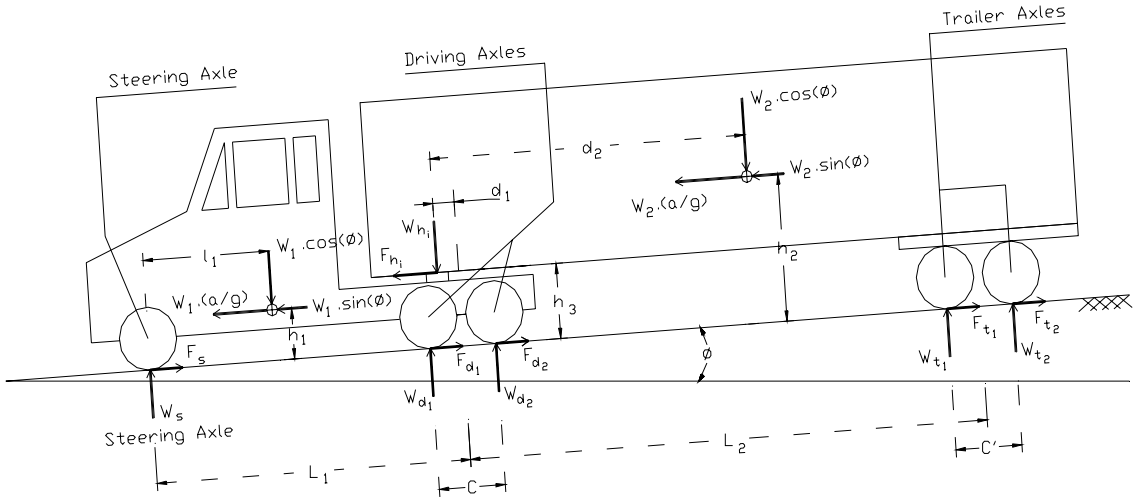

Figure E2c-1.1. Forces acting on a tractor-semitrailer during braking.

W_{h_i} and F_{h_i} are respectively the vertical and horizontal loads at the tractor-semitrailer articulation; "a" is the linear deceleration of the truck along the longitudinal axis; g is the deceleration due to gravity; W_1 and W_2 are respectively the tractor and semitrailer total weights; and θ is the angle of the slope with the horizontal (zero for level, positive for downhill and negative for uphill). W_s,, W_{d_1}, W_{d_2}, W_{t_1} and W_{t_2} are the tires normal loads. F_s,, F_{d_1}, F_{d_2}, F_{t_1} and F_{t_2} are the braking forces that originate from the brake system and developed on the tire-road interface.

In order to calculate the normal load on each axle, the tractor and the semitrailer are considered as free bodies separately and combined. The vertical, horizontal, and moment equilibrium equations for the tractor, semitrailer unit, and tractor-semitrailer combination can be written as a function of truck loads and geometry resulting in a total of eleven equilibrium equations, three characteristic equations, and fourteen unknowns (Hajj 2005).

For the tractor, the vertical and horizontal equilibrium are given by equations 1 and 2, respectively. The moment equilibrium around the rear and front tandem axle are given by equations 3 and 4, respectively.

$$W_s + W_{d_1} + W_{d_2} = W_1\cos\theta + W_{h_i} \tag{1}$$

$$F_s + F_{d_1} + F_{d_2} = \frac{a}{g}W_1 + W_1\sin\theta + F_{h_i} \tag{2}$$

$$W_s\left(L_1 + \frac{c}{2}\right) + W_{d_1}c = \frac{a}{g}W_1h_1 + W_1\left(L_1 + \frac{c}{2} - l_1\right)\cos\theta + W_1h_1\sin\theta + F_{h_i}h_3 + W_{h_i}\left(\frac{c}{2} + d_1\right) \tag{3}$$

$$W_s\left(L_1-\frac{c}{2}\right)+W_{h_i}\left(\frac{c}{2}-d_1\right)=\frac{a}{g}W_1h_1+W_1\left(L_1-\frac{c}{2}-l_1\right)\cos\theta+W_1h_1\sin\theta+F_{h_i}h_3+W_{d_2}c \quad (4)$$

For the semitrailer unit, the vertical and horizontal equilibrium are given by equations 5 and 6, respectively. The moment equilibrium around the front support point of the semitrailer and the trailer rear axle are given by equations 7 and 8, respectively.

$$W_{t_1}+W_{t_2}+W_{h_i}=W_2\cos\theta \quad (5)$$

$$F_{t_1}+F_{t_2}+F_{h_i}=\frac{a}{g}W_2+W_2\sin\theta \quad (6)$$

$$W_2d_2\cos\theta+F_{h_i}h_3=\frac{a}{g}W_2h_2+W_2h_2\sin\theta+W_{t_1}\left(L_2-\frac{c'}{2}+d_1\right)+W_{t_2}\left(L_2+\frac{c'}{2}+d_1\right) \quad (7)$$

$$W_{h_i}\left(L_2+d_1+\frac{c'}{2}\right)+F_{h_i}h_3+W_{t_1}c'=\frac{a}{g}W_2h_2+W_2h_2\sin\theta+W_2\left(d_2+L_2+\frac{c'}{2}-d_2\right)\cos\theta \quad (8)$$

For the tractor-semitrailer combination, the vertical and horizontal equilibrium are given by equations 9 and 10, respectively. The moment equilibrium around the steering axle is given by equation 11.

$$W_s+W_{d_1}+W_{d_2}+W_{t_1}+W_{t_2}=W_1\cos\theta+W_2\cos\theta \quad (9)$$

$$F_s+F_{d_1}+F_{d_2}+F_{t_1}+F_{t_2}=\frac{a}{g}(W_1+W_2)+(W_1+W_2)\sin\theta \quad (10)$$

$$\begin{aligned}W_1l_1\cos\theta+W_2(L_1+d_2-d_1)\cos\theta=&\frac{a}{g}W_1h_1+\frac{a}{g}W_2h_2+W_1h_1\sin\theta+W_2h_2\sin\theta\\&+W_{d_1}\left(L_1-\frac{c}{2}\right)+W_{d_2}\left(L_1+\frac{c}{2}\right)\\&+W_{t_1}\left(L_1+L_2-\frac{c'}{2}\right)+W_{t_2}\left(L_1+L_2+\frac{c'}{2}\right)\end{aligned} \quad (11)$$

From the above equations, the normal loads on the various axles can be expressed as follows:

Tractor front axle (steering axle),

$$W_s = W_2 \frac{\left[\left(a/g+\sin\theta\right)\left(h_2 d_1 + h_3 L_2\right) + d_1 \cos\theta\left(L_2 + d_1 - d_2\right)\right]}{L_1\left(L_2 + d_1\right)} + W_1 \frac{\left[\left(a/g+\sin\theta\right)h_1 + \left(L_1 - l_1\right)\cos\theta\right]}{L_1} - \left(F_{t_1} + F_{t_2}\right)\frac{h_3 L_2}{L_1\left(L_2 + d_1\right)} - \left(W_{t_1} - W_{t_2}\right)\frac{c' d_1}{2L_1\left(L_2 + d_1\right)} - \left(W_{d_1} - W_{d_2}\right)\frac{c}{2L_1} \tag{12}$$

Tractor rear axles (driving axles),

$$W_d = W_{d_1} + W_{d_2} = -W_2 \frac{\left[\left(a/g+\sin\theta\right)\left(h_2\left(d_1 - L_1\right) + h_3\left(L_1 + L_2\right)\right) + \left(d_1 - L_1\right)\left(L_2 + d_1 - d_2\right)\cos\theta\right]}{L_1\left(L_2 + d_1\right)} - W_1 \frac{\left[\left(a/g+\sin\theta\right)h_1 - l_1\cos\theta\right]}{L_1} + \left(F_{t_1} + F_{t_2}\right)\frac{h_3\left(L_1 + L_2\right)}{L_1\left(L_2 + d_1\right)} - \left(W_{t_1} - W_{t_2}\right)\frac{c'\left(L_1 - d_1\right)}{2L_1\left(L_2 + d_1\right)} + \left(W_{d_1} - W_{d_2}\right)\frac{c}{2L_1} \tag{13}$$

$$W_{d_1} = W_1 \frac{\left[-\left(a/g+\sin\theta\right)\left(h_3 - h_1\right) + \left(L_1 - l_1 - d_1\right)\cos\theta\right]}{c} + \left(F_s + F_{d_1} + F_{d_2}\right)\frac{h_3}{c} - W_s \frac{\left(L_1 - d_1\right)}{c} + W_d \frac{\left(d_1 + c/2\right)}{c} \tag{14}$$

$$W_{d_2} = W_1 \frac{\left[\left(a/g+\sin\theta\right)\left(h_3 - h_1\right) - \left(L_1 - l_1 - d_1\right)\cos\theta\right]}{c} - \left(F_s + F_{d_1} + F_{d_2}\right)\frac{h_3}{c} + W_s \frac{\left(L_1 - d_1\right)}{c} + W_d \frac{\left(c/2 - d_1\right)}{c} \tag{15}$$

Semitrailer axles (trailer axles),

$$W_t = W_{t_1} + W_{t_2} = W_2 \frac{\left[-\left(h_2 - h_3\right)\left(a/g+\sin\theta\right) + d_2\cos\theta\right]}{\left(L_2 + d_1\right)} - \left(F_{t_1} + F_{t_2}\right)\frac{h_3}{\left(L_2 + d_1\right)} + \left(W_{t_1} - W_{t_2}\right)\frac{c'}{2\left(L_2 + d_1\right)} \tag{16}$$

$$W_{t_1} = W_2 \frac{\left[\left(h_2 - h_3\right)\left(a/g+\sin\theta\right) - d_2\cos\theta\right]}{c'} + W_t \frac{\left(L_2 + d_1 + c'/2\right)}{c'} + \left(F_{t_1} + F_{t_2}\right)\frac{h_3}{c'} \tag{17}$$

$$W_{t_2} = W_2 \frac{\left[-\left(h_2 - h_3\right)\left(a/g + \sin\theta\right) + d_2\cos\theta\right]}{c'} - W_t \frac{\left(L_2 + d_1 - c'/2\right)}{c'} - \left(F_{t_1} + F_{t_2}\right)\frac{h_3}{c'} \quad (18)$$

The calculation of the normal loads on the various axles of the downhill braking 18-wheeler truck requires that the following characteristic properties be specified:

- Application (treadle) versus actuation (chamber) pressure at each axle: the application pressure is defined as the pressure produced at the output of the treadle valve, whereas the actuation pressure is the pressure experienced at the brake chamber. In the case where some sort of proportioning valve is used, these two pressures will differ significantly (Gillespie 1992; Gillespie and Balderas 1987).
- Brake force versus actuation pressure for the brakes on each axle: the braking force developed at the tire-road interface is determined by the actuation pressure applied to each brake and the gain of each (Gillespie 1992; Gillespie and Balderas 1987).

The braking force on individual wheels can be described by the following equation:

$$F_b = \frac{T_b}{r} = G\frac{P_{ac}}{r} \quad (19)$$

where, F_b = Brake force (lb), T_b = Brake torque (in-lb), r = Tire rolling radius (inch), G = Brake gain (in-lb/psi), and P_{ac} = Actuation pressure (psi).

The braking system properties of a standard United State (U.S.) 18-wheeler truck are taken from a National Highway Traffic Safety Administration (NHTSA) report that was conducted by T. D. Gillespie et al. (Gillespie and Balderas 1987). The NHTSA study considered a linear brake system (i.e., linear relationship between the application and the actuation pressure). Table E2c-1.1 summarizes the brake system properties of the U.S. eighteen-wheel.

Table E2c-1.1. Summary of a U.S. tractor-semitrailer brake system properties.

Truck unit	Axle	Torque gain[+] (in-lb/psi)	Pushout pressure (psi)
Tractor	Steering	1322.5	13.5
	Tandem leading driving	3280.0	5.8
	Tandem trailing driving	3280.0	5.8
Semi-trailer	Tandem leading trailer	2818.8	5.5
	Tandem trailing trailer	2818.8	5.5

[+] For a loaded truck-semitrailer

The extent to which vertical load is transferred during braking from the rear tandem tires to the front tandem tires is called the dynamic load transfer coefficient (α) and is defined as follows (Gillespie and Balderas 1987).

$$\alpha = \frac{W_{t_1} - W_{t_2}}{2\left(F_{t_1} + F_{t_2}\right)} = \frac{W_{d_1} - W_{d_2}}{2\left(F_{d_1} + F_{d_2}\right)} \quad (20)$$

The load transfer coefficient has a value of 0.0 when the loads on the front and rear tandem tires are equal (i.e., $W_{t_1} = W_{t_2}$; $W_{d_1} = W_{d_2}$).

By solving the system of equilibrium equations, the normal loads on the various axles during braking on a slope can be expressed as a function of W_1, W_2, a, θ, braking forces, and truck geometry.

Work Planned Next Quarter

Using the above derived equations to define the axle loads of an 18-wheeler traveling on level and sloped roads and to conduct the mechanistic analyses to identify the critical loading conditions of the 18-wheeler truck traveling at various speeds on level and sloped roads.

References

Gillespie, T. D., 1992, *Fundamentals of Vehicle Dynamics*, Textbook, ISBN 1-56091-199-9.

Gillespie, T. D., and L. Balderas, 1987, An Analytical Comparison of the Dynamic Performance of a European Heavy Vehicle and a Generic U.S. Heavy Vehicle. The University of Michigan Transportation Research Institute, Report No. UMTRI-87-17.

Hajj, E. Y., 2005, "Hot Mix Asphalt Mixtures for Nevada's Intersections," Dissertation, University of Nevada, Reno.

Wong, J. Y., 1993, *Theory of Ground Vehicles*, Second Edition, Textbook, ISBN 0-471-52496-4, Department of Mechanical and Aerospace Engineering Carleton University, Ottawa, Canada.

Subtask E2c-2: Conduct Mixture Evaluations

Progress This Quarter

No activity this quarter.

Work Planned Next Quarter

Mix designs will be completed for the following mixtures: one aggregate source (lockwood, NV), intermediate Superpave gradation with ½" nominal max size, and three binder grades of: PG52-22, PG58-22, PG64-22.

Subtask E2c-3: Develop a Simple Test

Progress This Quarter

No activity this quarter.

Work Planned Next Quarter

No work planned.

Subtask E2c-4: Develop a Standard Test Procedure

Progress This Quarter

No activity this quarter.

Work Planned Next Quarter

No work planned.

Subtask E2c-5: Evaluate the Impact of Mix Characteristics

Progress This Quarter

No activity this quarter.

Work Planned Next Quarter

No work planned.

Work element E2d: Thermal Cracking Resistant Mixes for Intermountain States (UNR Year 1 start)

Subtask E2d-1: Determine Parameters for an Aging Model for Asphalt Binders in HMA Mixtures Placed in the Intermountain Region

Progress This Quarter

Temperature Data: The objective of this effort is to collect and report actual temperature history and profile throughout the depth of HMA pavements within the intermountain region of the U.S. This objective will be achieved by identifying HMA pavements throughout the intermountain region with measured temperature hourly histories and profiles throughout the depth of the HMA layer. The following steps will be completed.

- Identify HMA pavements at various locations within the intermountain region of the U.S. that have information regarding the HMA temperature histories and profile. This will be achieved by contacting:
    - Nichols Consulting Engineers for LTPP SPS sites in the intermountain region
    - Nevada Automotive Test Center (NATC) for the Westrack project
- Collect mixture and binder properties for the various sites that offers the temperature histories and profiles, if available

In collaboration with Nichols Consulting Engineers, the ARC researchers identified and extracted pavement temperature histories and profiles, mixture and binder properties, pavement performance data, air temperature history, and project information for 14 different asphalt pavement sites located in the intermountain region of the United States. Figure E2d-1.1 shows the various LTTP site locations. Table E2d-1.1 shows the overall information of the various sites.

Figure E2d-1.1. LTPP sites locations in the intermountain region of the U.S.

Table E2d-1.1. LTPP Sites Locations in the Intermountain Region of the U.S.

State	Section	Functional classification of roadway	Number of lanes per direction	Pavement type	Estimated Annual ESAL applications on test lanes	Climatic classification
Arizona	040113	US highway, rural, principal arterial	2	AC	208.5 kESALs	Dry, no-freeze, SMP cell #5
Arizona	040114	US highway, rural, principal arterial	2	AC	208.5 kESALs	Dry, no-freeze, SMP cell #13
Arizona	041024	Interstate highway, rural, arterial	2	AC	936.7 kESALs	Dry, no-freeze, SMP cell #13
Colorado	081053	US highway	2	AC	61 kESALs	Dry-freeze, cell #3
Idaho	161010	US interstate highway	2	AC	147 kESALs	Dry-freeze, cell #15
Montana	300114	Interstate highway, rural arterial	2	AC	174 kESALs	Dry-freeze, SMP cell #11
Montana	308129	US highway	2	AC	45 kESALs	Dry-freeze, cell #3
Nevada	320101	Interstate highway, rural, arterial	2	AC	534 kESALs	Dry-freeze, SMP cell #15
New Mexico	351112	US highway	2	AC	26 kESALs	Dry, no-freeze, cell #13
South Dakota	469187	State highway	2	AC	NA	Dry-freeze, cell #3
Texas	481077	US highway	2	AC	184.1 kESALs	Dry, no-freeze, cell #1
Texas	481122	US highway	NA	AC	48 kESALs	Dry, no-freeze, cell #6
Utah	491001	US highway	1	AC	82 kESALs	Dry-freeze, cell #15
Wyoming	561007	US highway	1	AC	27 kESALs	Dry-freeze, cell #7

The following data were collected for the various 14 LTPP sites

- Temperature Data
  - Hourly Air/Precipitation data
  - Hourly subsurface temperature data
  - Subsurface thermistor depths/installation data

- Performance Data
  - Construction event dates and descriptions
  - IRI data

- Surface distress data
- Transverse profile data
- Report of characterization of transverse profile data for LTPP sites (explains transverse profile data reported)

- Mix/Binder Data
  - Results from LTPP laboratory testing
  - Mix/binder properties from agency inventory records
  - Mix/binder properties from agency rehabilitation records

- Project Information
  - PDF files of installation reports for each site (provides background info on the sites)
  - PDF files of maps indicating the approximate location of each site

The pavement temperature profiles are analyzed to determine the rate of daily temperature changes. Figures E2d-1.2 – E2d-1.4 show temperature profiles from three sensors located at different pavement depths for the test section 040113 located near Kingman, Arizona for the months of January and July, 2004. Figures E2d-1.5 – E2d-1.7 show the pavement temperature rates along with the minimum and maximum daily pavement temperatures for the month of January, 2004. Figures E2d-1.8 – E2d-1.10 show the pavement temperature rates along with the minimum and maximum daily pavement temperatures for the month of July, 2004.

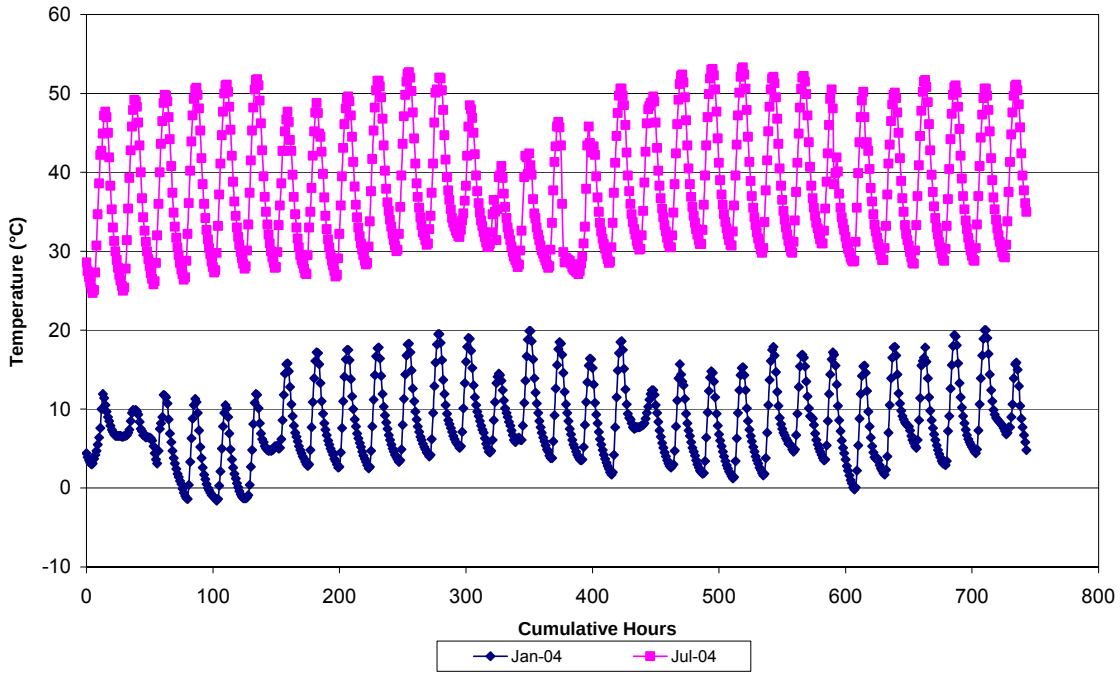

Figure E2d-1.2. Pavement hourly temperature profile for test section 040113 at sensor 1 (depth = 1.7 inches) for January and July of 2004.

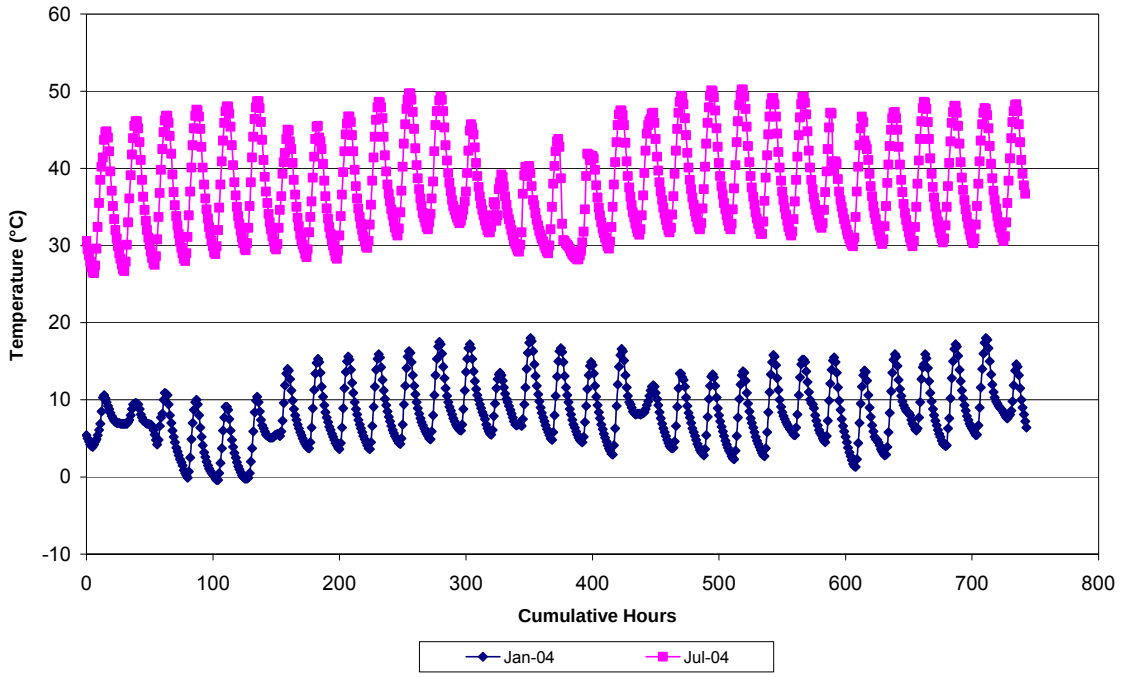

Figure E2d-1.3. Pavement hourly temperature profile for test section 040113 at sensor 2 (depth = 2.9 inches) for January and July of 2004.

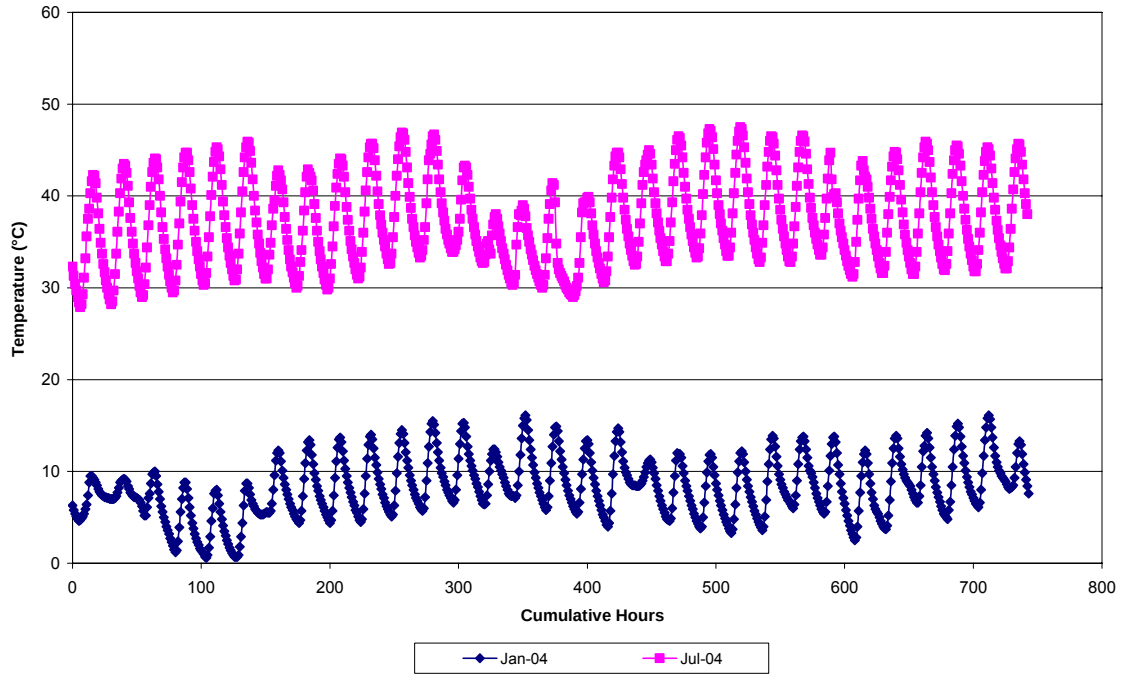

Figure E2d-1.4. Pavement hourly temperature profile for test section 040113 at sensor 3 (depth = 4.1 inches) for January and July of 2004.

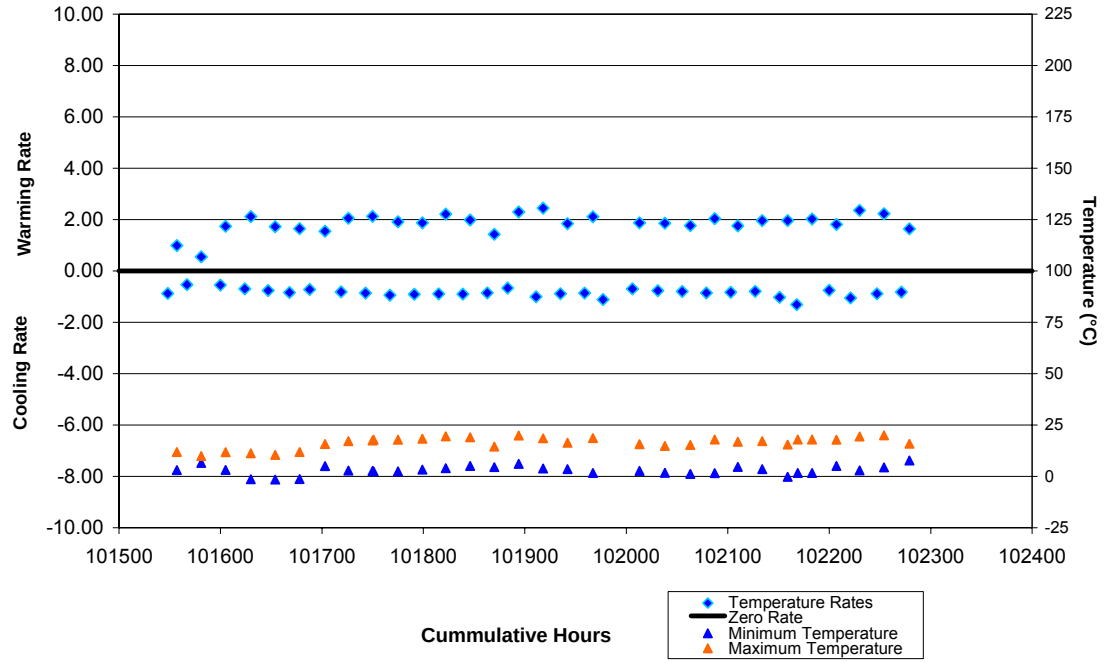

Figure E2d-1.5. Pavement temperature rates along with the maximum and minimum daily temperatures for test section 040113 at sensor 1 (depth = 1.7 inches) for January of 2004.

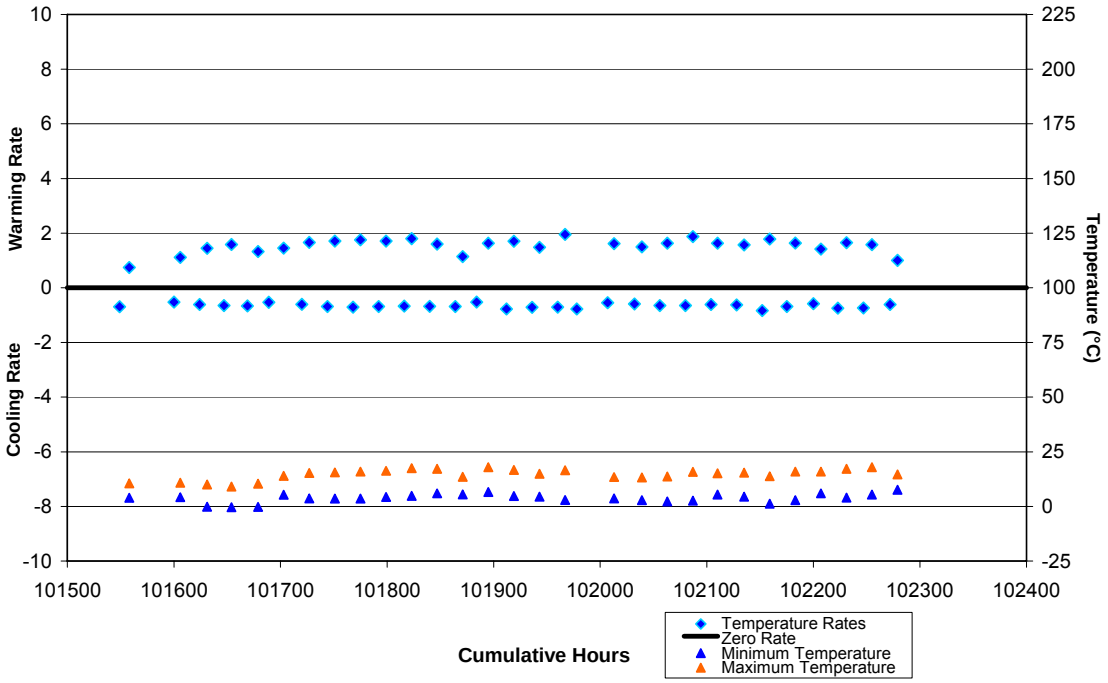

Figure E2d-1.6. Pavement temperature rates along with the maximum and minimum daily temperatures for test section 040113 at sensor 2 (depth = 2.9 inches) for January of 2004.

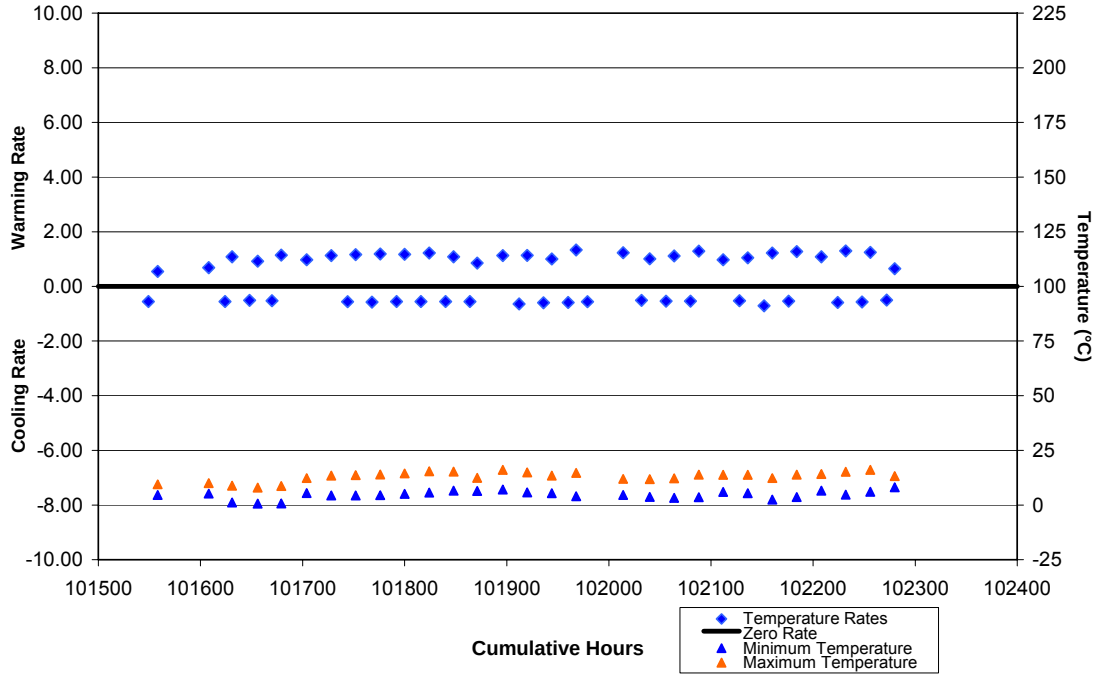

Figure E2d-1.7. Pavement temperature rates along with the maximum and minimum daily temperatures for test section 040113 at sensor 3 (depth = 4.1 inches) for January of 2004.

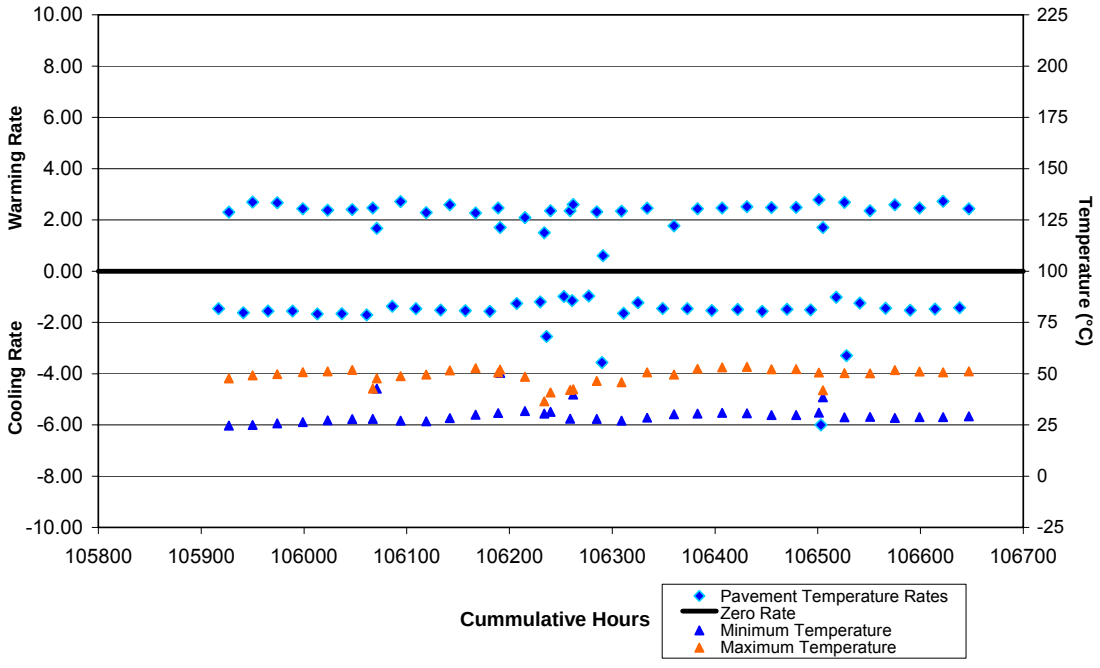

Figure E2d-1.8. Pavement temperature rates along with the maximum and minimum daily temperatures for test section 040113 at sensor 1 (depth = 1.7 inches) for July of 2004.

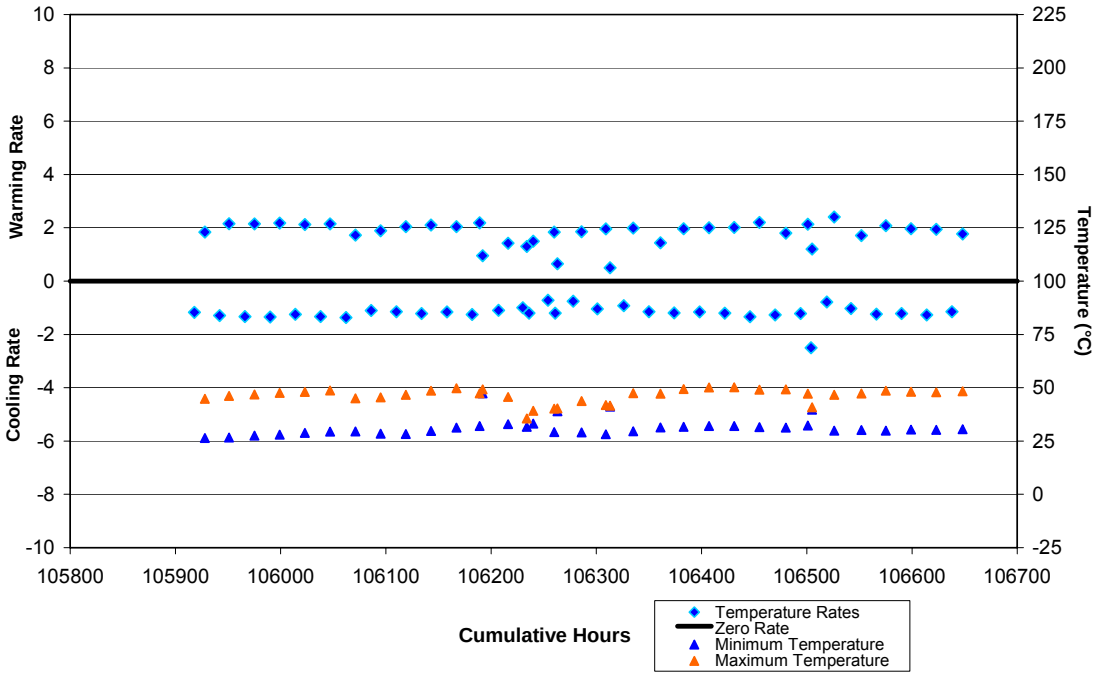

Figure E2d-1.9. Pavement temperature rates along with the maximum and minimum daily temperatures for test section 040113 at sensor 2 (depth = 2.9 inches) for July of 2004.

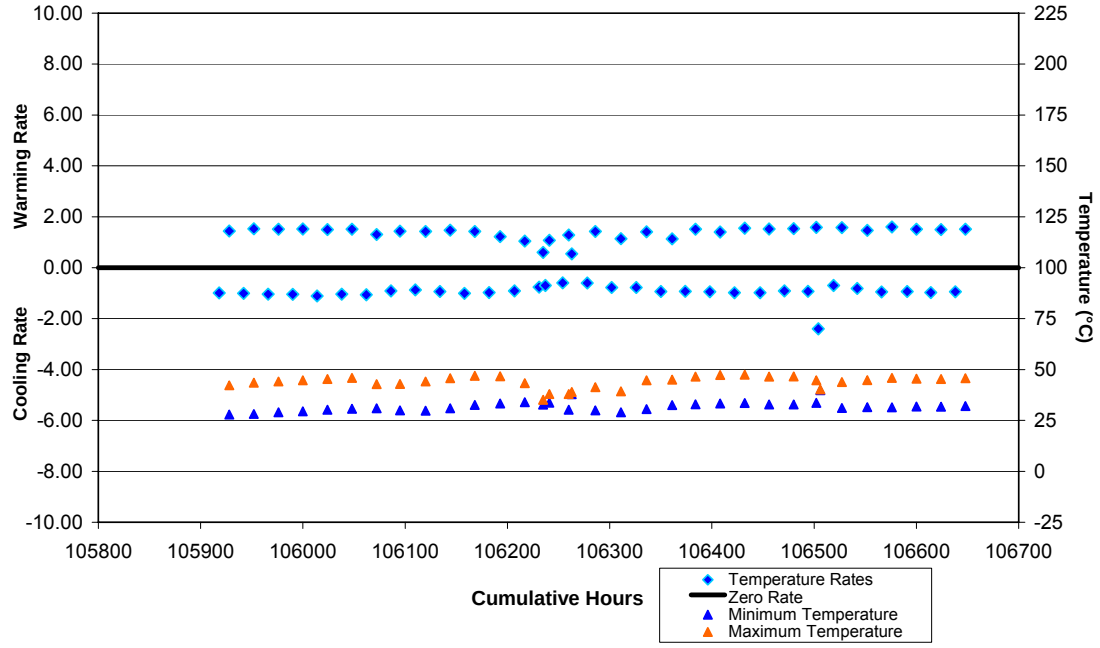

Figure E2d-1.10. Pavement temperature rates along with the maximum and minimum daily temperatures for test section 040113 at sensor 3 (depth = 4.1 inches) for July of 2004.

Additionally, UNR collected pavement temperature histories and profiles, mixture and binder properties, pavement performance data, air temperature history, and project information for the Westrack project in Nevada. Table E2d-1.2 summarizes the overall information of the three Westrack sections that had temperature sensors. Similar analysis is undergoing for the Westrack pavement temperature profile.

Table E2d-1.2. Overall information on Westrack test sections with temperature profiles.

	Section No.		
	12	**19**	**25**
Binder Grade/Source	PG 64-22; West Coast	PG 64-22; West Coast	PG 64-22; West Coast
Aggregate Source	Quarry near Dayton, Nevada (partially crushed fluvial deposit); Sand from Wadsworth, Nevada	Quarry near Dayton, Nevada (partially crushed fluvial deposit); Sand from Wadsworth, Nevada	Quarry near Dayton, Nevada (partially crushed fluvial deposit); Sand from Wadsworth, Nevada
HMA Thickness	6 inches	6 inches	6 inches
Aggregate Gradation Designation	Fine-Plus*	Fine-Plus*	Coarse
Design Asphalt Content	Optimum (Medium)	Optimum (Medium)	Optimum + 0.7% (High)
In-place Air Voids	4% (Low)	8% (Medium)	4% (Low)

* Fine gradation with 2% baghouse fines added

Work Planned Next Quarter

Continue the analysis of the field temperature data from the 14 LTPP sites and the 3 Westrack sections. Start the long-term oven aging of the binders to simulate binder aging with access to free oxygen.

Subtask E2d-2: Identify the Causes of the Thermal Cracking

Progress This Quarter

No activity this quarter.

Work Planned Next Quarter

No work planned.

Subtask E2d-3: Identify an Evaluation and Testing System

Progress This Quarter

During previous quarters, a dilatometric system for measuring binder properties was used to study the glass transition of 10 binders and a length change measuring system was used to measure the glass transition of asphalt mixtures. Results show a variation in the glass transition behavior as function of the binder grade and modification. Furthermore, the glass transition temperature (T_g) of the mixtures does not correlate with binder glass transition properties, which highlights the importance of aggregate characteristics and mixture compaction data in defining mixture thermo-volumetric properties. It is also found that the contraction and dilation behavior of mixtures shows a hysteretic response. These findings hint at a need for fundamental understanding of the effect of aggregate interaction in the thermal behavior of asphalt mixtures, and they also shed some light on the important aspect of thermal cracking of pavements and the measurements needed for better modeling.

We have developed a finite difference model that simulates the temperature gradient and strain distribution in 2.5-inch by 2.5-inch cross-section mix specimen during thermal cycling. This finite difference model solves the heat diffusion equation:

$$\frac{\partial T(x,z,t)}{\partial t} = k \cdot \left(\frac{\partial^2 T(x,z,t)}{\partial x^2} + \frac{\partial^2 T(x,z,t)}{\partial z^2} \right)$$

by discretizing it both in the space and time:

$$\frac{T(x_i,z_i,t_{i+1}) - T(x_i,z_i,t_i)}{\Delta t} = k \cdot \left(\begin{array}{l} \dfrac{T(x_{i+1},z_i,t_i) - 2T(x_i,z_i,t_i) + T(x_{i+1},z_i,t_i)}{\Delta x^2} \\ + \dfrac{T(x_i,z_{i+1},t_i) - 2T(x_i,z_i,t_i) + T(x_i,z_{i-1},t_i)}{\Delta z^2} \end{array} \right)$$

where T(x,z,t) is the temperature specimen in space and time, k is the thermal diffusivity, and Δx, Δz, and Δt are the space and time discretization intervals. By applying the chamber temperature as the time-varying boundary condition, the distribution of temperature throughout the specimen during heating and cooling cycles can be calculated (figure E2d-3.1). Furthermore, the combination of local temperatures with thermal expansion coefficients (including different thermal expansion coefficients above and below the glass transition temperatures) permit calculating both local and global thermal strains for any asphalt mixture specimens.

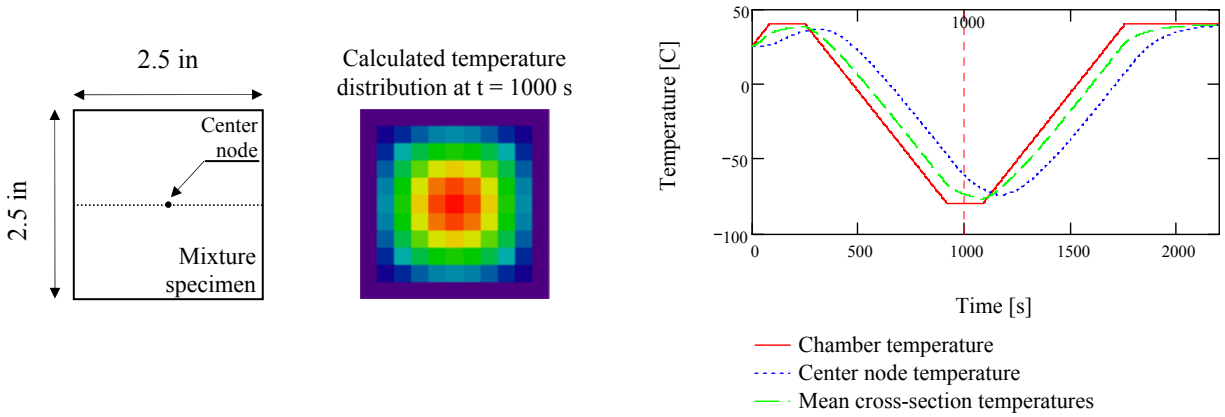

Figure E2d-3.1. Illustration and graphs. Finite difference model of temperature distribution on asphalt mixture specimens.

The ability to evaluate the temperature node by node across the specimen cross-section shows that using a single thermocouple to characterize the thermal behavior a whole specimen could mask the true response of the asphalt mixture. For example, figure E2d-3.2(a) shows how local measurements cannot be used to match the average temperature distribution in the specimen. This is important, as the average temperature distribution controls the overall thermal deformation. For example, figure E2d-3.2(b) shows the calculated thermal strain of a specimen plotting using thermal expansion for temperatures above and below the glass transitions temperature (Mamlouk et al. 2005; Ojo et al. 2008). Plotting these results versus local temperatures (either inside or outside the specimen, or the average of the two measurements), yields a loop response, while the cross-sectional average represents the true driving mechanism and it eliminates the looping in the response. It is seen that experimental measurements must be combined with numerical modeling to properly evaluate the response of the asphalt mixture system.

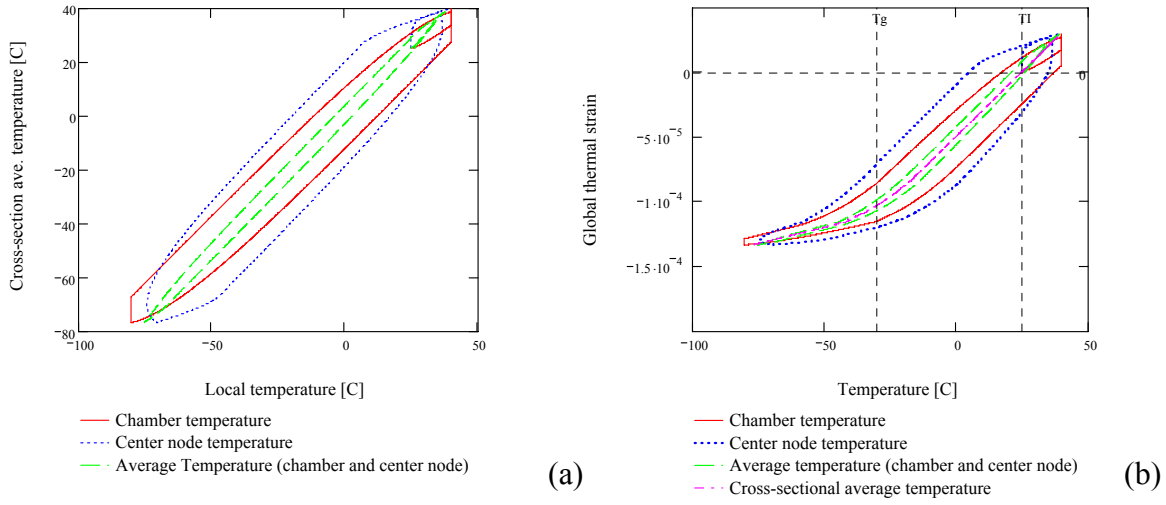

Figure E2d-3.2. Graphs. Modeled (a) thermal temperatures and (b) strain. The selection of local or global temperatures for the evaluation of system response may control the data interpretation.

Work Planned Next Quarter

Begin FTIR testing of aged asphalt binders. Determine thermal coefficients of asphalt binders and mixtures.

Subtask E2d-4: Modeling and Validation of the Developed System

Progress This Quarter

No activity this quarter.

Work Planned Next Quarter

No work planned.

Subtask E2d-5: Develop a Standard

Progress This Quarter

No activity this quarter.

Work Planned Next Quarter

No work planned.

Work element E2e: Design Guidance for Fatigue and Rut Resistance Mixtures (AAT Year 1 Start)

Subtask E2e-1: Identify Model Improvements

Progress This Quarter

This subtask was completed this Quarter. The recommended improvements are summarized in table E2e.1 and described in greater detail in the following sections

Table E2e.1. Summary of Recommended Improvements to the NCHRP Project 9-25 and 9-31 Composition to Engineering Property Models.

Model	Recommended Improvement
Hirsch Model for Dynamic Modulus	Curing time
	Low stiffness stress dependency
	Limiting maximum modulus
Resistivity Model for Rutting Resistance	Incorporate MSCR binder characterization
Continuum Damage Fatigue Model	Healing
	Damage tolerance
Permeability	Expand data set
	Aggregate size effect

Hirsch Model for Dynamic Modulus

Estimating the modulus of HMA is useful for a variety of purposes. It can serve as an aid during HMA testing, so that stress and strain levels can be properly set at the beginning of test procedures, including dynamic modulus, creep and fatigue testing. Estimates of |E*| values can be used in preliminary pavement designs, or for non-critical, low-volume pavement designs. Modulus estimates are also potentially useful in a variety of research situations, since many other HMA properties, such as fatigue resistance and rut resistance, are related to modulus.

The Hirsch model for estimating the modulus of hot-mix asphalt (HMA) was developed by engineers at Advanced Asphalt Technologies, LLC (AAT) as part of NCHRP Projects 9-25 and 9-31. It has been evaluated by several researchers independent of AAT and found to be more accurate and more rational than other similar models. There are however a number of improvements that can be made to the Hirsch model to improve its accuracy:

1. The modulus values of HMA specimens appears to gradually increase with time after specimen compaction. This is similar to curing of Portland cement concrete specimens, although not nearly as pronounced. This increase is probably due to a number of effects, including steric hardening of the asphalt binder, and continued, slow absorption of binder by the aggregate. The accuracy of the Hirsch model—and most other models for estimating HMA modulus values—could be significantly improved if the effect of curing time on HMA modulus could be at least approximately quantified.
2. Although it is generally assumed that the modulus of HMA is independent of stress level at relatively low stress levels, in reality, it is likely that some stress dependency exists even at very low stress levels at high temperatures and/or low loading frequencies/long loading times. The lower equilibrium modulus in the Hirsch model (and other similar models, such as the Witczak model) is assumed to be constant, but in fact probably varies slightly with stress level. The structure of the Hirsch model is such that this non-linearity can easily be accounted for if adequate data is collected to characterize typical stress dependency in HMA.

3. An important feature of the Hirsch model is the upper equilibrium modulus, or glassy modulus value. This is the maximum modulus value reached by an HMA at high frequencies/short loading times and/or low temperatures. The value of this limiting modulus is approximately 4 million psi. It is assumed constant in the Hirsch model, but as explained in item 1 above, probably varies somewhat with curing time. Another important factor affecting the glassy modulus of an HMA mix is the aggregate type used in the mixture. Theoretically, the maximum modulus for most HMA mixtures should be directly related to the modulus of the aggregate. Unfortunately, the data set used to develop the Hirsch model was not well suited for evaluating this effect. Being able to estimate the relationship between aggregate type and the glassy modulus of a mixture would significantly improve the accuracy of the Hirsch model.

Resistivity Model for Rutting Resistance

The resistivity/rutting model was developed during NCHRP Projects 9-25/9-31 as a way of relating HMA composition to rut resistance. The model predicts that rutting resistance increases with decreasing VMA, increasing aggregate surface area, decreasing in-place (or as tested air voids), increasing design air voids, and increasing asphalt binder modulus or viscosity. The nature of the model is consistent with the results of other studies relating HMA composition and properties to rut resistance. The model is promising, with in-place rutting predictions within about a factor of two of observed values. However, the model does not deal well with modified binders; in order to obtain reasonable accuracy, an indicator value must be used to allow for significantly greater rut resistance for polymer-modified binders as compared to non-modified binders. Recently, the multiple-stress creep and recovery (MSCR) test has been proposed as an alternative to the standard dynamic shear rheometer (DSR) test for evaluating and specifying the properties of binders at the critical temperature for rutting, T_c. The MSCR test directly measures permanent and non-permanent deformation in a binder at two different stress levels, and potentially is much more useful in characterizing the flow properties of modified binders as they relate to HMA rut resistance.

Continuum Damage Fatigue Model

During NCHRP Projects 9-25, 9-31 and 9-33, a model for estimating the fatigue resistance of HMA mixtures was developed based upon continuum damage theory (CDT). The model related certain fundamental constants in the CDT fatigue model to various aspects of HMA composition, including effective binder content, design and in-place/as tested air voids, and binder properties. The model was verified by independently predicting the results of flexural fatigue tests, with a degree of accuracy approaching that of typical fatigue tests. The CDT model is potentially very useful, and also can be applied in rapid laboratory fatigue testing of HMA mixtures. There are however two improvements needed in the CDT fatigue model in order to make it useful in predicting the performance of HMA mixtures in situ. These two improvements involve a better understanding of damage tolerance and healing. CDT does a very good job of predicting how the modulus of an HMA mixture degrades under continued loading. This is certainly important in understanding fatigue damage in flexible pavements, but it is not sufficient for a thorough understanding of this failure mode. CDT predicts the way modulus decreases due to micro-

cracking and other forms of micro-damage. It does not address crack propagation, or even the point at which micro-cracks coalesce into a major flaw and crack propagation begins to occur. Damage tolerance refers to the amount of damage an HMA mixture can withstand before macro-cracking, or crack propagation occurs; this is often referred to as "localization" in CDT terminology. Healing is equally important to understanding the manner in which fatigue damage occurs in real flexible pavement systems. CDT tests are generally performed by applying a continuous sinusoidal load to a specimen. In real pavement system, loading is not continuous, but sporadic, with numerous opportunities for healing to occur in the HMA. Although some preliminary work with promising results has been performed on developing a practical model for modeling healing within the context of CDT, additional work is needed to verify the principle concepts of this model and to refine it.

Permeability

A model to estimate mixture permeability was also developed in NCHRP Projects 9-25/9-31. This model relates the coefficient of permeability to the air void content and surface area of the mixture. Since this model was developed, a substantial amount of additional permeability data has been published by other researchers. This additional data will complied and the model will fit the expanded database. Emphasis will be placed on quantifying the nominal size effect reported by other researchers.

Work Planned Next Quarter

No work planned. The subtask is complete.

Subtask E2e-2. Design and Execute Laboratory Testing Program

Progress This Quarter

No activity this quarter.

Work Planned Next Quarter

Experimental plans for each of the improvements identified in subtask E2e-1 will be prepared. Preliminary experimental plans will be prepared for the Year 2 Work Plans. These preliminary experimental plans will be revised based on comments received from the AOTR, and detailed experimental plans will then be prepared.

Subtask E2e-3. Perform Engineering and Statistical Analysis to Refine Models

Progress This Quarter

Later start.

Work Planned Next Quarter

No work planned.

Subtask E2e-4. Validate Refined Models

Progress This Quarter

Later start.

Work Planned Next Quarter

No work planned.

Subtask E2e-5. Prepare Design Guidance

Progress This Quarter

Later start.

Work Planned Next Quarter

No work planned.

PROGRAM AREA: VEHICLE-PAVEMENT INTERACTION

CATEGORY VP1: WORKSHOP

Work element VP1a: Workshop on Super-Single Tires (UNR)

Progress This Quarter

The Workshop on Wide-Base Tires was held at FHWA TFHRC on October 25-26, 2007. FHWA has prepared draft minutes of the Workshop. All attendees have been reimbursed for their travel expenses.

Work Planned Next Quarter

The final version of the Workshop minutes will be posted on the ARC website after the minutes are received from FHWA. This will complete this will complete this work element.

CATEGORY VP2: DESIGN GUIDANCE

Work element VP2a: Mixture Design to Enhance Safety and Reduce Noise of HMA (UWM)

Subtask VP2a-1: Evaluate Common Physical and Mechanical Properties of Asphalt Mixtures with Enhanced Frictional Skid Characteristics
Subtask VP2a-2: Evaluate Pavement Macro and Micro-textures and Their Relation to Tire and Pavement Noise-generation Mechanisms
Subtask VP2a-3: Develop a Laboratory Testing Protocol for the Rapid Evaluation of the Macro and Micro Texture of Pavements
Subtask VP2a-4: Run Parametric Studies on Tire-pavement Noise and Skid Response
Subtask VP2a-5: Establish Collaboration with Established National Laboratories Specialized in Transportation Noise Measurements. Gather Expertise on Measurements and Analysis
Subtask VP2a-6: Model and Correlate Acoustic Response of Tested Tire-pavement Systems
Subtask VP2a-7: Proposed Optimal Guideline for Design to Include Noise Reduction, Durability, Safety and Costs

Note: These subtasks will be reported together.

Task Lead: Dante Fratta

One important emphasis of the new transportation bill is safety. Although safety, comfort, and noise control are known to be direct functions of macro- and micro-texture, there are no significant efforts on integrating these design parameters into asphalt pavement mixtures (Bernhard and Wayson 2005; Guisik and Bahia 2006; Noyce et al. 2007). It is also not well known if binders and mastics can change friction characteristics and sound generation and

absorption properties of asphalt mixtures. University of Wisconsin-Madison researchers have been working with a number of DOT's in the Midwest to look at new procedures for measuring macro- and micro-texture and enhancing the methods for estimating micro-texture.

Micro-texture is the fine-scale (≤ 1 mm depth) grittiness on the surface of the coarse aggregates. The micro-texture makes direct tire-pavement contact and thus provides the resistance to skidding on the prevailing road surface. Macro-texture is the large-scale roughness that is present on the pavement surface due to aggregate arrangements and provides the drainage ability of the pavement. The combination of macro and micro-textures, and their changes with traffic and climate factors, make up the overall resistance to skidding. Furthermore, the proper macro-texture design contributes to the reduction of roadway noise generation, increases the noise absorption behavior of pavements, and drains rain water faster, but improvements in these areas can come at the expense of skid friction (Newcomb and Scofield 2004; Jones 2005). Quiet pavement-tire systems have been implemented in Japan and many European countries because of the strong regulatory framework created by the European Community (EU). European regulations try to reduce noise at the source rather than using the noise barrier systems typically used in the United States. Several innovative techniques employed in Denmark, the Netherlands, France, Italy, and the United Kingdom have been able to reduce noise level in ranges that vary from 3 to 17 dB (Danish Road Institute 2005; Gibbs et al. 2007). Promising noise-reduction techniques include the use of porous elastic pavements (e.g., single and double layers porous asphalt, stone mastic asphalt, silent block pavements, etc.), recycled porous layers, emulsified asphalt concrete surfacing, use of a dense or semi-dense gradation in low-to-medium speed traffic roadways, and texturing of newly constructed concrete pavements for enhanced skid resistance and reduced pavement-tire noise.

This work element focuses on evaluating and modifying mixture design procedures to enhance safety and noise-reduction properties of asphalt mixtures for flexible pavements. In particular, this work element will develop a laboratory test procedure and/or prediction models for the evaluation of macro- and micro-textures of asphalt pavements. It will also focus on comparing these measurements with field measurements of skid resistance and pavement-tire noise. Results from this work will evolve into the development of pavement mixture design protocols that will not only include structural strength and durability, but also traffic safety, comfort and reduced pavement-tire noise.

The overall objectives of this work element are:

- To study the state of the art on pavement-tire friction coefficient and quiet pavement-tire design techniques.
- To develop a surrogate laboratory test procedure to measure pavement macro- and micro texture, as well as predict safety and noise related properties.
- To establish criteria for the holistic mixture design protocol that optimizes mechanical properties, durability, economy, skid resistance, and noise generation.

The final result of this work element will be the development of a mixture design protocol that will incorporate macro- and micro-structure of mixtures that produce pavement surface layers with enhanced frictional response while reducing pavement-tire noise levels

Table VP2.1. Summary of research team effort this quarter.

% Complete for Year 1	***Effort in Months*** *(1 month = 160 Hrs)*				
	Principal Investigator	Task Lead	Research Assistants	Secretarial	Cost Share
25	0	15%	15%	0	0

Progress This Quarter

The University of Wisconsin-Madison research team performed an extensive literature review of the state of the art in the areas of skid resistance and quiet pavement. Emphasis is placed on evaluating commonality of parameters that have shown in practice to enhance skid resistance. The evaluation of parameters is helping in establishing not only the commonality of interacting factors, but it also helps in establishing areas of research needs. A preliminary summary table is presented in table VP2.1. The research team is also evaluating different testing methodology for the evaluation of surface parameters and acoustic properties of pavement mixtures.

Acoustic properties of asphalt mixtures: Two different parameters need to be evaluated. The first one is the generation of noise at the tire-asphalt interface. The second parameter is the sound absorption behavior pavement mixtures.

To evaluate the noise generation at the type-asphalt pavement interface, the research team is considering creating a setup similar to the British pendulum (Liu et al. 2003; Noyce et al. 2007) with the addition of microphones. This setup will allow measuring both the skid resistance and the sound generation at the interface.

To evaluate the sound absorption behavior of pavement surfaces, the research team is evaluating and designing an impedance tube (waveguide device) that will allow the testing of different asphalt mixture specimen geometries (i.e., 6-in diameter specimens and slab specimen). The geometry and testing geometry that is being favored is the one proposed by NCAT (Sound absorption setup – Hanson et al. 2004; Crocker et al. 2004), as this geometry allows the testing of both specimen types.

These two tests will allow the evaluation of the acoustic properties of a large number of pavements mixtures, specially those mixtures that have the desirable strength and dynamic properties of pavements. Finally, to indirectly evaluate the sound absorption properties of asphalt pavements, permeability tests should be run to determine not only the acoustic absorption but also the drainage properties of the pavement. Drainage properties are important in the evaluation of skid friction and the aquaplaning susceptibility of the pavement surface.

Table VP2.2. Asphalt mixture parameters and performance factors

	Rutting Resistance	Fatigue Resistance	Moisture Damage Resistance	Thermal Cracking Resistance	Economy	Skid Resistance	Noise Reduction
Gradation (fine/coarse)	High number of contact points within the mix provide high internal friction that resists permanent deformation.	Gradations that have greater resistance to deformation distribute stresses more evenly and results in less damage from bottom-up cracking.			Fine aggregates are typically more cost effective. However, gradation affects aggregate structure in the pavement, controlling the compactive effort needed.	Coarse gradation increases skid resistance	Higher proportion of fines makes for smoother and quieter surfaces.
Aggregate angularity	High aggregate interlock provides a more structurally stable material that results in stiffer mixes	High aggregate interlock provides a more structurally stable material that results in stiffer mixes			Crushed aggregates are typically more expensive due to processing costs.	Increase angularity increases skid resistance	Smoother aggregates create less tire vibration from adhesive effects.
Aggregate mineralogy			Mineralogy controls hydrophilic (moisture susceptible) or hydrophobic (moisture resistance) of aggregates		Softer aggregates are cheaper to process. Availability of the type of aggregate ultimately drives price, however.		
Maximum aggregate size						Uniform gradation distribution may lead to denser structures and smoother surfaces that may yield lower drainage and reduced skid friction.	Smaller aggregates provide quieter characteristics due to smoother surfaces.
Binder properties	Superpave binder specifications are in place in order to ensure the binder is stiff enough at operating temperatures to resist permanent deformation	Binder can be highly susceptible to fatigue damage. Binders that have a combination of high damage resistance and high healing potential typically lead to good fatigue resistance.		Binder should be ductile at low temperatures in order to relax the stresses induced from thermal restraint. Also, aggregates themselves have no tensile strength, so the tensile strength added by the binder is mostly responsible for resistance to tensile thermal cracking.	Stiffer binders increase compactive effort at similar temperatures, so increased heating is needed to achieve the correct viscosity.		
Asphalt content	Low asphalt contents, known as "dry" mixes, are typically thought of to be more rutting resistant due to less lubrication between the aggregates due to the binder.			The asphalt content should control the expansion and contraction thermal coefficients.	Higher asphalt content increases cost of mix.		
Additives	Many additives are available to stiffen the binder at operating temps, which adds strength to the pavement.	Some polymer additives can add fatigue resistance to materials		Polymers that add ductility to the asphalt can help prevent brittle failure.		Unclear	High damping additives, such as elastic polymers and crumb rubber, have been used to aid in the dissipation of vibration energy. Also, polymers may be used in high void mixes to help increase structural stability.

Skid resistance characteristics. There are a number of both direct and indirect testing techniques to evaluate the skid friction properties of pavements. The direct testing techniques measure the friction coefficient (or a related parameter) of the pavement surfaces. These testing methodologies include the British pendulum (BP – Liu et al. 2003; Noyce et al. 2007) and dynamic friction tester (DFT – Brown et al. 2001). The research team will favor the use of the British Pendulum as it has simpler geometry for the monitoring of noise generation on different asphalt mixtures.

Indirect methods include for example, the sand patch method (SPM - ASTM E965), circular texture meter (CTM – Hanson and Prowell 2004), and Ames texture scanner (ATS – Ames Engineering 2007). The SPM is an indirect and inexpensive measurement technique of the asphalt pavement surface macrostructure. The biggest problem with this methodology is that SPM yields an index parameter (mean texture depth - MTD) that may or may not be able to describe the complexity of the skid friction and noise generation and absorption. Alternatively, the circular texture scanner and the AMES texture scanner use laser profilometry to completely profile the surface of the pavement. These profiling methodologies yield a number of surface measurement parameters that can be used to better correlated noise and skid friction behavior of asphalt pavements but at a greater cost. These portable instruments cost more than $12,000 per unit.

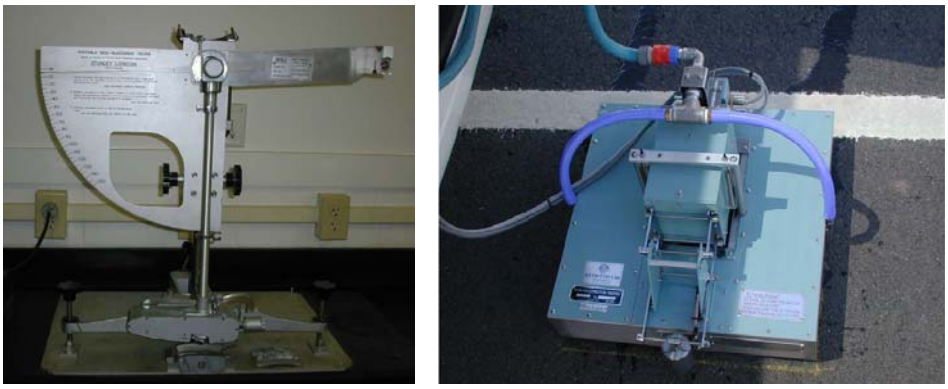

Figure VP2.1. Photos. Skid resistance measurement devices: British pendulum and dynamic friction tester (Image source: Brown et al. 2001).

Figure VP2.2. Photos. Asphalt pavement texture measurement techniques: sand patch method, circular texture meter, and Ames texture scanner (Image sources: Hanson and Prowell 2004). Ames Engineering 2007).

Problems Encountered and Solutions

None

Work Planned Next Quarter

During the first quarter of 2008, the research team will continue correlating mixture pavement design parameters with good practices on skid friction and low-noise of pavements. The research team will also define a finite number of test methodologies to help evaluate the most important parameters for the development of a surrogate test or several surrogate tests. Then, in Year 2, the research team will develop a testing matrix to evaluate how binder and texture contribute to the design of skid resistant and quite pavement surface.

References

Ames Engineering, 2007, *Company Web Site*, URL: http://www.amesengineering.com/ amestexturescanner.html (Accessed November 2007).

Bernhard, R. J., and R. L. Wayson, 2005, *An Introduction to Tire/Pavement Noise*. SQDH 2005-1 HL 2005-2. URL: http://meweb.ecn.purdue.edu/~sqdh/ (Accessed November 2007).

Brown, E. R., P. S. Kandhal, and J. Zhang, 2001, *Performance Testing for Hot Mix Asphalt*. NCAT Report 01-05, National Center for Asphalt Technology, Auburn University, AL.

Crocker, M. J., D. Hanson, Z. Li, R. Karjatkar, and K. S. Vissamraju, 2004, Measurement of Acoustical and Mechanical Properties of Porous Road Surfaces and Tire and Road Noise. Transportation Research Record: *Journal of the Transportation Research Board*, No. 1891, TRB, National Research Council, Washington, D.C., pp. 16–22.

Danish Road Institute, 2005, *Noise reducing pavements in Japan - study tour report*. DRI-DWW Noise Abatement Program Road and Hydraulic Engineering Institute, 68 pp.

Gibbs, D. C., R. H. Iwasaki, R. J. Bernhard, J. F. Bledsoe, D. D. Carlson, C. Corbisier, F. W. Fults, T. M. Hearne, Jr., K. W. McMullen, D. E. Newcomb, J. H. Roberts, J. L. Rochat, L. A. Scofield, and M. E. Swanlund, 2007, *Quiet Pavement Systems in Europe*. FHWA Report. URL: http://international.fhwa.dot.gov/quiet_pav/index.htm (Accessed November 2007)

Guisik, K., and H. U. Bahia, 2004, *Incorporating Road Safety into Pavement Management*. MRUTC 04-04 Technical Report.

Hanson, D. I., R. S. James, and C. NeSmith, 2004, *Tire/Pavement Noise Study*. NCAT Report 04-02, National Center for Asphalt Technology, Auburn University, AL.

Hanson, D. I., and B. D. Prowell, 2004, *Evaluation of Circular Texture for Measuring Surface Texture of Pavements*. NCAT Report 04-05, National Center for Asphalt Technology, Auburn University, Auburn, AL.

Jones, W., 2005, A Quiet Pavement – Coming to Highway Near You. *Asphalt*, Summer 2005, pp. 24-25.

Liu, Y., T. F. Fwa, and Y. S. Choo, 2003, Finite-Element Modeling of Skid Resistance Test. *Journal of Transportation Engineering*, 129(3): 316-321.

Newcomb, D., and L. Scofield, 2004, Quiet Pavement Raise the Roof in Europe. *Hot Mix Asphalt Technology*, September/October 2004, pp. 22-28.

Noyce, D. A., H. U. Bahia, J. Yambo, J. Chapman, and A. Bill, 2007, *Incorporating Road Safety into Pavement Management: Maximizing Surface Friction for Road Safety Improvements*, MRUTC Project 04-04, 241 pp.

CATEGORY VP3: MODELING

Work element VP3a: Pavement Response Model to Dynamic Loads (UNR Later start)

Progress This Quarter

No activity this quarter.

Work Planned Next Quarter

No work planned.

PROGRAM AREA: VALIDATION

CATEGORY V1: FIELD VALIDATION

Work element V1a: Use and Monitoring of Warm Mix Asphalt Sections (Year 1 start)

Progress This Quarter

Analysis of warm-mix materials from the Yellowstone National Park (YNP) sections was begun.

Work Planned Next Quarter

Continue analysis of YNP materials.

Work element V1b: Construction and Monitoring of additional Comparative Pavement Validation sites (Year 1 start)

Progress This Quarter

Communication with State DOT's is continuing in order to build additional validation sites.

Work Planned Next Quarter

It is planned to continue to communicate with State DOT's and other possible agencies to build additional validation sites.

CATEGORY V2: ACCELERATED PAVEMENT TESTING

Work element V2a: Scale Model Load Simulation on Small Test Track (Later start)

Progress This Quarter

No activity this quarter.

Work Planned Next Quarter

No work planned.

Work element V2b: Construction of Validation Sections at the Pecos Research & Testing Center (Later start)

Progress This Quarter

No activity this quarter.

Work Planned Next Quarter

No work planned.

CATEGORY V3: R&D VALIDATION

Work element V3a: Continual Assessment of Specifications (UWM Year 1 start)

Work Element Lead: Hussain Bahia

Progress This Quarter

During last quarter the review of the PG-Plus practices as document in literature was completed and a conceptual plan for the work in this work element was developed. The work focused on three areas of the PG binder specifications:

1. PG Rutting Parameter

   A review of the findings of a project on PG grading for airfield pavements, sponsored by AAPTP (Project 04-02), was conducted. Table V3a.1, taken from that study, gives a summary of the Plus specifications for the different states in 2006. The study included testing of binders using PG-Plus as well as MSCR and repeated creep testing. Figures V3a.1 and V3a.2, also from the same study, compare elastic recovery (ER) result and percent recovery from the MSCR test. It can be seen that the testing at various stresses (100 and 3200 Pa) does not make a significant difference in correlations with ER from ductility test. The analysis of the data indicates that a stress level higher than 3200 Pa is required to measure the critical stress sensitivity of the binders tested in that project. Work on the stress level continued under this task and it was show that stresses on the order of 20,000 - 30,000 Pa are needed to show a distinction between binders. In task E1b-1 on binder rutting it was also discovered that binders show tertiary flow and that the starting of the tertiary flow depends on temperature and stress level. In addition, it was found that geometry of testing could make a difference as the accumulated permanent strain, after a significant number of cycles, was significantly different.

   Pictures were taken of the sample with parallel plate and with cone and plate when the tertiary flow was observed. It was discovered that the tertiary flow appears to start when the sample edge start separating in the middle and a rapid reduction in sample area propagated. Although binders vary by the strain level at which the geometry change

starts, the tertiary flow does not appear to be a material property as much a change in geometry that depends on binder viscosity. This observation requires further analysis and it could mean that total cycles, or a minimum total strain, should be required to assess performance differences between binders.

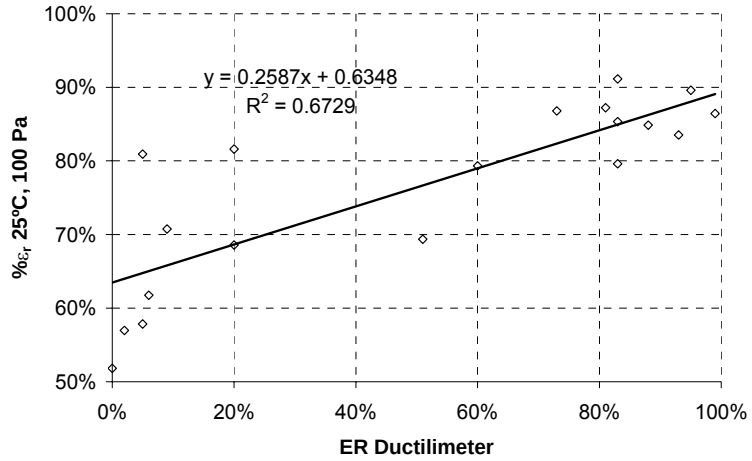

Figure V3a.1. ε_r% at 25 ºC and 100 Pa vs. ER (after project 04-02).

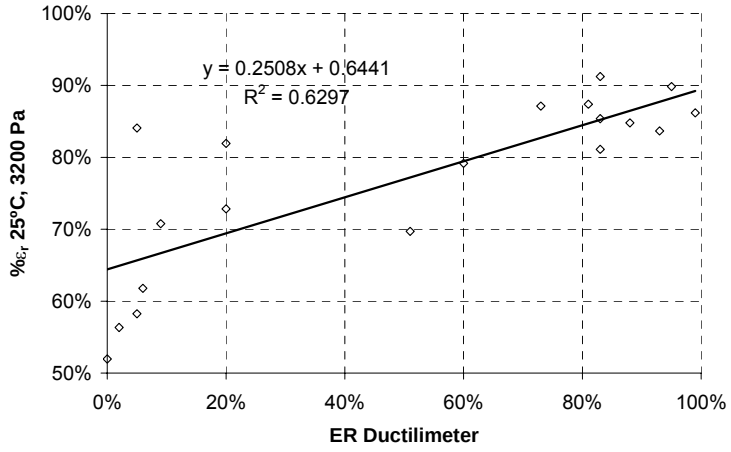

Figure V3a.2. Chart. ε_r% at 25 ºC and 3200 Pa vs. ER (after project 04-02).

Table V3a.1. Superpave-Plus specification details by state (part I) (after project AAPTP 04-02).

State	Superpave Plus Specifications
Alabama	Polymer type (Elastomer), Quantity (%) and Quality (Measured with Infrared Trace)
Alaska	Softening point. Toughness & Tenacity at 25 ºC (Alaska DOT test method)
Arizona	Polymer type (SBS or CRA) Quantity (%) plus the following requirements: • For SBS modified: solubility in TCE, phase angle, elastic recovery at 10 ºC and softening point • For CRA modified: rotational viscosity, penetration ant 4 ºC, softening point and resilience
Arkansas	Polymer type (Elastomer) and Elongation Recovery at 25 ºC
California	NO
Colorado	Ductility, Toughness & Tenacity at 25 ºC, Elastic Recovery at 25 ºC
Connecticut	NO
Delaware	Rotational viscosity at 165 ºC
Florida	Spot Test, Smoke test, Phase Angle, Solubility in TCE, Absolute Viscosity at 60 ºC
Georgia	Phase Angle, Separation, Solubility in TCE
Hawai	NO
Idazo	Elastic Recovery at 25 ºC
Illinois	Separation, Force Ratio at 4 ºC, Toughness & Tenacity at 25 ºC, Elastic Recovery at 25 ºC
Indiana	NO
Iowa	NO
Kansas	Separation, Elastic Recovery at 25 ºC
Kentucky	Solubility in TCE, Elastic Recovery at 25 ºC
Louisiana	Solubility, Separation, Force Ductility Ratio, Force Ductility, Elastic Recovery at 25 ºC, Ductility at 25 ºC
Maine	NO
Maryland	Critical cracking temperature
Massachusetts	Polymer type (SBR)
Michigan	Polymer type (SBS or SBR, others need approval), Solubility in TCE, separation, Elastic Recovery at 25 ºC, plus the following requirements: • For SBS modified: Force Ratio • For SBR modified: Toughness & Tenacity at 25 ºC
Minnesota	NO
Mississippi	Polymer type (SBS or SBR, others need approval), Quantity (%), Temperature - Viscosity Curve
Missouri	Separation, Elastic Recovery at 25 ºC
Montana	Ductility at 25 ºC

Table V3a.2. Superpave-Plus specification details by state (part II) (after project AAPTP 04-02).

Nebraska	Phase Angle, Elastic Recovery at 25 ºC
Nevada	Ductility, Sieve, Toughness & Tenacity at 25 ºC, Polymer Content
New Hampshire	NO
New Jersey	Elastic Recovery at 25 ºC
New Mexico	NO
New York	Elastic Recovery at 25 ºC
North Carolina	Polymer type (Elastomer)
North Dakota	To implement in 2005
Ohio	Penetration at 25 ºC, Phase Angle, Separation, Homogeneity, Elastic Recovery at 25 ºC
Oklahoma	Separation, Solubility in TCE, Spot Test, Elastic Recovery at 25 ºC
Oregon	Only for Chip Seal Asphalt
Pennsylvania	Separation, Softening Point, Elastic Recovery at 25 ºC
Puerto Rico	Unknown
Rhode Island	NO
South Carolina	Polymer type (Elastomer)
South Dakota	Elastic Recovery at 25 ºC
Tennessee	Polymer type (Elastomer), Viscosity at 135 ºC (Contractor Plant Testing), Softening Point, Elastic Recovery at 10 ºC, Screen Test.
Texas	Elastic Recovery at 10ºC
Utah	Phase Angle, Elastic Recovery at 25 ºC
Vermont	NO
Virginia	Elastic Recovery at 25 ºC
Washington	NO
West Virginia	Elastic Recovery at 25 ºC
Wisconsin	To be implemented in 2005
Wyoming	Elastic Recovery at 25 ºC

2. PG Fatigue Parameter

The work conducted on fatigue for the ETG for the last 3-4 years was reviewed last quarter. There is little doubt that the current fatigue parameter $G^*\sin\delta$ is not a good choice for measuring contribution of binder to fatigue resistance. In collaboration with FHWA, a set of binders was tested for binder fatigue and also for mixture fatigue. Results are shown in figure V3a.3, which shows the lack of relationship between $G^*\sin\delta$ and mixtures fatigue. The test procedure for binder fatigue testing is the time sweep in the DSR. In an attempt to compare using different rheometers to examine the repeatability of the test, a few binders were tested in two rheometers by same operator. It was observed that minor variation in the time setting of the time sweep could change

fatigue behavior significantly. Figure V3a.4 shows the change in correlation when the testing sequence for the same binders, using the same DSR, was changed very slightly. Figure V3a.5 shows the results of the strain-controlled time sweep with various setting on the DSR. The results showed that any binder fatigue test that includes a time sweep should consider the possible variation in load history.

These results raise questions about importance of healing and the need to consider the details of loading rate and sequence. It also suggests that a successful fatigue specification test should include healing rate. This work will continue in coordination with other fatigue tasks in this project.

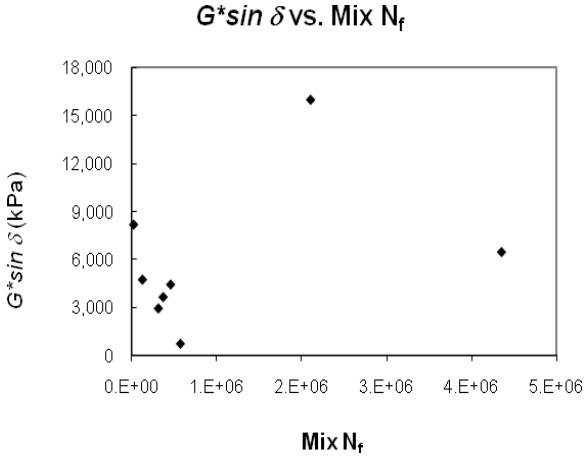

Figure V3a.3. Chart. Plot of *G*sin* δ values against mixture fatigue life.

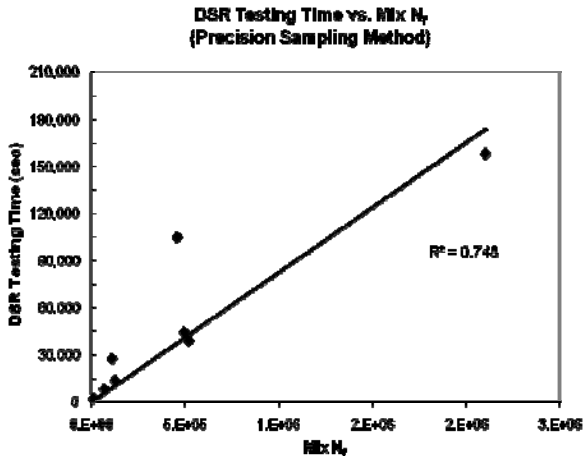

(a)

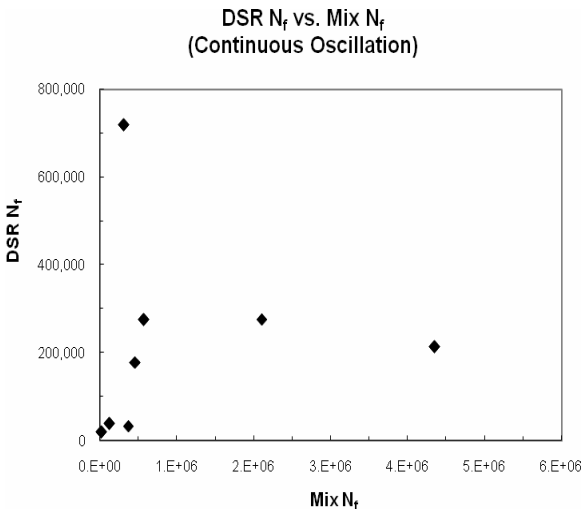

(b)

Figure V3a-4. Chart. Plot of DSR testing time-to-failure against mixture cycles until failure for (a) the precision sampling method, (b) continuous oscillation.

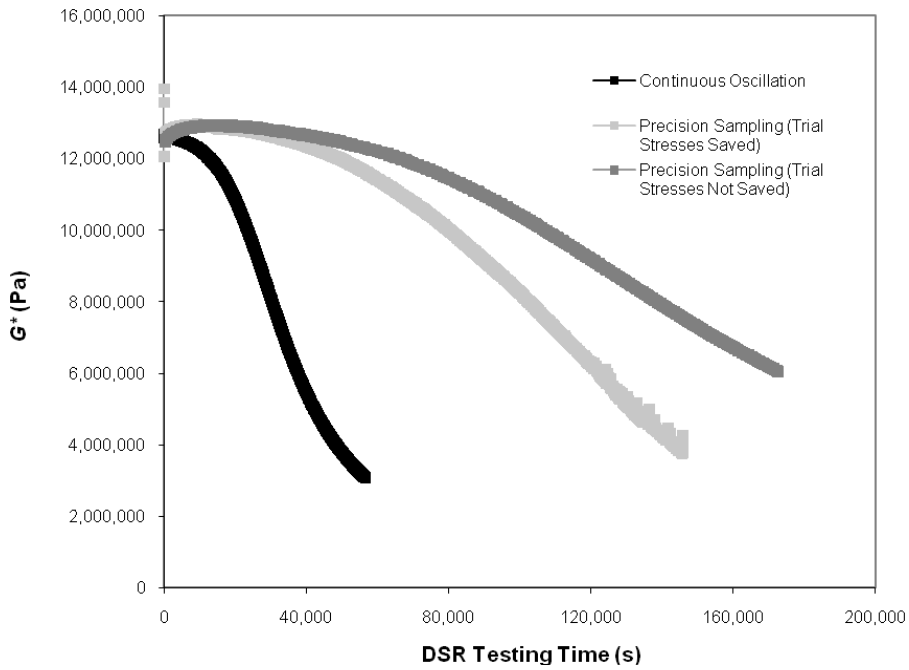

Figure V3a.5. Chart. Plot of binder stiffness against testing time for different types of fatigue tests.

3. PG Low Temperature Parameter

   It appears that the majority of agencies are not using – and do not plan on using – the Direct Tension Test (DTT). It also appears that the equipment manufacturers are not selling the DTT, and it is almost impossible to get the existing machines serviced by the manufacturers. Therefore, there is a critical need for a binder failure test to replace the Direct Tension Test. There are two potential tests that were reviewed last quarter: The Single Edge Notched Beam (SENB) test, that is used in Canada and was introduced by Professor Hesp, and the ABCD test developed by Dr. S. Kim of Ohio University. The SENB test geometry could be applied in a modified BBR device and thus is more attractive. Last quarter, a plan for adding a stepped motor to the BBR, to conduct a constant deformation rate test was developed. An analysis of the notched beam geometry and consideration of various steps for conducting the test was pursued. There is a great potential for simple modification of the BBR to conduct a version of the SENB test while using a modified mold and notch procedure.

Last quarter the Year 2 work plan was developed. Figure V3a.6 show the general approach developed for this task. This effort will be coordinated with the binder ETG and the asphalt institute.

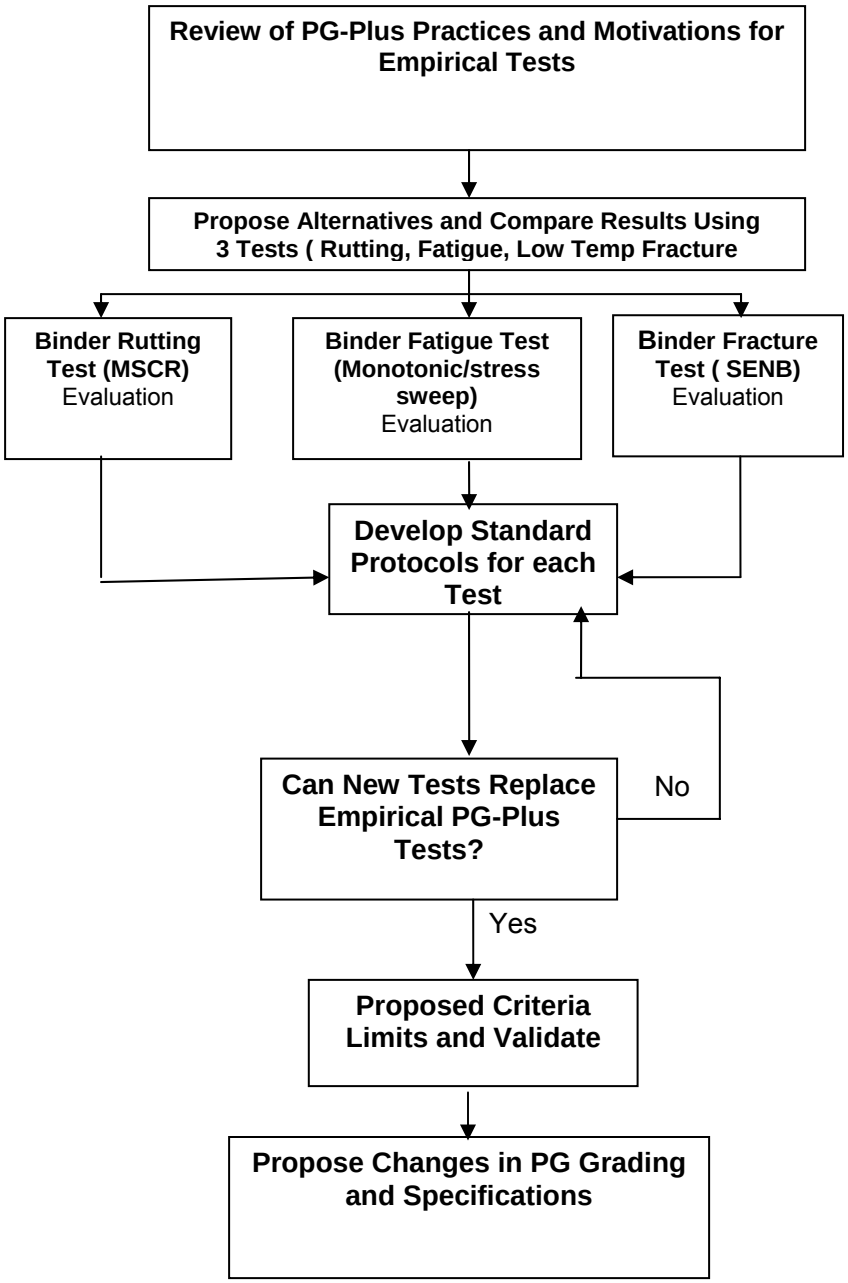

Figure V3a.6. Chart. Flow chart for research approach.

Work Next Quarter

The activities for all three areas will continue next quarter. An outreach effort to collect Elastic Recovery data will be conducted to examine the success of this test in meeting DOT expectations and what are the challenges faced. Also, an assessment of the willingness to change to the MSRC test, or a derivative of it, will be explored. Similar effort will be conducted to evaluate other PG plus practices and conduct a thorough review of whether the new fatigue and low

temperature facture tests can replace the empirical tests used today to complement the PG specifications. The following specific tasks will be pursued:

a. Coordinate work with the fatigue studies to propose a surrogate test using the DSR. The stress sweep and the binder monotonic tests are both promising and could yield a solution.
b. Work on further development of the SENB test and the modification of the BBR.
c. Evaluate the new aging procedure and the new procedure for estimating the mixing and compaction temperatures.

References

Christensen, D., R. Delgadillo, H. Bahia, and R. McQueen, 2007, AAPTP Project 04-01-PG Binder Grade Selection for Airfield Pavements, Draft Final Report, November 2007.

Masad, E., N. Somevadan, H. U. Bahia, and S. Kose, 2001, Modeling and Experimental Measurements of Strain Distribution in Asphalt Mixes. *Journal of Transportation Engineering*, 127 (6), Nov/Dec. 2001, pp. 477 – 485.

Witczak, M., K. Kaloush, T. Pellinen, M. El-Basyouny, and H. Von Quintus, 2002, Simple Performance Tests for Superpave Mix Design. NCHRP Report 465, Transportation Research Board, Washington, DC.

D'Angelo, J., R. Kluttz, R. Dongré, K. Stephens, and L. Zandotto, 2007, Revisions of the Superpave High Temperature Binder Specification: The Multiple Stress Creep and Recovery Test. *Proc.*, Association of Asphalt Paving Technologists, 2007 meeting, San Antonio, Texas.

D'Angelo, J., 2005, Development of Standard Practice for Superpave Plus Specifications. Presented at the NEAUPG 2005 meeting.

Delgadillo, R., D-W Cho, and H. Bahia, 2006, Non Linearity of Repeated Creep and Recovery Binder Test and the Relationship With Mixture Permanent Deformation. *Transportation Research Records: Journal of the Transportation Research Board*, No 1962, TRB, National Research Council, Washington DC, pp. 3 – 11.

Drakos, C., R. Roque, and B. Birgisson, 2001, Effect of Measured Tire Contact Stresses on Near-Surface Rutting. *Transportation Research Record: Journal of the Transportation Research Board*, No.1764, TRB, National Research Council, Washington, D.C., pp. 59 – 69.

Performance Graded Specifications & Test Method Tolerances. Combined State Binder Group (Iowa, Michigan, Minnesota, North Dakota, South Dakota & Wisconsin DOTs & Nebraska DOR), January 2006.

Reinke G., S. Glidden, S. Engber, and D. Herlitzka, 2005, Properties of Polymer Modified Bitumens Related to Mixture Resistance to Permanent Deformation. Presented at 4th Mexican Asphalt Congress. August 24-26, 2005, Guadalajara, Mexico.

Witczak, M. W., K. E. Kaloush, and H. Von Quintus, 2002, *Journal of the Association of Asphalt Paving Technologists*, 71: 671-691.

Work element V3b: Validation of the MEPDG Asphalt Materials Models Using New MEPDG Sites and Selected LTPP Sites. (UNR, UWM)

Subtask V3b-1: Design and Build Sections (UNR Start Year 1, Year 2, and Year 3)

Progress This Quarter

Discussions were held with the MEPDG Lead States Team and several other state highway agencies to solicit their cooperation on this work element. At this point the following states have indicated their willingness to further consider their cooperation on this effort: New Jersey, Virginia, Texas, Nevada, Wisconsin, Idaho, Montana, and South Dakota. Other states that have been contacted but not responded yet include: New Mexico and Washington

Work Planned Next Quarter

Continue discussions with the states to select field section for the MEPDG validations sites.

Subtask V3b-2: Additional Testing (UNR Start Year 2, Year 3, and Year 4)

Progress This Quarter

No activity this quarter.

Work Planned Next Quarter

No work planned.

Subtask V3b-3: Select LTPP Sections (UWM, AAT Start Year 1 thru Year 5)

Task Lead: Haifang Wen

Progress This Quarter

In this quarter, the team looked into the LTPP database for possible data retrieval. Some of the preliminary findings in the area of fatigue are ready to be validated. For instance, the fracture energy from the constant strain-rate tests has the potential to be used as an indicator to fatigue performance of asphalt binder. Fracture energy correlated well with the performance of asphalt binders at the FHWA ALF pavements. One of the plans is to validate this finding. LTPP SPS9 sections were designed to validate the Superpave mix design and materials. These sections could be good candidates for validation. A list of the sections is shown in the table V3b.1.

The team will coordinate with FHWA LTPP to procure the asphalt binder samples. A series of tests will be conducted, including constant strain-rate tests. The parameters from these tests will be correlated with the field performance of these materials. It is noted that there are many variable affecting the field performance, such as climate, aggregate, traffic, thickness, base and soil conditions. To take into account of these factors, as many as samples should be included for any meaningful statistical analysis.

Table V3b.1. Candidate pavement sections for validation.

SHRP_ID	PG_HIGH_TEMP	PG_LOW_TEMP	SOURCE_OTHER
0902	64	-28	HUDSON OIL COMPANY, PROVIDENCE, R.I.
0903	64	-22	HUDSON OIL COMPANY, PROVIDENCE, R.I.
0961	58	-34	HUDSON OIL COMPANY, PROVIDENCE, R.I.
0962	58	-28	HUDSON OIL COMPANY, PROVIDENCE, R.I.
0902	58	-28	ULTRAMAR, ST. RUMUALD, QE
0902	52	-40	BITUMAR, MONTREAL, QE
0903	58	-28	ULTRAMAR, ST. RUMUALD, QE
0903	52	-34	PETRO CANADA, MONTREAL, QE
0901	64	-22	CITGO, PERTH AMBOY, NJ
0902	64	-22	CITGO, PERTH AMBOY, NJ
0902	58	-28	SUIT-KOTE, CORTLAND, NY
0903	64	-22	CITGO, PERTH AMBOY, NJ
0903	52	-28	SUIT-KOTE, CORTLAND, NY
0960	64	-22	CITGO, PERTH AMBOY, NJ
0960	64	-22	CITGO, PAULSBORO, NJ
0961	64	-22	CITGO, PERTH AMBOY, NJ
0961	76	-28	SUIT-KOTE, CORTLAND, NY
0962	64	-22	CITGO, PERTH AMBOY, NJ
0902	64	-22	CITGO
0902	64	-22	CITGO
0902	64	-22	CITGO
0903	70	-22	CITGO
0903	70	-22	CITGO
0903	70	-22	CITGO

SHRP_ID	PG_HIGH_TEMP	PG_LOW_TEMP	SOURCE_OTHER
A902	58	-22	Shell Canada, Montreal
A902	52	-40	Bitumar, Montreal
A903	58	-22	Shell Canada, Montreal
A903	52	-34	Petro Canada, Montreal
0902	58	-40	McAsphalt ON
0903	58	-34	McAsphalt ON
0960	58	-28	McAsphalt ON
0961	58	-34	McAsphalt ON
0962	58	-40	McAsphalt ON
0902	58	-40	McAsphalt ON
0903	58	-34	McAsphalt ON
0960	58	-28	McAsphalt ON
0961	58	-34	McAsphalt ON
0962	58	-40	McAsphalt ON
0901	64	-22	AMOCO, ST.LOUIS
0901	64	-22	AMOCO, ST.LOUIS
0902	64	-28	POLYMER ASPHALT, ST.LOUIS
0902	64	-28	POLYMER ASPHALT, ST.LOUIS
0903	64	-28	POLYMER ASPHALT, ST.LOUIS
0903	58	-28	POLYMER ASPHALT, ST.LOUIS
0959	64	-22	AMOCO, ST.LOUIS
0959	64	-22	AMOCO, ST.LOUIS
0960	64	-22	AMOCO, ST.LOUIS
0960	64	-28	POLYMER ASPHALT, ST.LOUIS
0961	64	-22	AMOCO, ST.LOUIS
0961	64	-22	AMOCO, ST.LOUIS
0962	64	-28	POLYMER ASPHALT, ST.LOUIS
0962	70	-28	POLYMER ASPHALT, ST.LOUIS
0963	64	-28	POLYMER ASPHALT, ST.LOUIS
0963	64	-16	POLYMER ASPHALT, ST.LOUIS
0964	64	-28	POLYMER ASPHALT, ST.LOUIS
0964	64	-28	POLYMER ASPHALT, ST.LOUIS

SHRP_ID	PG_HIGH_TEMP	PG_LOW_TEMP	SOURCE_OTHER
A901	64	-22	POLYMER ASPHALT, ST.LOUIS
A901	64	-22	POLYMER ASPHALT, ST.LOUIS
A902	64	-28	POLYMER ASPHALT, ST.LOUIS
A902	64	-28	POLYMER ASPHALT, ST.LOUIS
A959	64	-28	POLYMER ASPHALT, ST.LOUIS
A959	64	-28	POLYMER ASPHALT, ST.LOUIS
A903	58	-28	POLYMER ASPHALT, ST.LOUIS
A903	58	-28	POLYMER ASPHALT, ST.LOUIS
A960	70	-28	POLYMER ASPHALT, ST.LOUIS
A960	70	-28	POLYMER ASPHALT, ST.LOUIS
A961	64	-16	POLYMER ASPHALT, ST.LOUIS
A961	64	-16	POLYMER ASPHALT, ST.LOUIS
0902	64	-22	MARATHON OIL;MEMPHIS, TN
0903	58	-22	MARATHON OIL, MEMPHIS, TN
0903	70	-22	
0903	58	-22	
0902	64	-22	
0959	64	-10	
0901	64	-16	Citgo Savannah, GA
0902	64	-16	Citgo, Savannah, GA
0903	58	-16	Citgo, Savannah, GA
0959	76	-16	Citgo, Savannah, GA
0902	64	-16	
0903	64	-16	
A902	64	-16	
A903	64	-16	
B902	76	-10	EOTI / Neste Oil
B903	70	-10	Koch Asphalt
0902	64	-34	Montana Refining Company
0903	64	-22	Montana Refining Company
A902	52	-34	Husky Oil
A903	46	-34	Husky Oil

Work Planned Next Quarter

Next quarter the research team will coordinate with FHWA LTPP to procure binder samples and possibly start testing.

Subtask V3b-4: Testing of Extracted Binders from LTPP Sections (UWM, AAT Start Year 1)

Progress This Quarter

ARC team members reviewed the plans for the extracted binder testing that were recommended by the LTPP Materials Expert Task Group and LTPP Protocols P27 (DSR) and P28 (BBR). The recommended testing includes standard DSR and BBR testing of extracted binders at a single temperature selected based on the location of the LTPP project site. ARC team members believe that adding this data to the LTPP database will be of minimal value. Additionally ARC team members are having difficulty securing the necessary cost share to perform this testing.

Work Planned Next Quarter

Considering recent efforts within the LTPP program to provide estimated dynamic modulus measurements for the LTPP sections, the ARC team recommends that the extracted binder testing plan recommended by the LTPP Materials Expert Task Group be reconsidered. The LTPP program currently has a project with Nichols Consulting Engineers to review various models and recommend an approach for estimating mixture dynamic modulus values for the LTPP database. Dr. Richard Kim, an ARC subcontractor, has a key role in this LTPP effort. Dr. Bonaquist will schedule a meeting with the FHWA LTPP Team to discuss a revised plan for the extracted binder testing.

Subtask V3b-5: Review and Revisions of Materials Models (UNR Start Year 2, Year 3, Year 4, and Year 5)

Progress This Quarter

No activity this quarter.

Work Planned Next Quarter

No work planned.

Subtask V3b-6: Evaluate the Impact of Moisture and Aging (UNR Start Year 3, Year 4, and Year 5)

Progress This Quarter

No activity this quarter.

Work Planned Next Quarter

No work planned.

PROGRAM AREA: TECHNOLOGY DEVELOPMENT

Work element TD1: Prioritize and Select Products for Early Development (Year 1)

Progress This Quarter

Identification of viable Early Development projects was completed by the Consortium partners and executive summaries were prepared. The executive summaries were transmitted to the AOTR on January 9, 2008 for distribution to the ETG Chairs. Table TD1.1 presents a summary listing of the projects, the anticipated product, and the Expert Task Group(s) (ETG) that would have major interest in the project. All of these projects deal with further development of test methods that were conceived during research under Federal Highway Administration (FHWA) project "Fundamental Properties of Asphalt and Modified Asphalts."

Table TD1.1. Summary Listing of Early Technology Delivery Projects.

Project	Product	ETG
Automated Flocculation Titrimetric Analysis	Draft AASHTO Standard Test Method for evaluation the propensity of an asphalt or mixture of asphalts to exhibit phase separation	Binder
Determination of Polymer in Asphalt	Draft AASHTO Standard Test Method to determine the quantity of polymer and the nature of the polymer(s) in asphalt	Binder Mixture and Construction
Dynamic Mechanical Analysis	Draft AASHTO Standard Test Method for torsional fatigue testing of the fine aggregate matrix of asphalt concrete	Mixture and Construction Binder Fundamental Properties and Advanced Modeling
Simplified Continuum Damage Fatigue Test	Draft AASHTO Standard Method of Test for fatigue testing of asphalt concrete that can be used with the Simple Performance Test System	Mixture and Construction Fundamental Properties and Advanced Modeling
Universal Sorption Device	Draft AASHTO Standard Method of Test for measuring the surface free energy components of aggregates	Binder Mixture and Construction Fundamental Properties and Advanced Modeling
Wilhelmy Plate Test	Draft AASHTO Standard Method of Test for measuring the surface free energy components of the asphalt binder	Binder Mixture and Construction Fundamental Properties and Advanced Modeling

Work Planned Next Quarter

Upon receipt of authorization from the AOTR, the executive summaries will be distributed to the appropriate ETG membership for comment and rating. The results of the ETG ratings and

recommended projects for development in work element TD2 will be compiled and reported to the AOTR.

Work element TD2: Develop Early Products (Year 2)

Progress This Quarter

Later start.

Work Planned Next Quarter

No work planned.

Work element TD3: Identify Products for Mid-Term and Long-Term Development (Year 2, 3, and 4)

Progress This Quarter

Later start.

Work Planned Next Quarter

No work planned.

Work Element TD4: Develop Mid-Term and Long-Term Products (Years 3, 4, and 5)

Progress This Quarter

Later start.

Work Planned Next Quarter

No work planned.

PROGRAM AREA: TECHNOLOGY TRANSFER

CATEGORY TT1: OUTREACH AND DATABASES

Work element TT1a: Development and Maintenance of Consortium Website (UNR Year 1 through Year 5)

Progress This Quarter

The ARC website was maintained and updated. Quarterly progress reports, the ARC Newsletter, and the ARC presentations at ETG meetings have been posted.

Work Planned Next Quarter

Continue maintaining and updating the ARC website.

Work element TT1b: Communications (UNR Year 1 through Year 5)

Progress This Quarter

The first ARC Newsletter was published. It can be accessed from the ARC website at www.ARC.UNR.EDU

Work Planned Next Quarter

Collect information for the ARC newsletter.

Work element TT1c: Prepare Presentations and Publications (All)

Progress This Quarter

Presentations were made at the Materials Selection meeting at TFHRC in November.

Work Planned Next Quarter

Several presentations are planned by Consortium members at the Transportation Research Board meeting in January 2008.

Work element TT1d: Development of Materials Database (UNR Year 2 through Year 5)

Subtask TT1d-1: Identify the Overall Features of the Web Application
Subtask TT1d-2: Identify Materials Properties to Include in the Materials Database System
Subtask TT1d-3: Define the Structure of the Database
Subtask TT1d-4: Create the Database

Progress This Quarter

Some preliminary material properties were identified at the Materials Selection meeting at TFHRC in November 2007.

Work Planned Next Quarter

No work planned.

Work element TT1e: Development of Research Database (UNR Year 2 through Year 5)

Subtask TT1e-1: Identify the Information to Include in the Research Database System
Subtask TT1e-2: Define the Structure of the Database
Subtask TT1e-3: Create the Database

Progress This Quarter

No activity this quarter.

Work Planned Next Quarter

No work planned.